Master's thesis

NTNU
Norwegian University of Science and Technology
Department of Materials Science and Engineering

Gjermund Lie Solbakk

The Effect of Varying CaO/SiO2 Ratios and Reductant Addition in Silicon Production by Aluminothermic Reduction of Silica Based Slags

Master's thesis in MTMT
Supervisor: Gabriella Tranell
Co-supervisor: Harald Philipson
June 2021

NTNU
Norwegian University of
Science and Technology

Gjermund Lie Solbakk

The Effect of Varying CaO/SiO2 Ratios and Reductant Addition in Silicon Production by Aluminothermic Reduction of Silica Based Slags

Master's thesis in MTMT
Supervisor: Gabriella Tranell
Co-supervisor: Harald Philipson
June 2021

Norwegian University of Science and Technology
Department of Materials Science and Engineering

NTNU
Norwegian University of
Science and Technology

Preface

This thesis titled, "The Effect of Varying CaO/SiO_2 Ratios and Reductant Addition in Silicon Production by Aluminothermic Reduction of Silica Based Slags" was written for the course TMT4905 and was carried out at the Department of Materials Science and Engineering at the Faculty for Natural Sciences at the Norwegian University of Science and Technology (NTNU), during the spring semester of 2021.

The project has received funding from the European Union's Horizon 2020 research and innovation program under Grant Agreement N° 869268.

I would like to thank my supervisor, professor Gabriella Tranell for all al guidance, insight, and feedback throughout this master period. I would also like to thank my co-supervisor PhD candidate Harald Philipson, for all help with the experimental parts, for help with FactSage calculations, as well as helping me to contextualise the results through helpful discussions and sharing previous experiences. It has been a pleasure working with you this past year and I hope that we will meet again in the near future, either through work on this or other future exciting projects. I wish you all the best in your continued studies.

A large thanks goes to Dmitry Slizovskiy and Arman Hoseinpur Kermani for helping me with lab equipment, training, and of course answering my stupid questions regarding the experimental setup. I would also like to thank Morten Peder Raanes for all the help with the EPMA.

Finally, I would like to thank my classmates that I am proud to call my friends. You have helped me through, not only this writing process, but all of these five wonderful (but also tiresome) years. We are even still relatively sane... It has been hard work yet incredibly fun. I have loved every hour we have been studying together, exercised together, partied together, and of course the hours we have "wasted" on the breakroom (a.k.a "Paus") together. I once heard someone say, "Time you enjoy wasting, is not wasted time". So maybe I have not wasted so much time after all.

Abstract

The aim of this work was to investigate how different CaO/SiO_2 ratios in slags, as well as how different reductants additions affects aluminothermic reduction of silica in said slags. The SisAl Pilot project aims to make this process a viable alternative to the traditional carbothermic reduction of silica used in today's silicon industry. In order scale this process up to industrial scale will a good understanding of how different input materials affect the process, and the end products be of utmost importance. The process will use $CaO\text{-}SiO_2$ based start slags, and the temperature will be between 1600-1700˚C. As there are only a certain interval of CaO/SiO_2 ratios that has a low enough melting temperature to meet the requirements of the planed process, will investigations into this interval be of interest.

Three different slags were investigated. One with CaO/SiO_2 ratio of 1.1 (dubbed REC slag) with a melting temperature well within the planed operating temperature, and two slags with CaO/SiO_2 ratio of 0.79 and 1.26 respectively (called acidic- and basic slag). SiO_2 into the system was keep close to constant between slags, meaning that the acidic slag had a lower input mass than the basic slag due to its higher SiO_2 content. Two different reductant/SiO_2 ratios were investigated for all three slags: ~0.9*stoichiometric- and stoichiometric reductant addition. Three parallels were conducted for each experiment. Two parallels with 1.18*stoichiometric reductant addition were also investigated for the acidic slag. All experiments were conducted by adding the reductant (pure Al bares) and slag in to a graphite crucible that was then heated up to 1650˚C in an induction furnace. The samples were held for 60 minutes at T=1650˚C after the operation temperature was reached. All results were compared to expected equilibrium compositions, simulated in FactSage.

The results showed that a higher reductant addition led to a lower concentration of Si in the produced metal, though with a higher overall Si recovery. It was also found that the Si concentration, as well as the Si recovery increased with decreasing CaO/SiO_2 ratio, while the Ca concentration in the metal generally decreased. The simulated equilibrium values and experimental values showed the same trends, though there were significant deviations from the expected values. It is theorised that some of the reductants are lost as it forms carbides as it reacts with the crucible walls, leading to a higher-than-expected Si concentration-, but lower than expected Si recovery to the metal. There was also a general trend of lower-than-expected Ca concentration in the produced metal. This was the case for all slags and stoichiometries. One explanation is that equilibrium has not been reached due to slow reaction rate of CaO, though theory and observations indicated that this was not the problem. It was therefore theorised that the small Ca concentration could be due to either error in the simulated equilibrium values, or that the transport of Ca to the metal was slow due to the formation of Si_2Ca phase (observed in all slags). The Si_2Ca seemed to have a low interfacial tension with the slag, so the driving force for it to coalesce with the rest of the metal would be low. This could not be concluded in this thesis however, but would be an interesting thing to look into at a later date.

Experiments conducted with the REC slag had consistent results with regards to metal composition and yield. This was not the case for the acidic- and basic slag however. The variations were theorised to be due to temperature problems, though for different mechanisms. The acidic slag had problems with a low Si recovery, as the metal from some of its parallels did not coalesce. This was attributed to the slag's high viscosity at low temperatures, thereby reducing the transport of SiO_2 for reactions, and general transport of metal droplets to a main metal phase. The Basic slag had variations in its composition, though it did not have problems with coalescing. There were signs that indicated that the slag did not melt completely due to the high CaO/SiO_2 ratio. A partial melted slag will lead to unstable results for the composition. This, coupled with a potential higher energy consumption, due to both high melting temperature and a high CaO reduction rate makes slags this high in CaO content impractical for use in the SisAl process. The temperature dependence of both the basic and the acidic slag should be investigated further, as too little data was collected to draw concrete conclusions.

Sammendrag

Målet med dette arbeidet var å se på hvordan forskjellige CaO/SiO_2 forhold i slagger, samt hvordan forskjellige reduktant tilsatser påvirker aluminotermisk reduksjon av silika i nevnte slagger. SisAl Pilot prosjektet har som mål å gjøre denne prosessen til et mulig alternativ for den tradisjonelle karbotermiske reduksjonen av silika, brukt i dagens silisium produksjon. For å kunne skalere prosessen opp til industriell skala er en god forståelse av hvordan forskjellige råvarer påvirker prosessen, samt sluttproduktene av stor betydning. Prosessen vil bruke $CaO\text{-}SiO_2$ baserte slagger, og foregå på temperaturer mellom 1600-1700˚C. Ettersom at det kun er et visst intervall av CaO/SiO_2 forholdet som har et lavt nok smeltepunkt for å møte kravene til den planlagte prosessen, vil etterforskning av dette intervallet være av interesse.

Tre slagger ble sett på. En med CaO/SiO_2 forhold på 1,1 (kalt REC slagg) som har en smeltetemperatur godt innenfor den planlagte operasjonstemperaturen, og to slagger ned CaO/SiO_2 forhold på 0.79 og 1.26 (kalt sur- og basisk slagg). SiO_2 inn i systemet var holdt tilnærmet konstant mellom slaggene, hvilket betyr at massen inn av den sure slaggen var mindre enn for den basiske slaggen grunnet sitt høye SiO_2 innhold. To forskjellige reduktant/SiO_2 forhold ble etterforsket for alle tre slaggene, ~0,9*støkiometrisk og støkiometrisk reduktant tilsats. Tre paralleller ble gjennomført for hvert eksperiment. To paralleller med 1,18*støkiometrisk reduktant tilsats ble også sett på for den sure slaggen. Alle eksperimentene ble gjennomført ved at reduktanten (rene Al barrer) og slagg ble tilsatt i en grafittdigel som så ble varmet opp til 1650˚C i en induksjonsovn. Prøvene ble holdt 60 minutter på 1650˚C etter at temperaturen ble nådd. Alle resultantene ble sammenlignet med forventede likevekts sammensetninger, simulert i FactSage.

Resultatene viste at en høyere reduktant tilsats førte til en lavere Si-konsentrasjon i metall produktet, men en høyere Si utvinning. Det ble også funnet at Si-konsentrasjon, samt Si-utbyttet økte med synkende CaO/SiO_2 forhold, mens Ca-konsentrasjonen sank. De simulerte likevekts verdiene og de eksperimentelle verdiene viste samme trend, men det var signifikante avvik fra eksakte verdier. Det er spekulert at en del av reduktanten er tapt til karbider ettersom at det reagerer med digel veggen, noe som førte til et høyere enn forventet Si-konsentrasjon, men et lavere enn forventet Si-utbytte i metallet. Det var også en generell trend av lavere enn forventet Ca-konsentrasjon i produsert metall. Dette var tilfellet for alle slagger og støkiometrier. En forklaring på dette kan være at likevekt ikke er nådd grunnet treg reaksjons rate av CaO, men teori samt observasjoner indikerer at dette ikke var et problem. Det ble derfor spekulert om det var feil i de simulerte likevekts verdiene, eller om transporten av Ca til metallet var tregt grunnet dannelsen av Si_2Ca fasen (den var observert i slagg). Si_2Ca latet til å ha lave grensesjikt spenninger med slagg, så de drivene kreftene for at denne fasen skal samle seg til en metallfase er lave. Dette kunne ikke konkluderes i denne oppgaven, men det ville vært interessant å se nærmere på dette ved en senere anledning.

Eksperimenter hvor REC-slagg var brukt hadde konsistente resultater med tanke på metall komposisjon og utbytte. Dette var ikke tilfellet for den sure- eller den basiske slaggen. Det var spekulert at variasjonene skylles problemer med temperaturen, men forskjellige mekanismer. Den sure slaggen hadde problemer med lavt Si utbytte, ettersom at metallet ikke samlet seg i noen av parallellene. Dette ble forklart med slaggens høye viskositet på lave temperaturer, dermed redusere transport av SiO_2 for reaksjoner, og den generelle transporten av metall dråper til hoved metallfasen. Den basiske slaggen hadde variasjoner i sammensetning, men ikke problemer med at metallet ikke samlet seg. Det var tegn på at alt av slagg ikke smeltet grunnet den høye CaO/SiO_2 forholdet. En delvis smeltet slagg vil føre til et ustabilt resultat for sammensetningen. Dette, sammen med det potensielle høyere energi bruken grunnet høy smeltetemperaturen og en høy CaO reduksjons rate gjøre at slagger med høyt CaO innhold upraktisk for bruk i SisAl prosessen. Hvordan de to slagen avhenger av temperaturen ville vært interessant å se på senere, ettersom at for lite data ble funnet for å si noe helt sikkert.

Table of Contents

Preface ..... **i**
Abstract ..... **iii**
Sammendrag ..... **v**
List of Tables ..... **x**
Table of Figures ..... **xi**
1 Introduction **1**
1.1 Background and motivation 1
1.2 Objective 1
2 Literature study **2**
2.1 Overview of silicon use and production 2
2.1.1 Silicon use 2
2.1.2 Silicon production 2
2.1.3 Problems with silicon production 3
2.2 Alternatives to carbothermic reduction 4
2.2.1 Reduction using Hydrogen 4
2.2.2 Silicon production using Electrolysis 4
2.2.3 Metallothermic reduction 5
2.2.4 Aluminothermic reduction 5
2.2.5 The SisAl Process 6
2.3 Slag properties 7
2.3.1 Slag basicity 7
2.3.2 Interfacial properties 9
2.3.3 Viscosity 9
2.4 Reaction rate and transport in a metal-SiO_2-Al_2O_3-CaO system 11
2.4.1 The rate constant 11
2.4.2 Mass transport 12
2.4.3 Rate determining step 12
2.5 Metal-SiO_2-Al_2O_3-CaO system 13
2.5.1 Factors affecting the composition 13
2.5.2 CaO-SiO_2 system 15
2.5.3 Metal interaction with carbon 15
3 Experimental **17**
3.1 Slag Making 18
3.1.1 Apparatus and Material for Slag Making 18
3.1.2 Slag Making Process 18
3.2 Aluminothermic reductio 20

3.2.1 Apparatus for Aluminothermic Reduction 20
3.2.2 Aluminothermic Reduction of SiO_2 in Different CaO-SiO_2-Slags 22
3.3 Characterisation 24
3.3.1 Sample Preparation 24
3.3.2 Composition analysis 24
3.3.3 Electron Probe Microanalysis (EPMA) 24
3.3.4 X-Ray Fluorescence (XRF) 25
3.3.5 Inductive Coupled Plasma Mass Spectrometry (ICP-MS) 25
3.4 Thermodynamic Modelling with FactSage 25
4 Results 26
4.1 XRF-analysis of master slag 26
4.2 Temperature observations 28
4.2.1 Acidic Slag 28
4.2.2 REC Slag 30
4.2.3 Basic Slag 31
4.3 Metal-yield 32
4.4 Observations 34
4.4.1 Visual inspection, differences between the input slags 34
4.4.2 Observable outliers 35
4.4.3 BSE images and WDS analysis 37
4.5 Chemical composition 46
4.5.1 EDS area analyses of metal and slag 47
4.5.2 Metal dispersed in Slag 49
4.5.3 Mass balance 51
4.6 Simulated equilibrium values 55
4.6.1 Metal yield 55
4.6.2 Simulated composition of metal and slag 56
5 Discussion 57
5.1 Master slags and experiments stoichiometries 57
5.2 Composition of metal and slag 57
5.2.1 Effect of reduction amount 58
5.2.2 Effect of slag composition 60
5.3 Metal yield/mass balance 62
5.3.1 Metal losses 62
5.3.2 Elemental balance for Acidic Slag 63
5.3.3 REC Slag 67
5.3.4 Basic Slag 70

5.4 Effect of temperature and time on reaction rate and transport 73
5.4.1 Outliers from the Acidic slag 73
5.4.2 Basic slag temperature dependence 74
5.5 Interfacial tension 75
6 Conclusion 76
6.1 Concentrations 76
6.2 Si recovery to metal 76
7 Further work 77
8 Bibliography 78
Appendix 80
A. XRF results of the master slags 80
B. All WDS results 81
C. Results from the ICP-MS analysis 83
D. EPMA analysis of slag on low and high magnification 84
E. EPMA results for all parallels 85
F. Plotted analysed and simulated values with C introduced 86
G. Calculated metal yield from analysed composition 87

List of Tables

Table 3-1: Input material and mass for the two separate batches of slag made. 18
Table 3-2: Input mass of metal and slag for the different aluminothermic reduction experiments. 22
Table 3-3: Experimental matrix, showing number of experiments conducted for the different slags and different reductant amounts. 24
Table 4-1: XRF results of the three master slags 26
Table 4-2: Stoichiometry for the different aluminothermic reduction experiments, calculated form XRF-analyses of the master slags 27
Table 4-3: Mass lost during furnace run (mass of crucible in – mass of crucible out). There is no values for basic slag as losses when the crucible was too large to use. Values marked with "*" are samples where pieces of alumina tubes were stuck in the graphite tubes. 32
Table 4-4: Mass of metal separated from the different experiments. Note: 1. basic slag and stoichiometric do not have a value as the metal was to brittle/flaky to be separated without too large loss. 1. acidic slag and 1.1*stoichiometric do not have a value as the metal did not coalesce 32
Table 4-5: The EDS analysis of the third parallel with basic slag and stoichiometric reduction amount. The error are the standard deviation between the 3 measurements done. 49
Table 4-6: Simulated metal yield in for the different input materials with no carbon in the system. 55
Table 4-7: Amount of input C and output SiC for the simulated metal yield to match the experimental metal yield. 56
Table 4-8: Simulated compositions for metal and slag, both for system with, and without carbon introduced. Values are the 3 main elements and impurities. 56
Table 5-1: The metal loss of theoretical metal mass in g and wt%. Theoretical mass calculated from analysed metal composition, and theoretical mass form the FactSage simulation. 62
Table 5-2: Show the maximum calculated wt% of slag that is entrapped metal. There are here assumed no losses during separation, nor to carbides. 63
Table 1: Results for all parallels of XRF analysis of the three master slags. 80
Table 2: All WDS results of phases seen in metal (left), and slag (right). Samples with bold numbers in slag are identified as metal of SiC.(The results goes from brightest (heaviest) to darkest (lightest) in the BSE-images. 81
Table 3: ICP-MS results of three main elements (Si, Al, and Ca) in metal and slag, for REC slag with stoichiometric reduction amount. 83
Table 4: EPMA results for all metal samples. 85
Table 5: EPMA results for all slag samples. Calculated to pure elements (not oxides). 85

Table of Figures

Figure 2.1: Illustration of silicon production in a typical submerge arc furnace (SAF) [6] 2
Figure 2.2: Si recovery as a function of T. The graph is produced by Schei et al.[7], from estimation of measurements by Ozturk and Fruehan [11]..... 4
Figure 2.3: Hydrogen consumption as a function of T. The graph is produced by Schei et al. [7], from estimation of measurements by Ozturk and Fruehan [11]..... 4
Figure 2.4: Schematic representation of the SisAl process [1]..... 7
Figure 2.5: Depiction of how a network modifier (CaO) breaks apart network formers (SiO_2). 8
Figure 2.6: Iso-viscosity (poise) contours of CaO-Al_2O_3-SiO_2 melt at 1500˚C from [7]. More recent data shows that the values should be 20% lower. 10
Figure 2.7: Relationship between viscosity and CaO/Al_2O_3 mass fraction for a 10SiO_2-CaO-Al_2O_3 [24]. 11
Figure 2.8: Relationship between viscosity and mass ratio of CaO/Al_2O_3 at 1823K. For a CaO-5MgO-Al_2O_3-SiO_2 [25]. 11
Figure 2.9: Si-Ca-Al phase diagram created in FactSage using the FTLite database [35]..... 14
Figure 2.10: Ternary phase diagram of the SiO_2-Al_2O_3-CaO system created in FactSage 14
Figure 2.11: CaO-SiO_2 phase diagram [38]. The red lines marks the compositions of the three master slags investigated in this thesis..... 15
Figure 3.1: Flowchart presenting the experimental work. The blue squares illustrate main experimental work, the beige hexagons illustrate preparation of samples, while the round boxes illustrate input output materials/parameter where blue are different slags and grey are reductant amount. 17
Figure 3.2: Crucible, cast and the slag produced (CaO/SiO_2) directly after casting 19
Figure 3.3: Illustrating how slag was crushed down to smaller pieces with a hammer, the tungsten carbide discs used for the crushing, and the resulting slag powder..... 20
Figure 3.4: The closed induction furnace used for the aluminothermic experiments. Left, shows the furnace closed. Right, shows the inside of the furnace, marked are the gas inlet, gas outlet, and Cu coil. 21
Figure 3.5: Graphite crucibles used for the aluminothermic reduction experiments..... 21
Figure 3.6: Left, the graphite tubes that is used to contain the thermocouples in the graphite crucibles, (the indent 67mm from the top was filed in so it would be possible to fasten the tube 30mm over the bottom of the crucible). Right, the graphite lid used to reduce the amount of fuming (the holes are for the two thermocouples). 22
Figure 3.7: Illustrate the charging process with empty crucible (left), charged with the Al used as reductant (middle), and charged with slag on top of the reductant (right). (NB! The graphite paper observed inside the crucible was tested out, but not used for the experiments described here due to problems that arose when used) 23
Figure 4.1: Illustrate the CaO (square) and SiO_2 (circle) concentrations of the three master slags assumed during the experiments (solid masks), and the results from XRF analysis (outline). 27
Figure 4.2: Temperature over time for acidic slag and 0.9*stoichiometric reductant amount. Solid lines are control thermocouple, and dashed line are from top thermocouple. Parallel: 1. (black), 2. (red), and 3. (grey). 28
Figure 4.3: Temperature change per second over time for control thermocouple. Acidic slag and 0.9*stoichiometric reductant amount. Parallel: 1. (black), 2. (red), and 3. (grey)..... 28
Figure 4.4: Temperature over time for acidic slag and stoichiometric reductant amount. Solid lines are control thermocouple, and dashed line are from top thermocouple. Parallel: 1. (black), 2. (red), and 3. (grey). 29
Figure 4.5: Temperature change per second over time for control thermocouple. Acidic slag and stoichiometric reductant amount. Parallel: 1. (black), 2. (red), and 3. (grey)..... 29

Figure 4.6: Temperature over time for acidic slag and 1.1*stoichiometric reductant amount. Solid lines are control thermocouple, and dashed line are from top thermocouple. Parallel: 1. (black) and 2. (red)). 29
Figure 4.7: Temperature change per second over time for control thermocouple. Acidic slag and 1.1*stoichiometric reductant amount. Parallel: 1. (black), and 2. (red). 29
Figure 4.8: Temperature over time for REC slag and 0.9*stoichiometric reductant amount. Solid lines are control thermocouple, and dashed line are from top thermocouple. Parallel: 1. (black), 2. (red), and 3. (grey). 30
Figure 4.9: Temperature change per second over time for control thermocouple. REC slag and 0.9*stoichiometric reductant amount. Parallel: 1. (black), 2. (red), and 3. (grey). 30
Figure 4.10: Temperature over time for REC slag and stoichiometric reductant amount. No top thermocouple was used in these experiments. Parallel: 1. (black), 2. (red), and 3. (grey). 30
Figure 4.11: Temperature change per second over time for control thermocouple. REC slag and stoichiometric reductant amount. Parallel: 1. (black), 2. (red), and 3. (grey). 30
Figure 4.12: Temperature over time for basic slag and 0.9*stoichiometric reductant amount. Solid lines are control thermocouple, and dashed line are from top thermocouple. Parallel: 1. (black), 2. (red), and 3. (grey). 31
Figure 4.13: Temperature change per second over time for control thermocouple. Basic slag and 0.9*stoichiometric reductant amount. Parallel: 2. (red), and 3. (grey). 31
Figure 4.14: Temperature over time for basic slag and stoichiometric reductant amount. Solid lines are control thermocouple, and dashed line are from top thermocouple. Parallel: 1. (black), 2. (red), and 3. (grey). 31
Figure 4.15: Temperature change per second over time for control thermocouple. Basic slag and stoichiometric reductant amount. Parallel: 1. (black), 2. (red), and 3. (grey). 31
Figure 4.16: The average metal yield separated from the slag for each slag and input reductant divided by the input Al in the reductant addition 33
Figure 4.17: Main metal lump separated form (parallel 3) acidic slag and stoichiometric reduction amount (left). Metal pieces comprising the metal yield form (parallel 3) basic slag and stoichiometric reductant amount, after separation (right). 33
Figure 4.18: Illustrate cross section of samples with input material: acidic slag and Stochiometric Al (Left), REC slag and 0.9*Stoichiometric Al (Right). 34
Figure 4.19: Cacked crucible after experiment conducted with basic master slag. Illustrate grey powder found in bottom off all experiments with basic slag, as well as the cross section of metal and slag form this parallel. 35
Figure 4.20: 1. Parallel of acidic slag with 0.9*stoichiometric Al amount: illustrate the cross section of the sample with a small coalesced metal ball, and metal droplets dispersed in the slag. 36
Figure 4.21: 1. Parallel of acidic slag with 1.1*stoichiometric Al amount: illustrate the top (left), and cross section of the sample. The metal had not coalesced in this sample, there were instead a dense dispersion of metal droplets in the top half of the slag. 36
Figure 4.22: 3. Parallel of basic slag with stoichiometric Al amount: 1) illustrate the top of the slag clad coalesced metal (2 metal droplets on top). 2) side view of same lump. 3) said lump cracked in two. 4) illustrate the two metal droplets form the top of the coalesced metal, and the result of one after it was flattened with a hammer. 37
Figure 4.23: BSE-images; acidic slag and 0.9*stoichiometric reductant, parallel 1. (Left) shows phases in metal sample. (Middle) and (Right) shows phases in slag sample. 38
Figure 4.24: BSE-images; acidic slag and 0.9*stoichiometric reductant, parallel 2 and 3. (Left) shows phases in metal sample for parallel 2. (Right) shows phases in slag sample for parallel 3. 38
Figure 4.25: BSE-images; acidic slag and stoichiometric reductant. (Left) shows phases in metal sample for parallel 1. (Right) shows phases in slag sample for parallel 3. 39
Figure 4.26: BSE-images; acidic slag and 1.1*stoichiometric reductant, parallel 1. Metal droplets trapped in slag, (top part of the crucible). 39

Figure 4.27: BSE-images; acidic slag and 1.1*stoichiometric reductant, parallel 1. (Left) shows slag form the top part of the crucible (in between the metal droplets. (Right) shows slag from the bottom part of the crucible. 40
Figure 4.28: BSE-images; acidic slag and 1.1*stoichiometric reductant, parallel 2. Metal droplets trapped in slag, (top part of the crucible). 40
Figure 4.29: BSE-images; acidic slag and 1.1*stoichiometric reductant, parallel 2. (Left) shows slag with 40x magnification. (Right) shows slag phases at 1000x magnification. 41
Figure 4.30: BSE-images; REC slag and stoichiometric reductant, parallel 3. (Left) shows metal with 40x magnification. (Right) shows slag phases at 1000x magnification. 41
Figure 4.31: BSE-images; REC slag and stoichiometric reductant, parallel 2. (Left) shows metal with 100x magnification. (Right) shows slag phases at 600x magnification. 42
Figure 4.32: BSE-images; Basic slag and 0.9*stoichiometric reductant. (Left) shows metal with 40x magnification from the first parallel. (Right) shows slag phases at 1000x magnification from the third parallel. 42
Figure 4.33: BSE-images; Basic slag and stoichiometric reductant, parallel 1. (Left) shows metal with 40x magnification from the first parallel. (Right) shows slag phases at 1000x magnification. 43
Figure 4.34: BSE-images; Basic slag and stoichiometric reductant, parallel 2. (Left) shows metal with 40x magnification from the first parallel. (Right) shows slag phases at 1000x magnification. 43
Figure 4.35: BSE-images; Basic slag and stoichiometric reductant, parallel 3. (Left) shows metal with 40x magnification from the first parallel. (Right) shows slag phases at 1000x magnification. 44
Figure 4.36: BSE-images; Basic slag and stoichiometric reductant, parallel 3. Metal pearl at 40x magnification (left) and 400x magnification (right). 44
Figure 4.37: BSE-images of grey slag powder from all experiments using basic slag. (Left) show an overview of the powder at 40x magnification, showing a compact slag and cracked particles. (Right) show a 600x magnification of the cracked particles (1.) and the compact particles (2.). 45
Figure 4.38: BSE-images; Acidic slag and 1.1*stoichiometric reductant, parallel 2. Shows: Al metal close to the crucible wall (2), an aluminium carbide phase in between the wall and Al phase (1), two slag phases (3) and (4), as well as SiC particles dispersed throw-out the slag phase (5) and (6). 46
Figure 4.39: Average wt% Si in metal for the different input slags and reductant amount. (Red x) under stoichiometric, (black diamantes) stoichiometric, and (blue square) over stoichiometric. The error bars are the standard deviation between the parallels. 47
Figure 4.40: Average wt% SiO_2 in slag for the different input slags and reductant amount. (Red x) under stoichiometric, (black diamantes) stoichiometric, and (blue square) over stoichiometric. The error bars are the standard deviation between the parallels. 47
Figure 4.41: Average wt% Al in metal for the different input slags and reductant amount. (Red x) under stoichiometric, (black diamantes) stoichiometric, and (blue square) over stoichiometric. The error bars are the standard deviation between the parallels. 48
Figure 4.42: Average wt% Al_2O_3 in slag for the different input slags and reductant amount. (Red x) under stoichiometric, (black diamantes) stoichiometric, and (blue square) over stoichiometric. The error bars are the standard deviation between the parallels. 48
Figure 4.43: Average wt% Ca in metal for the different input slags and reductant amount. (Red x) under stoichiometric, (black diamantes) stoichiometric, and (blue square) over stoichiometric. The error bars are the standard deviation between the parallels. 48
Figure 4.44: Average wt% CaO in slag for the different input slags and reductant amount. (Red x) under stoichiometric, (black diamantes) stoichiometric, and (blue square) over stoichiometric. The error bars are the standard deviation between the parallels. 48
Figure 4.45: Illustrate the difference between how much metal that can be in a area scan of a slag sample at 40x magnification (left), and 600x magnification (right). The slag are the second parallel with basic slag and stoichiometric reduction addition. 49
Figure 4.46: Difference in analysed SiO_2 with EPMA EDS area scan between 40x and 600x magnification. 50

Figure 4.47: Difference in analysed Al_2O_3 with EPMA EDS area scan between 40x and 600x magnification 50
Figure 4.48: Difference in analysed CaO with EPMA EDS area scan between 40x and 600x magnification 51
Figure 4.49: Illustrate the distribution between extracted metal yield and the presumed slag for all experiments. (S stands for stoichiometric) 52
Figure 4.50: Illustrate the distribution of input Si in the output metal and slag for all experiments. (S stands for stoichiometric) 53
Figure 4.51: Illustrate the distribution of input Al in the output metal and slag for all experiments. The samples that had a combined higher Al content in output slag and metal than the input, has a thicker outline around the bar. The samples where only the slag had a higher Al content than the output has a thick outline around the slag bar. (S stands for stoichiometric) 54
Figure 4.52: Illustrate the distribution of input Ca in the output metal and slag for all experiments. The samples that had a combined higher Ca content in output slag and metal than the input, has a thicker outline around the bar. The samples where only the slag had a higher Ca content than the output has a thick outline around the slag bar. (S stands for stoichiometric) 55
Figure 5.1: Simulated and experimental Si concentration in metal. 58
Figure 5.2: Simulated and experimental SiO_2 concentration in slag. 58
Figure 5.3: Simulated and experimental Al concentration in metal. 59
Figure 5.4: simulated and experimental Al_2O_3 concentration in slag. 59
Figure 5.5: Simulated and experimental Ca concentration in metal. 59
Figure 5.6: Simulated and experimental CaO concentration in slag. 59
Figure 5.7: Calculated Si recovery for Acidic slag, compared with the simulated values with and without C. 65
Figure 5.8: Calculated Al recovery for Acidic slag, compared with the simulated values with and without C. 66
Figure 5.9: Calculated Ca recovery for Acidic slag, compared with the simulated values with and without C. 67
Figure 5.10: Calculated Si recovery for REC slag, compared with the simulated values with and without C. 68
Figure 5.11: Calculated Al recovery for REC slag, compared with the simulated values with and without C. 69
Figure 5.12: Calculated Ca recovery for REC slag, compared with the simulated values with and without C. 70
Figure 5.13: Calculated Si recovery for Basic slag, compared with the simulated values with and without C. 71
Figure 5.14: Calculated Al recovery for Basic slag, compared with the simulated values with and without C. 72
Figure 5.15: Calculated Ca recovery for Basic slag, compared with the simulated values with and without C. 73
Figure 1: Average wt% SiO_2 (40x magnification) in slag for the different input slags and reductant amount. (Red x) under stoichiometric, (black diamantes) stoichiometric 84
Figure 2: Average wt% SiO_2 (600x magnification) in slag for the different input slags and reductant amount. (Red x) under stoichiometric, (black diamantes) stoichiometric 84
Figure 3: Average wt% Al_2O_3 (40x magnification) in slag for the different input slags and reductant amount. (Red x) under stoichiometric, (black diamantes) stoichiometric 84
Figure 4: Average wt% Al_2O_3 (600x magnification) in slag for the different input slags and reductant amount. (Red x) under stoichiometric, (black diamantes) stoichiometric 84
Figure 5: Average wt% CaO (40x magnification) in slag for the different input slags and reductant amount. (Red x) under stoichiometric, (black diamantes) stoichiometric 84

Figure 6: Average wt% CaO (600x magnification) in slag for the different input slags and reductant amount. (Red x) under stoichiometric, (black diamantes) stoichiometric 84
Figure 7: Simulated (with C) and experimental Si concentration in metal. 86
Figure 8: Simulated (with C) and experimental SiO_2 concentration in metal. 86
Figure 9: Simulated (with C) and experimental Al concentration in metal. 86
Figure 10: Simulated (with C) and experimental Al_2O_3 concentration in metal. 86
Figure 11: Simulated (with C) and experimental Ca concentration in metal. 86
Figure 12: Simulated (with C) and experimental CaO concentration in metal. 86

1 Introduction

1.1 Background and motivation

The use of MG-Si (Metallurgical Grade Silicon) is today divided between three main industries: additives in alloys (mainly aluminium), for silicones production, and the photovoltaics industry [1]. All of these industries are in growth. Though photovoltaics has a relatively small share in the global power marked, is it growing, and will continue to grow rapidly. The Compound Annual Growth Rate (CAGR) of photovoltaics installations was 36.8% between 2010-2018 [1], [2].

Silicon-based products are used in a number of "green"- applications. The production of this resource is an energy intensive process as well as a large contributor to CO_2-emissions. There is efficiently no commercial alternative to the traditional Submerge Arc Furnace (SAF) production route used today. Production in SAF uses carbothermic reduction to produce silicon.

The EU H2020 funded SisAl-pilot project introduces a new production route for silicon. Utilising aluminothermic reduction as an alternative to carbothermic will lead to a reduction in the energy consumption needed, as well as a reduction in the direct CO_2-emissions. The SisAl process will allow silicon production to stay in an ever increasingly carbon-lean Europe [1].

The SisAl process utilises SiO_2 as fines or lumps in combination with CaO as the silicon source. The flux mix is melted at 1600-1700˚C, after which an aluminium source (end of life scrap, dross, etc.) is added. This results in a reduction of the silica to silicon metal, and the oxidation of aluminium to alumina in a CaO-Al_2O_3 based slag. The produced slag is separated from the metal, and the CaO- and Al_2O_3 components are separated through leaching. CaO will go back into the process while the Al_2O_3 can be sent to aluminium primary production or to be used in ceramic applications. A schematic insulation of the material flow is presented in Figure 2.4. The process is described in further detail in section 2.2.5.

1.2 Objective

It is important to have a good understanding of what input parameters that is of interest to test, as the SisAl project moves forward with its upscaling of experiments for industrial use. The main objective of this thesis is to investigate the affect different slag compositions, as well as the effect different reduction amount have on the end product, both metal and slag composition. Slags with three different CaO/SiO_2 mass ratios was investigated; 0.79, 1.1, and 1.26. The input of reductant addition investigated was; 0.9*stoichiometric and stoichiometric addition, corresponding to the reduction of silica with aluminium, (these was later revealed to be somewhat higher than intended for each slag). Three parallels were conducted for each stoichiometry, on each of the slags. Two experiments with 1.18*stochiometric reductant addition were also conducted on the high silica slag. This was done to investigate the effect over stoichiometric reductant amount has on the process as a whole, but especially to investigate how pure (free of SiO_2) the slag could become in practise. As a slag high in Al_2O_3 and low in SiO_2 are preferable for leaching and later use. The experiments were conducted on 1650˚C at 60 minutes holding time. Metal and slags samples were characterised by EPMA (Electron Probe Micro Analysis), where the overall bulk compositions, as well as phases were identified. Thermodynamical modelling of the systems was conducted in FactSage 7.3. This was done to compare the expected equilibrium compositions, and metal yields with experimental compositions, and metal yields.

2 Literature study

2.1 Overview of silicon use and production

2.1.1 Silicon use

Silicon use has exploded in later years as it is critical element in a wide range of modern technologies and applications. MG-Si (Metallurgical Grade Silicone) usage was in 2016 split between three main industries; additives in aluminium alloys (50%), silicones (30%), and for solar photovoltaics (PV) (17%) [1]. All of with are markets in continued growth. Europe are today consuming about one quarter of the worlds produced MG-Si, despite only producing between 10-12% [1], [2]. This, together with the fact that China produces two thirds of the worlds silicon, lead to silicon being classified as a critical raw material by the EU in 2014 [3]. This is despite the fact that silicon is the second most abundant element in the earth's crust after oxygen.

2.1.2 Silicon production

Commercial production of silicon varies little in between companies and plants. Though there are differences in operations like charging and input material, plant design, size, etc. the principle is the same for all producers as of today. In the submerged arc furnace (SAF), quartz (SiO_2), carbon material (coke, coal, charcoal, and/or wood chips), and heat from electrical energy are mixed to produce silicon by carbothermic reduction. The energy is supplied through electrodes and it takes 11-13MWh to produce one tonne of silicon [4], [5]. A schematic illustration of a SAF is depicted in Figure 2.1.

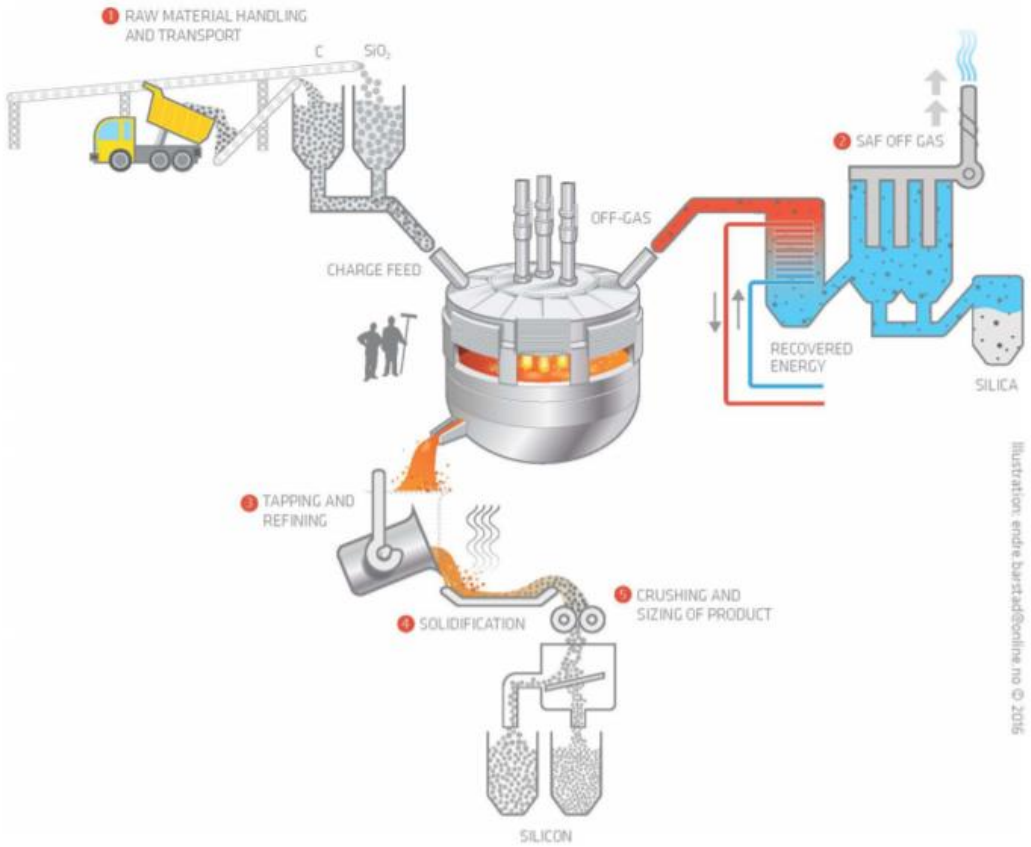

Figure 2.1: Illustration of silicon production in a typical submerge arc furnace (SAF) [6]

The simplified ideal reaction showing the reduction of silica to silicon is describing in eq. (2.1), (the real process has several intermediate products before silica goes to silicon, complicating the process). The bottom of the furnace where most of the silicone are produces is kept at an operation temperature of

1900-2000˚C. The large amount of energy supplied is necessary to keep the needed operation temperature stable, as the production is endothermic.

$$SiO_{2(s)} + 2C_{(s)} \rightarrow Si_{(l)} + 2CO_{(g)} \quad (2.1)$$

There are several factors that contribute to metal losses in the silicon production. The largest reason for the reduction in yield is by far that silicon exits the furnace as SiO-gas, eq. (2.2). SiO and CO exits the top of the furnace and react with oxygen in the atmosphere to produce SiO_2 (microsilica), CO_2 and heat, see eq. (2.3). (It should be mentioned that captured microsilica is sold as a product to a number of different industries). The silicon yield depends on a number of factors like carbon material, stoking, surface temperature, etc. but there is found that a typical yield is in between 80-90% [7].

$$(1+x)SiO_{2(s)} + (2+x)C_{(s)} \rightarrow Si_{(l)} + xSiO_{(g)} + (2+x)CO_{(g)} \quad (2.2)$$

$$xSiO_{(g)} + (2+x)CO_{(g)} + (1+x)O_2 \rightarrow xSiO_{2(micorsilica)} + (2+x)CO_{2(g)} + heat \quad (2.3)$$

2.1.3 Problems with silicon production

Looking at eq. (2.1) and eq. (2.3) it becomes clear that silicon production contributes to the release of CO_2 into the atmosphere. In fact, ignoring the emissions related to energy production, the pre-processing of carbon materials (charge and electrode), and assuming 100% silicon yield, the emissions from the reduction (described in eq. (2.1)) alone would be 3.1 tonne CO_2 per tonne silicon produced. This is not an ideal world though, so emissions will be considerable higher. How much higher will depend on factors like; furnace operation, carbon sources, etc.[5], [8]. In addition to CO_2 emissions are there several other problems related to silicon production.

Methane (CH_4) and other volatile hydrocarbons are generated during combustion of carbon materials, like the carbon-based electrodes and carbon material in the charge (coal, coke, woodchips, etc.). The emission levels of the hydrocarbons are mainly decided by the type of carbon material, but it is also strongly dependant on how the furnace are operated as well as the charging mechanism. There is high variation and uncertainty in the data reported, as the factors that these types of emissions depend on are numerous. Lindstad et al. [9] compared data from Norwegian Si and FeSi smelters (available at norskeutslipp.no[10]) and found discrepancies in an order of 10.

Nitrogen oxides often referred to as NO_x, are another emission type that arise from silicon production. NO_x is linked to a number of different environmental problems. In the SAF are there mainly two formation mechanisms that is dominant for the formation of NO_x: fuel NO_x is formed from the oxidation of the nitrogen present in the fuel, while thermal NO_x is formed by oxidation of nitrogen in the atmosphere at temperatures above 1400˚C (the fume hood is frequently observed with temperatures around 1400˚C). Typical NO_x emissions was found to be around 22 kg/tonne Si produced in a batch process, while it was found to be around 11 kg/tonne Si produced in a semi-continuous process [6].

Polycyclic Aromatic Hydrocarbons (PAH) are organic molecules composed of two or more aromatic (benzene) rings. These compounds come from incomplete combustion (pyrolysis) of the carbon material (charge and electrodes). Several of these PAH are linked to different chronic illnesses and health problems. Though emissions vary due to furnace operations and carbon materials, data from Norwegian plants suggest a yearly emission between 10-70 kg of PAH per site [6].

Though most of the greenhouse gasses together with other dangerous emissions from the silicon production comes from the carbon materials used, there are other steps in the value chain that are contributing to the emissions. Raw material like quartz needs to be mined and transported. There is a number of requirements that needs to be met, in regards to the quartz that is used in the SAF. The purity is important, but there are also strict requirements to the size (this means that sand of high purity can not be used in traditional production). To small particles in the furnace reduces the gas permeability which increases the likelihood of blow-outs due to gas build-up [7].

2.2 Alternatives to carbothermic reduction

In order to address the problems described in the section 2.1.3 have new production methods been proposed as an alternative to traditional carbothermic reduction in SAF.

2.2.1 Reduction using Hydrogen

The carbon material (coal, coke, etc.) used in silicon production is the main source of impurities, the largest contributor to damaging emissions for both health and environment, and have the disadvantage of being a finite resource (with the exception of wood chips and charcoal). All of these problems can be circumvented by replacing carbon with hydrogen as a reductant [7].

The most important parameter in production is the efficiency of the process. When hydrogen is used will the efficiency be defined as the silicon recovery (number of mol Si produced per mol SiO_2 consumed. The losses will be in SiO), and as hydrogen consumption (the number of mol H_2 consumed per mol Si produced). Equilibrium calculations can be done on eq. (2.4) that is the system silicon production by hydrogen reduction would be in [7].

$$xSiO_{2(l,s)} + yH_2 \rightarrow zSi_{(l)} + aSiO_{(g)} + bH_2O_{(g)} + cH_g + dH_{2(g)} \quad (2.4)$$

Plotting the silicon recovery as a function of temperature for a number of different pressures, was it found that the pressures needed to be incredible high (up to 100 000 bar) to get a relatively high silicone recovery, see Figure 2.2.

Hydrogen consumption as a function of temperatures at different pressures was plotted as well, see Figure 2.3. It becomes clear that production of silicon using hydrogen as a reductant will be incredible inefficient and borderline impossible to do on a large scale [7].

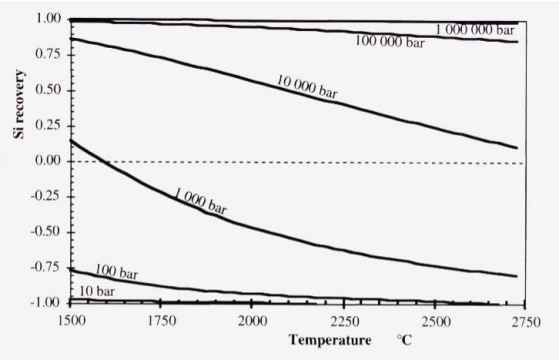

Figure 2.2: Si recovery as a function of T. The graph is produced by Schei et al.[7], from estimation of measurements by Ozturk and Fruehan [11].

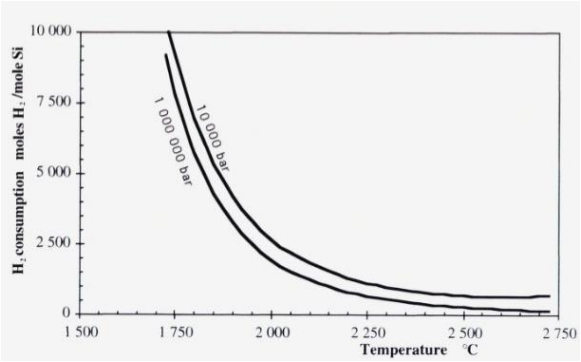

Figure 2.3: Hydrogen consumption as a function of T. The graph is produced by Schei et al. [7], from estimation of measurements by Ozturk and Fruehan [11].

2.2.2 Silicon production using Electrolysis

The possibility of silicon production through electrolysis has been investigated in order to minimise the disadvantages stemming from the carbothermic reduction (see section 2.1.3). Similar to the Hall-Héroult process used for aluminium production, SiO_2 can be dissolved in cryolite and then be electrolyzed. The electrolyte bath is traditionally kept at 1000˚C which is well above the melting temperature of aluminium. Silicone however, melts at temperatures above 1400˚C which means that it will exit the cell as a solid. [7]

Nohira et al. [12] did a study where the removal of oxygen from solid SiO_2 in a molten $CaCl_2$ at 850˚C, as well as in a molten LiCl-KCl-$CaCl_2$ at 500˚C was done through electrolysis. A contact electrode in the form of a metal wire (molybdenum wire) were contacted to the SiO_2 piece, where the conductor supplied electrons to selected areas of the insulating SiO_2. It was believed that when deoxygenation would occur at the three-phase interface between SiO_2, the conducting material, and the molten salt,

when the electrode potential of the conducting material was more negative than the reduction potential of SiO_2. This was mainly done as proof of concept for smaller processes in silicone semiconductor technology, and high-purity silicone production, with high purity SiO_2.

A later study conducted by Yasuda et al. [13] looked closer into direct electrolytic reduction of SiO_2 in molten $CaCl_2$ at 850˚C, at 1.10 V for one hour. XRF-analysis confirmed the reduction of the amorphous SiO_2 sample to crystalline Si. It was found that the rate determining step was the diffusion of O^{2-} through the molten $CaCl_2$ in the vacant space that appeared as a consequence of the volume decrease as SiO_2 transformed to Si.

Though there is some promise in solid state electrolysis of silicon for high purity production (as long as the SiO_2 source is pure, and little contact with electrode material) the reaction rate is relatively slow when compared to mass transport in liquid. This type of production has a problem with the high operation temperature required. The temperature needs to be over the melting temperature of silicon, but increased temperature means increased tear on the furnace material and increased energy usage. Several salt fluxes have been studied, where the one that shows the most promise is a SiO_2-BaO-BaF_2 mix. Small scale experiments found a current efficiency of only 40%, though it was expected to increase with increasing scale of operation [7], [14].

Elwell and Rao [14] conducted a literature review comparing different electrolysis methods of silicon. When compared to carbothermic reduction was it found that electrolysis had a higher purity. The lower reaction rate and relatively high cost means that electrolytic production of silicone makes it less viable commercially in comparison too carbothermic reduction [7], [14].

2.2.3 Metallothermic reduction

Reducing a chemical compound like halides or oxides to a pure metal using a more reactive metal has been documented as far back as 1808, when Humphry Davy manage to isolate alkali metals [15], [16]. Though the method has been used for a number of applications, the first industrial use for the method was for aluminium production. Aluminium was produced from a reduction of the chemical compound aluminium chlorides with the highly reactive alkali metal, sodium. This was the main production rout of aluminium up to 1888 when the American, Charles Martin Hall and the Frenchman, Paul Louis Toussaint Héroult came up with the idea of using electrolysis for aluminium production.

Metallothermic reduction can be described by the generic equation illustrated in eq. (2.5). The A is the metal that get reduced, B is the reductant, and X is the oxidation agent (oxygen, sulphur, or halogens like chlorine or fluorine).

$$AX + B \rightarrow A + BX \tag{2.5}$$

The metals most commonly used as reducing agents are aluminium, calcium, ferrosilicon, magnesium, and sodium. There are several factors that is considered when choosing a reductant, whereas the most critical/general are [16]:

- They need to have a high affinity to oxygen/halogens.
- They should have a high boiling point.
- They should have a low vapor pressure.
- They should produce slag that can be removed easily by melting or leaching.
- They should not produce intermetallic compound with the produced metal
- They should be easy to handle, and be cheap.

2.2.4 Aluminothermic reduction

Aluminothermic reduction can be an alternative to the traditional carbothermic reduction, utilising ether SiO_2 or $SiCl_4$ as a silicon source [17]. There has been multiple studies into the subject of aluminothermic

silicon production with a special focus on high purity silicon for the photovoltaic industry [17]–[19]. The background for this use is that the largest contributor of impurities like carbon as well boron, in silicon are carbon materials used as reductants in traditional SAF operation [18].

Yasuda et al. [17] utilised $SiCl_4$ and SiO_2 as silicone sources, together with aluminium in order to produce high-purity silicon metal (see eq. (2.6) and eq. (2.7)). Aluminium must be supplied in solid or liquid form (not as gas) due to its high vapor pressure. Reduction of SiO_2 with Al (eq. (2.6)) is an exothermic reduction, which means that it will release a lot of energy when as the silicon is produced. The by-product in eq. (2.7), $AlCl_3$ will be removed as vapor, making the by-product and product easy to separate.

$$3SiO_{2(l)} + 4Al_{(s,l)} \rightarrow 3Si_{(l)} + 2Al_2O_{3(s)} \tag{2.6}$$

$$3SiCl_{4(g)} + 4Al_{(s,l)} \rightarrow 3Si_{(s)} + 4AlCl_{3(g)} \tag{2.7}$$

Aluminothermic reduction of quarts means that a smaller generation of SiO will occur as there is no carbon present. This means that it is possible to use quartz sand as silicon source, as there no longer is need for the good gas permeability through the charge, which is crucial for carbothermic reduction [1], [18].

Fluxes containing SiO_2 (like CaO-SiO_2) is also a possible oxidizing agent. Using a SiO_2 containing slag will serve two purposes; a source of silicon, and the slag (CaO) will work as a solvent for the produced Al_2O_3 [18]. There is important that all the oxides in the flux have a lower gibes free energy than Al_2O_3 (with the exception of SiO_2 of course), otherwise would aluminium reduce the other components in the slag as well, not just the SiO_2.

There are many advantages of producing silicon through aluminothermic reduction, but due to practical reasons most scientific research on the subject has focused on small scale, high purity silicon for the photovoltaics industry. Aluminothermic production of Metallurgical Grade Silicon (MG-Si), has not been economically viable due to the high price of aluminium compared to that of carbon materials. The next section will describe a process which tries to produce MG-Si through aluminothermic reduction.

2.2.5 The SisAl Process

The SiaAl Pilot Project funded by EU H2020, aims to demonstrate a novel industrial process as an alternative to the carbothermic silicon production used today. Switching from a carbothermic based process, to an aluminothermic based silicon production have a number of advantages related to environment, raw materials, energy consumption, etc. as outlined above. An overview of this process is illustrated in Figure 2.4. The following information is from the Proposal submission forms for the SisAl-pilot [1].

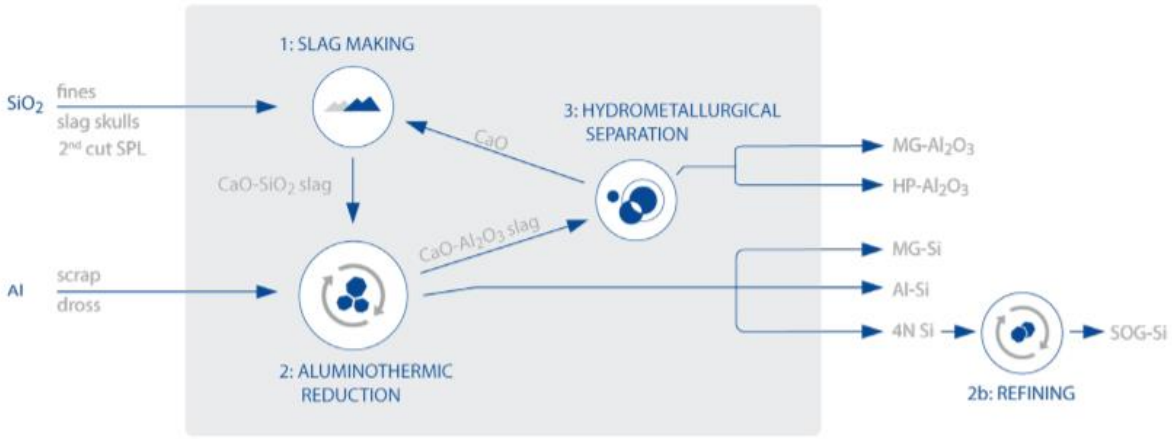

Figure 2.4: Schematic representation of the SisAl process [1].

The reductant used in the SisAl process will be aluminium form dross and scrap. The source of SiO_2 have fewer restrictions compared to the strict requirements set for the quartz used in SAF with carbothermic reduction. The process is comprised of three main steps as illustrated in Figure 2.4, and are as follows:

1. Combine SiO_2 (this can be less costly quarts sand and fines, instead of the highly size controlled quarts lumps used in SAF) and CaO to a CaO/SiO_2 mass ration of approximately 1. This is done on temperatures high enough to melt the mix, (temperatures between 1600-1700˚C).
2. Introducing an aluminium source (this can be scrap, dross etc.) to reduce most of the SiO_2 in the slag to silicon alloy, hence producing a Al_2O_3-CaO slag in accordance with eq. (2.8).

$$SiO_{2(in\ SiO_2-CaO\ slag)} + \frac{4}{3}Al_{(l)} \rightarrow Si_{(l)} + \frac{2}{3}Al_2O_{3(in\ Al_2O_3-CaO\ slag)} \quad \Delta H^\circ = -174.8\frac{kJ}{mol} \qquad (2.8)$$

   The metal and slag will then be separated. As the operation temperature are lower, as well as the fact that the reduction reaction is exothermic instead of endothermic when compared to carbothermic reduction in SAF, will the energy consumption be less the SisAl process.
3. Separate the Al_2O_3-CaO slag into Al_2O_3 and CaO components through a hydrometallurgical process. The Al_2O_3 can then be reintroduced back into primary aluminium production or refined into high purity alumina for sapphire production. The CaO will just be reintroduced back into the SisAl process. It should be mentioned that this third option can be skipped altogether as Al_2O_3-CaO slag can be sold for use in the refractory industry.

Observing eq. (2.8) it becomes obvious that a good understanding of the thermodynamics governing the SiO_2-Al_2O_3-CaO and metal system, as well as the transport mechanisms between these two will be crucial to control the SisAl process.

2.3 Slag properties

The SiO_2-Al_2O_3-CaO slag system is well known due to it being present in several metal production processes. The SiO_2-Al_2O_3-CaO system is of interest in the silicon industry when it comes to the topic of refining silicon [7]. To understand the slag system in metal process means to understand the process as a whole. Properties like viscosity, composition, the interfacial properties between metal and slag, thermodynamical equilibriums between the slag and melt, etc. are all important to define the interaction between metal and slag.

2.3.1 Slag basicity

The ion-oxygen parameter *I*, is an important parameter that is expressed by the coulombic force between cation and oxygen in an oxide. It is defined as follows:

$$I = \frac{2z}{(r_c + r_o)^2} \tag{2.9}$$

The z is the valence of the cation, the two is the valence of the oxygen, r_c and r_o are the radiuses of the cation and oxygen respectively (measured in Å). Large I values indicates strong interactions between cation and oxygen, while smaller values indicates weaker interactions [20]. Some oxides show good glass formability and are called "network formers" as they form large amorphous networks. These oxides have a strong interaction between cation and oxygen, meaning a high ion-oxygen parameter where $I > 1.7$ and they have oxygen coordination numbers of 3 or 4. The oxygen coordination numbers indicate that network formers create structures consisting of triangles or tetrahedral units. SiO_2 is an example of a network former that forms a network comprised of SiO_2^{4-} tetrahedra, (see eq. (2.10)).

$$SiO_2 + 2O^{2-} = SiO_4^{4-} \tag{2.10}$$

On the other side of the spectrum are oxides with weaker interactions between the cation and oxygen, leading to a lower ion-oxygen parameter $I < 0.7$. CaO is on such oxide. As the attracting forces between cation and oxygen are weak when compared to the network formers, will these oxides donate oxygen to the network formers when mixed. see eq. (2.11). The donated oxygen-ions will break apart the network formers, (see Figure 2.5), and are hence called "network modifiers".

$$CaO = Ca^{2+} + O^{2-} \tag{2.11}$$

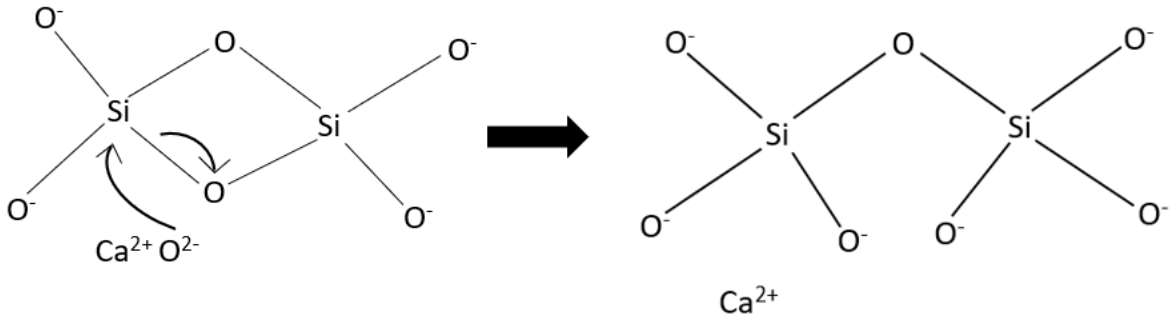

Figure 2.5: Depiction of how a network modifier (CaO) breaks apart network formers (SiO_2).

Oxides whom values for the ion-oxygen parameter are intermediate ($0.7 < I < 1.7$), are called "amphoteric" oxides. These will work as eater a network former or network modifier depending on the oxide melt environment. Al_2O_3 is an example of an amphoteric oxide [7], [20].

As network formers works much in the same way as a Lewis acid and networks modifiers as a Lewis base due to their ability to accept or donate O^{2-}, are slags with a high concentrations of network formers or network modifiers are termed acidic- or basic slags respectively. The term basicity was introduced in order to evaluate technical and chemical problems in pyrometallurgical processes where slags are present. Basicity does not have a set definition, but it is used to describe how basic the slag is. For a SiO_2-CaO system is a commonly used definition seen in eq. (2.12), while it is often defined by eq. (2.13) for a SiO_2-Al_2O_3-CaO system.

$$B = \frac{\%CaO}{\%SiO_2} \tag{2.12}$$

$$B = \frac{\%CaO}{\%SiO_2 + \%Al_2O_3} \tag{2.13}$$

These definitions vary between molar percent, mass percent, addition or subtractions of species, and how the concentrations are weighted. There is therefore important to specify the system when discussing actual values of basicity[20].

2.3.2 Interfacial properties

Mechanisms like reaction kinetics, nucleation and formation of solid particles, as well as droplets of one substance in another (like metal droplets in slag), are all influenced by interfacial properties. The interfacial properties are of a thermodynamical nature, and depends on the difference substances and phases that are in contact. The interfacial energy between these substances is defined as the work that is needed to expand the interface by one unit. The relation between temperature and surface energy (gas and liquid phase) usually follows the linear relation eq. (2.14) [7].

$$\sigma = \sigma_0 + \left(\frac{d\sigma}{dT}\right) * T \tag{2.14}$$

The T is absolute temperature, σ_0 and ($d\sigma/dT$) are constants found experimentally. Slags with high concentrations of SiO_2 are exceptional with regards to this relation as they are highly polymerized due to them being network formers [7].

A comprehensive literature review on slag properties like interfacial tension was done by Matsushita et al. [21]. It was found that the interfacial properties were less affected by the slag composition and more by the surface-active elements in the metal. Studies looking into systems with SiO_2-Al_2O_3-CaO slags and Fe-Si alloys had conflicting evidence regarding positive or negative change in the interfacial tension when Si concentration in the Fe-Si alloy was increased[22], [23]. Sun et al.[22] found that the interfacial tension between the metal phase and a CaO-SiO_2 slag increased slightly when the CaO/SiO_2 ratio increased.

2.3.3 Viscosity

Viscosity is defined as a fluids resistance to deformation at a given rate. It is an important parameter for the flow and transport properties of a melt, metal or slag. Viscosity of a metal or slag will vary depending on the composition, but a slag will general always have the higher viscosity due to the nature of the melt structure (polymerization). Viscosity of a fluid is naturally dependant on the temperature. The relationship between the temperature and the viscosity of certain types of melts (metal and simple ionic melts) is described by the Arrhenius equation (eq. (2.15)) [7], [20]:

$$\eta = \eta_0 * \ exp\left(\frac{E_\eta}{RT}\right) \tag{2.15}$$

The η_0 is a proportionality constant, R is the gas constant, E_η is the activation energy for viscous flow, and T is the absolute temperature. This relation between temperature and viscosity will no longer be valid for polymetric melts (i.e slags with high concentration of network formers), due to the de-polymerization that occur with rising temperatures, changing the E_η. Though eq. (2.15) no longer is reliable for acidic slags will this system to be highly temperature dependant, so a temperature increase and the subsequent de-polymerization will lead to a decrease in viscosity in most cases.

The viscosity in isothermal SiO_2-Al_2O_3-CaO slag systems will only depend on the concentration of the species. Acidic slags (high in silicates) will form networks that increase the viscosity, the network modifiers in basic slags (high in CaO) will decrease the polymerization of the slag, hence decrease the viscosity, while a slag high in amphoteric oxides (high in Al_2O_3) will depend on the composition of the whole system. These behaviours can be observed in Figure 2.6. As the Al_2O_3/SiO_2 is held constant will

the iso-viscosity lines lie perpendicular with the reduction of CaO, illustrating the fact that viscosity increases as the concentration of network modifiers decreases. A decrease in CaO and increase in Al_2O_3 content changes the iso-viscosity lines to become more parallel with the iso-concentration line of SiO_2. This is a clear indication of the amphoteric properties of Al_2O_3. In general it is found that Al_2O_3 works as a network former when $CaO/Al_2O_3 > 1$, and as a network modifier when $CaO/Al_2O_3 < 1$ [20], though this is just a rule of thumb and depends heavily on the composition of rest of the melt [24], [25].

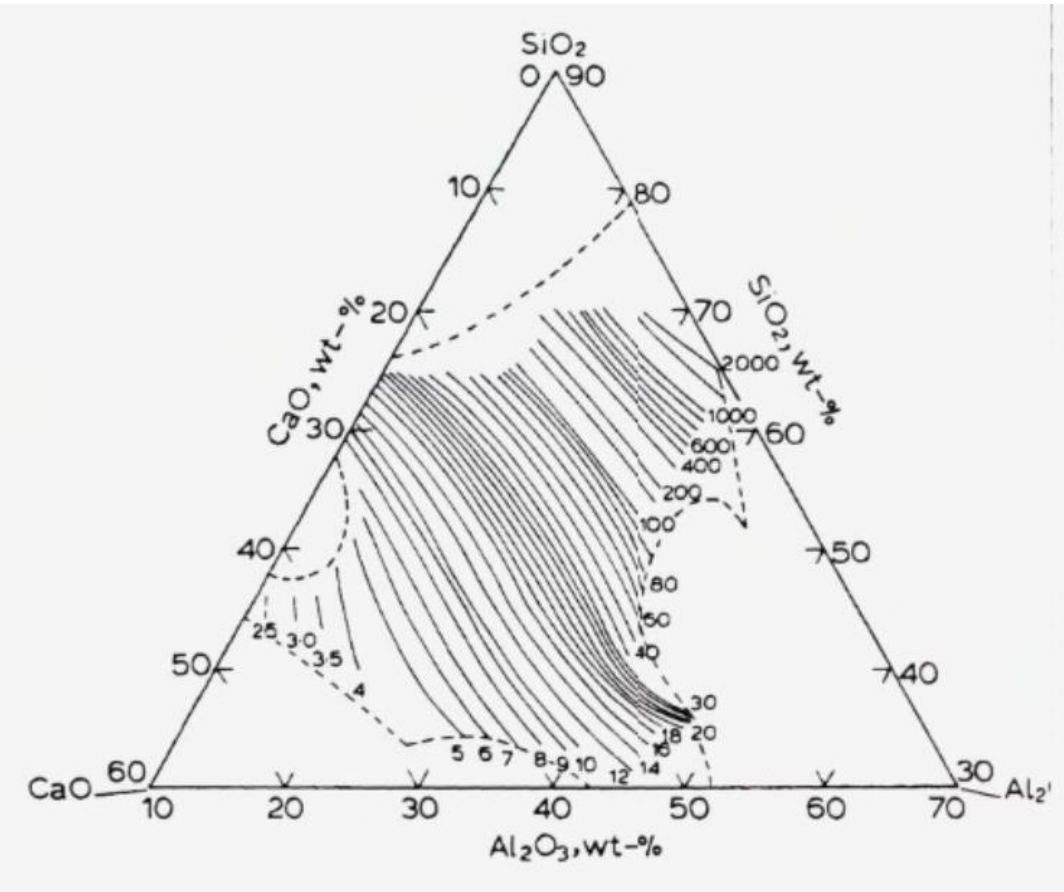

Figure 2.6: Iso-viscosity (poise) contours of CaO-Al_2O_3-SiO_2 melt at 1500˚C from [7]. More recent data shows that the values should be 20% lower.

In addition to the polymerization occurring in slags due to high concentration of network formers, the viscosity in a slag will increase if particles are present in the melt. The effect particles has on a melt is described by the relation eq. (2.16):

$$\eta_e = \eta(1 - 1.35\emptyset)^{-\frac{5}{2}} \tag{2.16}$$

Where η_e is the viscosity of the melt with particles, η is the viscosity of the pure melt, and $\emptyset$ is the volume fraction of the particles. (The particles are assumed to be spherical and of uniform size). Possible sources to these particles is slag not yet dissolved, particles formed through reaction with the crucible/refractory material (like SiC), or from primary precipitates of minerals at sub-liquidus temperatures [7].

Siafakas et al. [24] conducted a study, measuring the viscosity in a low SiO_2 (10-20 wt%)-CaO-Al_2O_3 system within a temperature interval (1623-2800˚C), varying the CaO/Al_2O_3 fraction. It became apparent that the viscosity was strongly dependant on the temperature as it decreased rapidly with rising temperature. The changes were more substantial for the lower end of the temperature scale as there still were a solid phase growing on the side of the crucible, reducing the viscosity. Al_2O_3 was shown to work

as a network former in a slag with 50 wt% CaO. This became obvious as the CaO were kept constant while the SiO_2/Al_2O_3 fraction was varied between 0.25-0.67 without substantial changes in the viscosity. There was a clear decrease in viscosity as the concentration of networks modifiers was increased (CaO/Al_2O_3 fraction were increased from 1.05-2.0, the SiO_2 concentration was kept at 10wt%). Thought there was a clear outlier as the viscosity increased after a steady decrease (CaO/Al_2O_3 = 1.57), see Figure 2.7. It was concluded that the reason for the sudden increase in viscosity was due to precipitation of ionic clusters in the melt at this specific composition.

Xu et al. [25] investigated the viscosity in a low silica CaO-5MgO-Al_2O_3-SiO_2, a slag system with much of the same attributes as the one that was discussed in the previous paragraph. They too found that viscosity decreased with increasing CaO/Al_2O_3 fraction, though further increase in CaO/Al_2O_3 eventually lead to an increase in viscosity (see Figure 2.8). It was concluded that the sudden increase in viscosity was due to the formation of low melting point material (such as $12CaO0.7Al_2O_3$) that forms at high CaO/Al_2O_3 fractions.

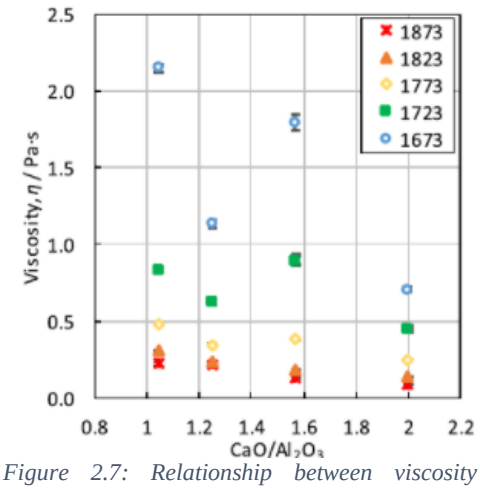

Figure 2.7: Relationship between viscosity and CaO/Al_2O_3 mass fraction for a $10SiO_2$-CaO-Al_2O_3 [24].

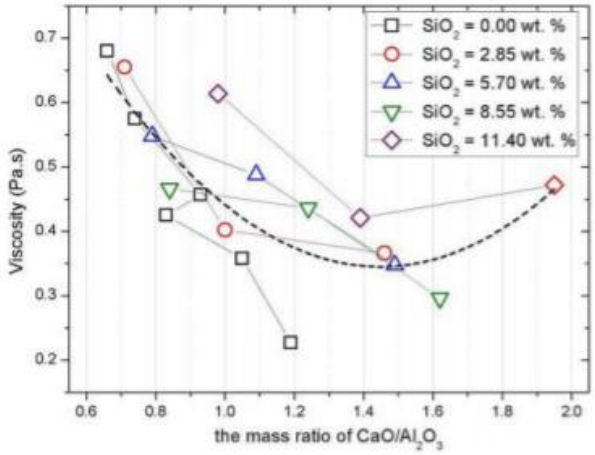

Figure 2.8: Relationship between viscosity and mass ratio of CaO/Al_2O_3 at 1823K. For a CaO-5MgO-Al_2O_3-SiO_2 [25].

2.4 Reaction rate and transport in a metal-SiO_2-Al_2O_3-CaO system

A reaction in a process that is thermodynamically favourable is not bound to occur within a reasonable time. This means that a good understanding of the kinetics and how different parameters affect the reaction rate, is crucial to make any metallurgical process practical and profitable.

2.4.1 The rate constant

In any chemical reaction will the reaction rate be dependent on a rate constant *k*, which is described in the Arrhenius equation:

$$k = k_0 * e^{\left(\frac{-E}{RT}\right)} \tag{2.17}$$

R is the gas constant, *T* is the absolute temperature, *E* is the activation energy of the given reaction, and k_0 is the frequency factor. It is observed that rate constant are highly dependent on the species reacting but also on temperature [26].

The reaction rate is described by the reaction:

$$-r_A = k * (C_A)^a * (C_B)^b \tag{2.18}$$

Here k is the rate constant, C_A and C_B is the concentrations of specie of the reactants A and B (can be more reactants), whilst the exponents are the stochiometric coefficient of the reactants. Eq. (2.18) shows that the reaction rate is highly dependent on access to reactants, but if the concentrations is stable will it only depend on the temperature in the system.

2.4.2 Mass transport

As describes above is it necessary for the reactants to be in contact with each other. For the aluminothermic reduction of silica used in the SisAl prosses is it necessary for the reductant (Al) to be transported through the boundary layer in the metal to the interface between the slag and metal. This will be true for the silica in the slag as well. The diffusivity driven flux of the reactants are described the equation:

$$J_A = D_i * \frac{dC_i}{ds} \tag{2.19}$$

C_i is the concentration of specie i, s is the distance, and D_i is the diffusivity coefficient. In liquids can the diffusivity coefficient (of a specie/particle) be described by the Stokes-Einstein equation:

$$J_A = \frac{k_B T}{6\pi\eta r} \tag{2.20}$$

Where T is the absolute temperature, k_B is the Boltzmann constant, r is the radius of a particle, and η is the viscosity of the liquid/melt [26]. As eq. (2.20) describes diffusivity of a spherical article will it not be entirely accurate for the system present in the SisAl system, but it gives a good indication of how factors like temperature and viscosity affect mass transport.

For a faster transport will forces like convection and conduction also help greatly.

Ahn et al [27] conducted a study where the time it takes for Si and a 22-9-69 wt% CaO-Al_2O_3-SiO_2 slag to approach equilibrium. A silica crucible was used at 1550˚C and the time was varied up to 24 hours. The time it to the system was stable was 6 hours, this was without stirring.

2.4.3 Rate determining step

For the an aluminothermic reduction of SiO_2 in a slag to occur is it 5 steps that need to occur, all of which can be the rate determining step [28]:

1. Transport of reactants (Al and SiO_2) to the boundary layer (diffusion, convection).
2. Transport of reactants (Al and SiO_2) through the boundary layer (diffusion).
3. Reaction between reactants (Al and SiO_2) to products (Si and Al_2O_3).
4. Transport of products (Si and Al_2O_3) away from the boundary layer (diffusion).
5. The products (Si and Al_2O_3) are transported into their respective bulk material (metal and slag).

A study into the reduction of SiO_2 with Al in a ferro-alloy found that the rate determining step was the transport of SiO_2 through the slag [29]. Though not confirmed, was it theorised that possible inclusion build up in the interface could lead to formation of solids. This was due to the increase in Al_2O_3 concentration at the interface. This could retard the reaction rate.

M. Sandell [30] investigated refining of Al and Ca from Si through the addition of SiO_2 with mechanical stirring, at a temperature of 1550˚C. It was discovered that the reaction was rapid as the equilibrium was reached after only 20 minutes. It was discovered however that the reaction rate for the reduction of Ca was higher than for Al. J. F. White [31] studied the interaction between a Si-metal and SiO_2-CaO-slag with mechanical stirring. The temperature was 1550˚C and the CaO/SiO_2 weight fraction varied between 1.17-0.59. It was concluded that the rate determining step was the transport of species in the slag. It was observed a high level of emulsion (metal droplets in the slag) for slags high in CaO. The level of

emulsion was as high as 18.3 wt% metallic Si in the slag, but dropped rapidly to a steady state of 2wt% metallic Si in the slag. This was explained by eq. (2.21).

$$\Delta G_{Tot} = \Delta G_{reaction} + \sigma A \quad (2.21)$$

ΔG_{Tot} is the total energy in the system, $\Delta G_{reaction}$ is the energy related to the reduction of CaO, σ is the interfacial tension between slag and metal, while A is the area between metal and slag. This means that as long as the energy related to the reduction is higher than that of the interface the emulation will persist so that there will be more surface where the reaction can occur. This observation was also confirmed by the Bjørnstad and Tranell [32] which investigated the formation of slag in oxidative ladle refining of silicon metal. It was found that the silica with its polymerisation properties is a highly surface-active specie. The introduction of Ca increased the surface between the slag and Si-metal, decrease the viscosity of the slag (thereby increasing the transport). Ca will make it more favourable for Al to oxidate and function as a network builder, as a Ca^{2+} coupled with two Al^{3+} would allow the Al^{3+} to act as Al^{4+} ion, mimicking the Si^{4+} polymer structure. This is found to be the lowest energy form of Al^{3+} in an oxide melt.

2.5 Metal-SiO_2-Al_2O_3-CaO system

2.5.1 Factors affecting the composition

Hassan [33] did a comprehensive study investigating the equilibrium between solar grade silicone (SoG-Si) and CaO-Al_2O_3 slags with 35-65wt% and 45-55 wt% composition. The metal/slag ratio was varied between 1/1-10/1, where the slag was kept at a constant 24g. This was heated up to 1650˚C and held for 60minutes. The results were compared with thermodynamical models of the system conducted in FactSage. It was concluded that increasing Si amount would unsurprisingly decrease the concentration of Ca and Al dissolved in the metal and increase the SiO_2 amount found in the slag. Trends of increasing Al in metal with decreasing CaO/Al_2O_3 values of the start slag was found. Consequently, a trend of increasing Ca in the metal was fond with increasing CaO/Al_2O_3 values in the start slag. The values found would be close to the simulated values, often following the expected trends, though the results were not 100 % in agreement.

A specialisation project conducted by the author [34] looked closer into the kinetics of the SisAl process, using dross as well as pure Al as reductant in a 47-51 wt% SiO_2-CaO slag (REC slag used in some of the experiments) at 1650˚C. Here it was found that pure Al reacted relatively fast as soon as the slag had melted, and that the changes in metal composition was small after 20minutes. It was assumed that equilibrium was reached after 60 minutes. The time to equilibrium was longer for dross. This was speculated to be due to the alumina that already encapsulated the Al, thereby increasing the transport time for the SiO_2 in the slag. The largest changes over time were the one in Al and Si, while it in the metal, Ca concentrations seamed to stabilize early. It was also concluded that Si concentration stayed relative the same for the different reductants, but that pure Al would have a higher Ca concentration, while dross would get a higher Al concentration in the metal as the slag would be saturated on the Al_2O_3 already present in the dross. All of the experiments ended up with 3 main phases in the metal, Si, $CaSi_2$, and $CaAl_2Si_2$. This was as expected when studding the phase diagram in Figure 2.9.

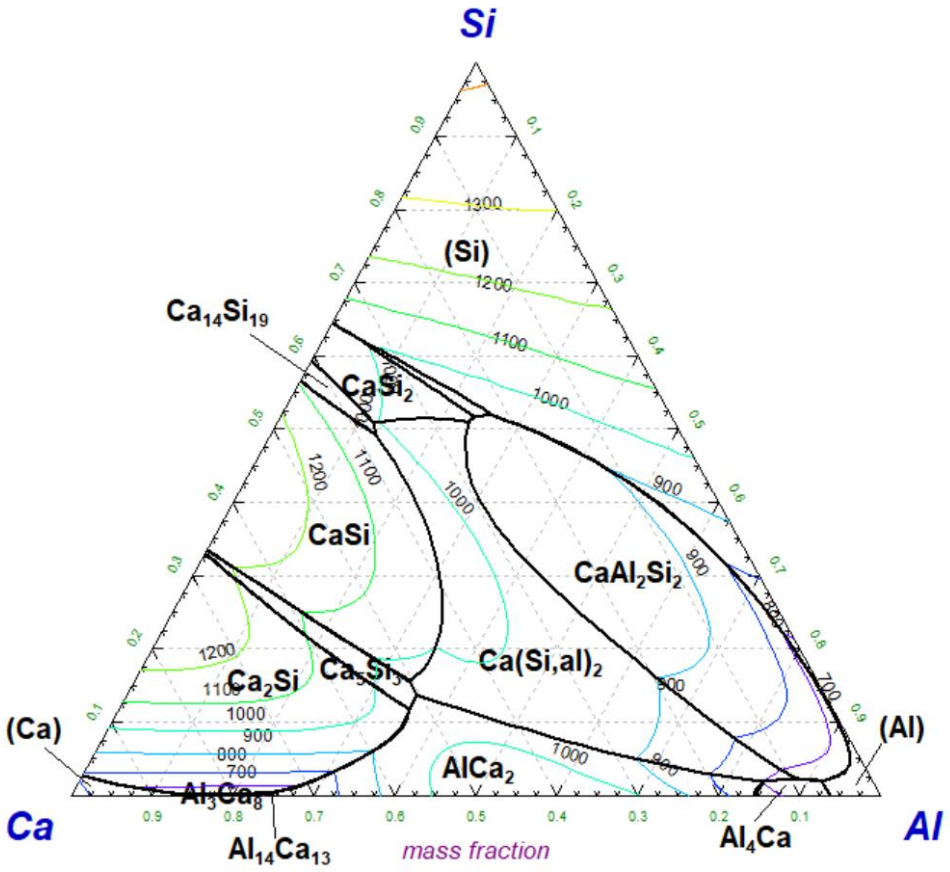

Figure 2.9: Si-Ca-Al phase diagram created in FactSage using the FTLite database [35].

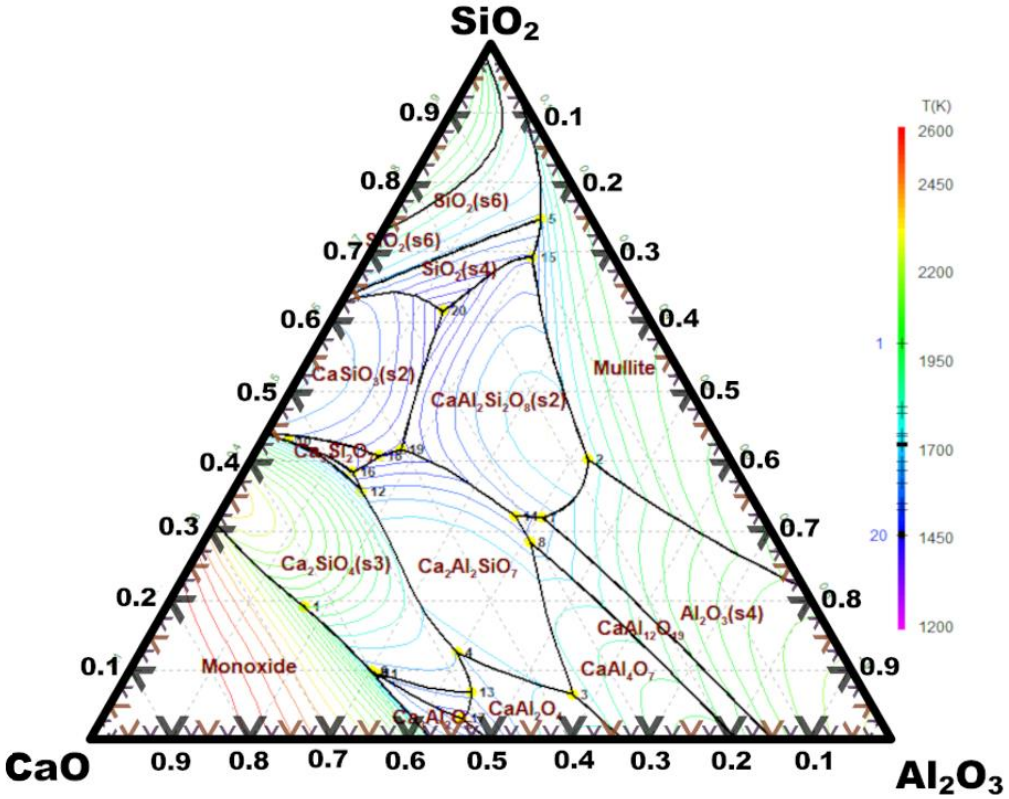

Figure 2.10: Ternary phase diagram of the SiO_2-Al_2O_3-CaO system created in FactSage

2.5.2 $CaO\text{-}SiO_2$ system

Though carbon used as a reductant is excluded from the SisAl project, carbon is used as lining in furnaces. The formation of SiC in SAF is a vell known fact [5]. Since the start slag in the SisAl project will be a $CaO\text{-}SiO_2$ slag the interaction between carbon and the slag will be of interest. White et al. [36] studied the reaction between a (46-54) and (63-37) wt% SiO_2-CaO slag at a carbon surface. They found that the reaction was highly dependent on material, but that the infiltration of slag into the carbon material increased with temperature. The formation of SiC was stagnated as the contact area along the carbon surface was depleted of SiO_2 thereby forming a solid CaO barrier which stopped further interactions between SiO_2 and C.

Studying the $CaO\text{-}SiO_2$ phase diagram Figure 2.11, it can be observed that there will be formed a Ca_2SiO_4 phase at lower SiO_2 concentration lower than 43wt%. This phase is well known both from slag, as well as concrete industries. This is due to the phase change that can occurs when Ca_2SiO_4 β-phase transforms to γ-phase at T=490˚C, where the material has a 12 vol% expansion. Thus, leading to self-depreciation of the concrete or other oxide material the phase are in [37].

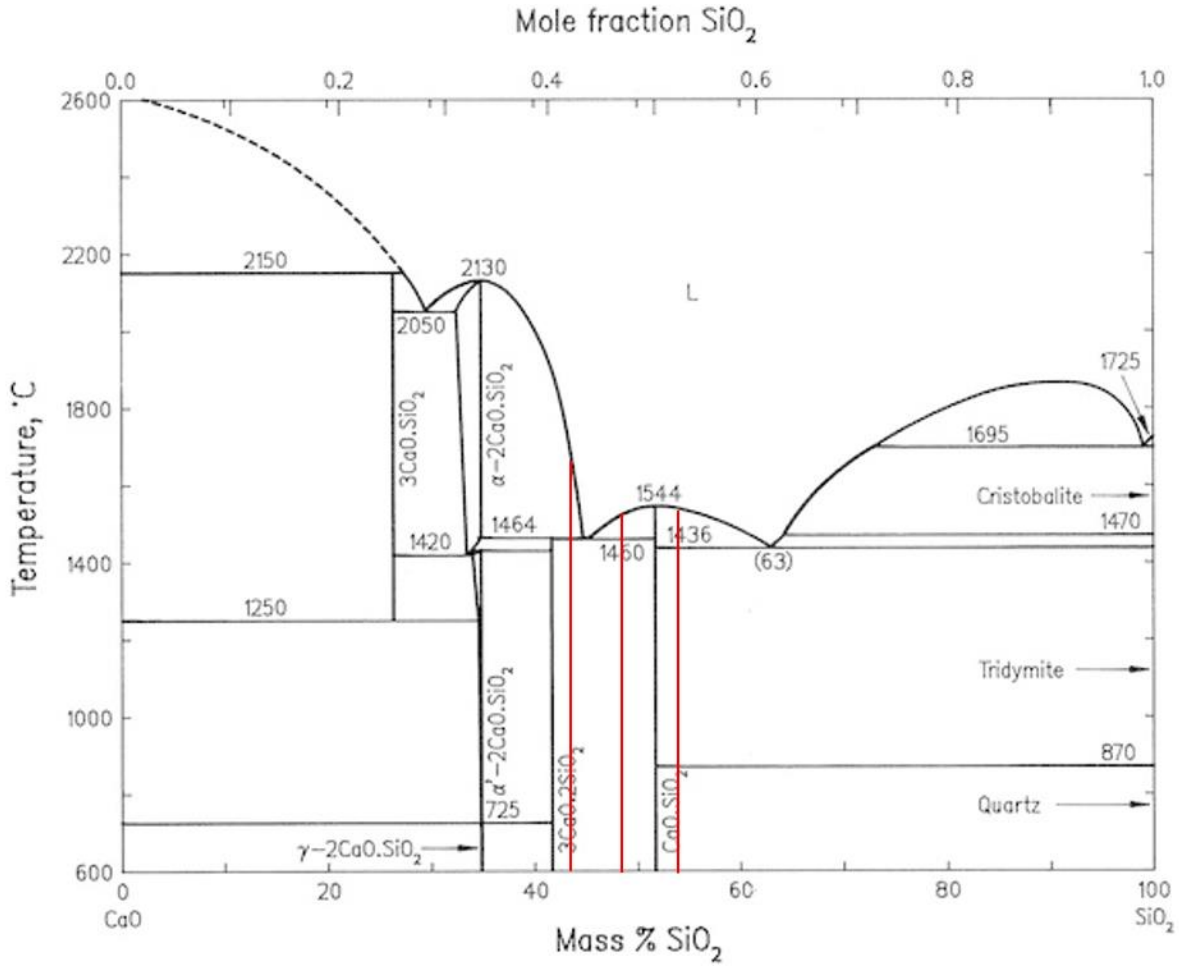

Figure 2.11: $CaO\text{-}SiO_2$ phase diagram [38]. The red lines marks the compositions of the three master slags investigated in this thesis.

2.5.3 Metal interaction with carbon

An investigation of Si and Si-20wt%Al in graphite crucibles was investigated by Hoseinpur and Safarian [39]. It was found that when pure Si was heated to 1500˚C SiC nuclei would be formed on the crucible surface. These would grow and for a SiC layer, thereby stop further grow. When the experiments were conducted at 1800˚C would the process be the same, though there was detached SiC crystals in the melt. It was concluded that the higher temperature would allow diffusion of Si through the grain boundaries

of the SiC layer. The diffused Si would start to form new SiC nuclei under the old grains, thereby pushing them of the wall. This process would then repeat.

Crucibles with Si-20wt%Al alloys would crack during experiments. It was concluded that the Si and Al would seep through the pore structure of the graphite crucible and form carbides, (SiC, Al_4C_3, and Al_4SiC_4 was found in the pores and crucible surface). The volume expansion of these would crack the crucible. It was concluded that the reason that the continues transport into the graphite was that Al, and Al alloys due have a higher wetting angle against graphite than Si. This led to a porous carbide layer on the surface.

3 Experimental

The goal of this thesis is to investigate the effect different CaO/SiO_2 ratios, and different reductant stoichiometries have on the process and end products of an aluminothermic reduction of conducted on 1650˚C. The experimental work conducted will be presented in this chapter. The equipment and process used to produce slags with different CaO/SiO_2 will be presented first. The apparatus and procedure for the main aluminothermic reduction experiments will then be presented. This will then be followed up with the different analyse methods used to investigate the produced samples. Lastly will the program and databases that was used to simulate expected equilibrium compositions for the experimental results, be presented. An overview of the experimental work is illustrated in Figure 3.1.

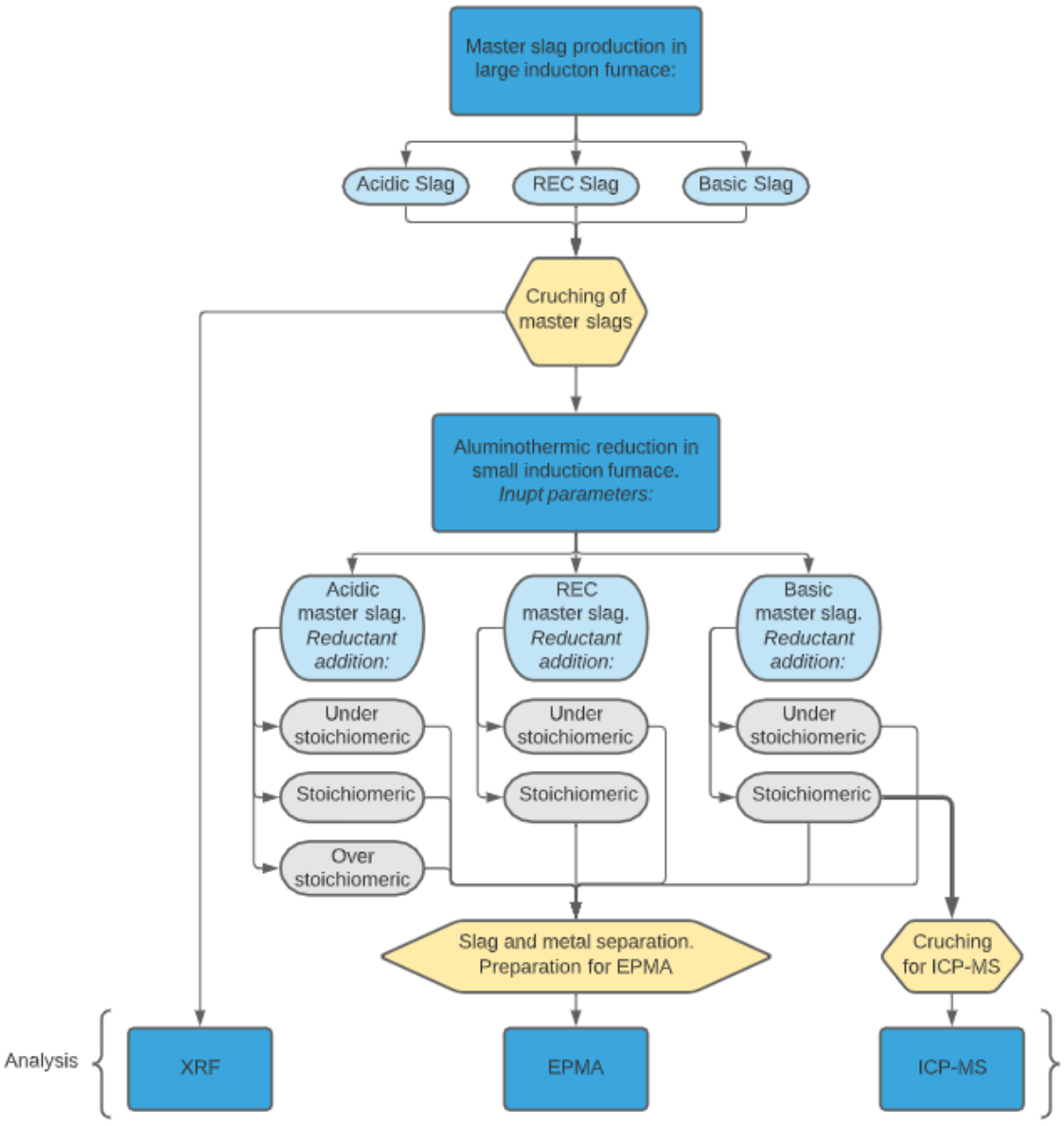

Figure 3.1: Flowchart presenting the experimental work. The blue squares illustrate main experimental work, the beige hexagons illustrate preparation of samples, while the round boxes illustrate input output materials/parameter where blue are different slags and grey are reductant amount.

3.1 Slag Making

Three different slags with the aimed for CaO/SiO_2-massratios (1, 1.2 and 0.7) were manufactured to be used in later experiments. The slag with mass ratio CaO/SiO_2=1 was a pre-fused slag provided by REC (later called REC slag). Two new master slags with mass ratio CaO/SiO_2=1.2, and CaO/SiO_2=0.7 was produced by supplementing the REC-slag with CaO and SiO_2 respectively (later called basic- and acidic slag respectively). This was done to make sure that the input slag for the aluminothermic experiments was homogeneous.

3.1.1 Apparatus and Material for Slag Making

The furnace used in the in the production of the acidic and basic master slags was an open 75kVA induction furnace.

The slag was produced in graphite crucibles with an inner diameter of 114mm and a hight of 400mm.

The different raw materials that were used to supplement the slag provided by REC (composition: 49wt% Si and 51wt% CaO) to produce the acidic and basic slag was a SiO_2-powder (99.5% purity) and CaO-powder respectively.

3.1.2 Slag Making Process

The acidic slag (CaO/SiO_2=0.7) was produced by adding the powdered REC-slag and SiO_2-powder in a container the and mixing it, see Table 3-1 for amount. The mixing of slag and SiO_2 before charging was done to reduce concentration gradients of the charge in the crucible, making the melting temperature more or less the same for the entire charge. A portion of the mixture was added in the crucible (ca. 3/5 of the volume was filled) and heated in the induction furnace up to 1800˚C. More powder was added gradually as the content in the crucible melted. This was done to avoid clogging as there are a relatively large temperature gradient in the furnace. The charge at the bottom will melt before the charge at the top, if the crucible is filled completely from the start. This can lead to gas build up and a blowout of the furnace. The gradually charging during the melting process also made it easier to increase the amount of slag produced as the powder mixture shrank as it melted. The slag was held on 1800˚C for 20 minutes after all of the slag was added and melted to be sure that the CaO and SiO_2 was properly mixed so that the slag was homogeneous. The crucible was then taken out and its content poured in a graphite cast, see Figure 3.2.

The basic slag (CaO/SiO_2=1.2) was produced in the same way as the acidic, with the difference that the REC-slag was supplemented with CaO instead of SiO_2, see Table 3-1 for the content. The CaO powder was heated up to 900˚C and held for 30 minutes, before mixing of the CaO and REC-slag. This was done to get rid of all possible CO_2 and H_2O that could have been bound to the CaO. Melting and charging process was the same as the acidic, described over. Significant fuming was observed as both acidic-, and basic slag was fused.

Table 3-1: Input material and mass for the two separate batches of slag made.

		Type and amount of input material		
		REC-slag [g]	*SiO_2 [g]*	*CaO [g]*
Master slag	*Acidic*	3002	716	-
	Basic	4423	-	345

Figure 3.2: Crucible, cast and the slag produced (CaO/SiO_2) directly after casting

The slag slabs were crushed into smaller pieces with a hammer, and then grounded down further in a Retsch RS 200 Disc Mill (see Figure 3.3 for process), after casting and cooling. This was done as the aluminothermic reduction experiments described in the next section used small amount of slag (250-323g) for each experiment. The grounding of the slags was crucial to make sure the input mass would be the same for each parallel, (as there was easier to consistently get the same mass of slag, when it was in the form of small particles compared to larger pieces.) The grounding also reduced the chance of using larger heterogeneous pieces in the different parallels, thereby reducing the risk of different input concentrations between them.

Figure 3.3: Illustrating how slag was crushed down to smaller pieces with a hammer, the tungsten carbide discs used for the crushing, and the resulting slag powder.

3.2 Aluminothermic reductio

3.2.1 Apparatus for Aluminothermic Reduction

The furnace used in the aluminothermic reduction experiments was a closed induction furnace, see Figure 3.4. The samples were heated in graphite crucibles illustrated in Figure 3.5. There was used 2 C-type thermocouples for each experiment. The thermocouples were placed in alumina tubes and then in the graphite tubes seen in Figure 3.6. This was done to investigate the temperature gradient in the crucible, as on graphite tube rests at the bottom while one is suspended so that there are 30mm between the tubes bottom and the bottom of the crucible. A lid was fashioned from a solid graphite cylinder to reduce the fuming from contaminating the furnace and to reduce mass loss, see Figure 3.6.

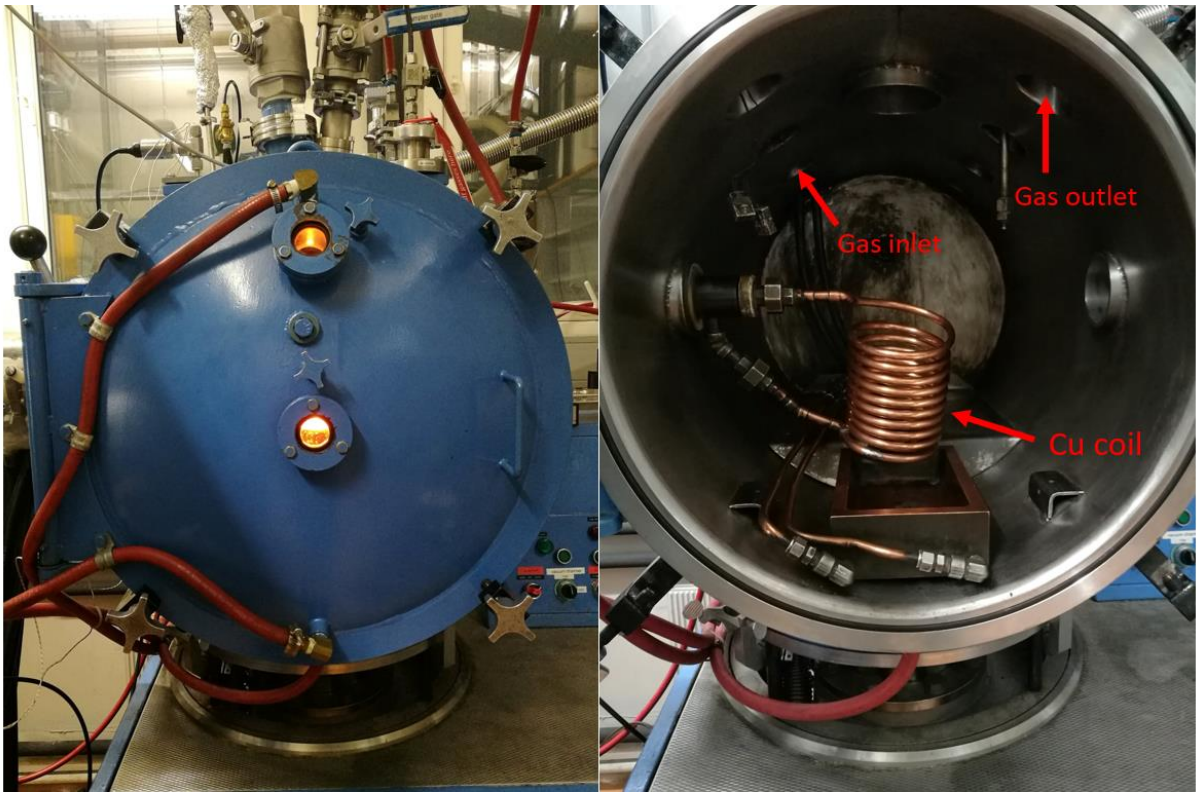

Figure 3.4: The closed induction furnace used for the aluminothermic experiments. Left, shows the furnace closed. Right, shows the inside of the furnace, marked are the gas inlet, gas outlet, and Cu coil.

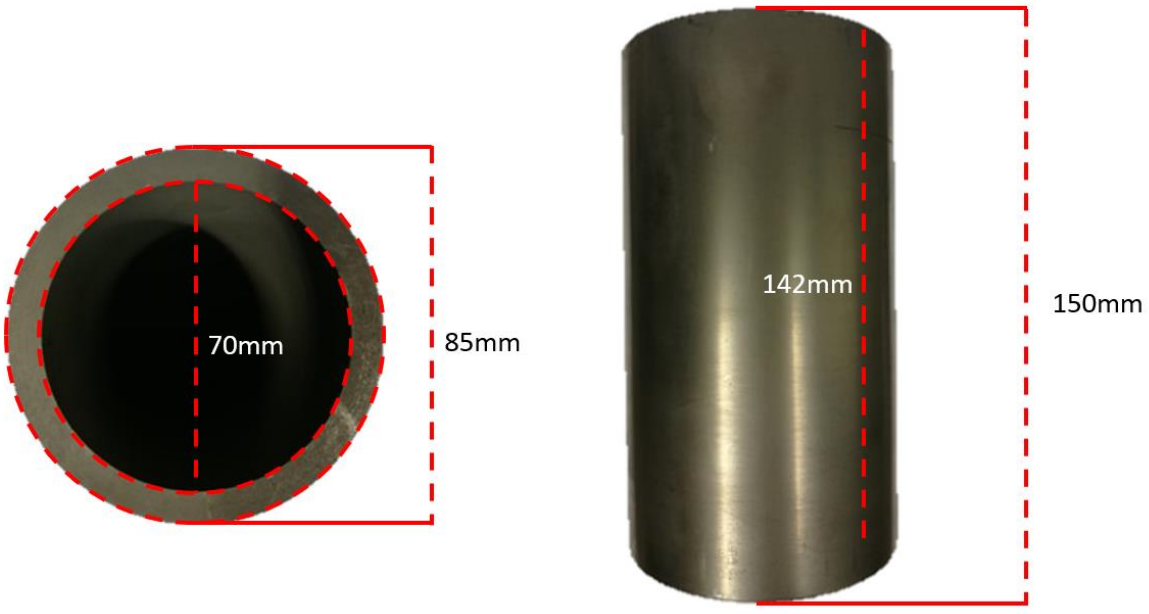

Figure 3.5: Graphite crucibles used for the aluminothermic reduction experiments.

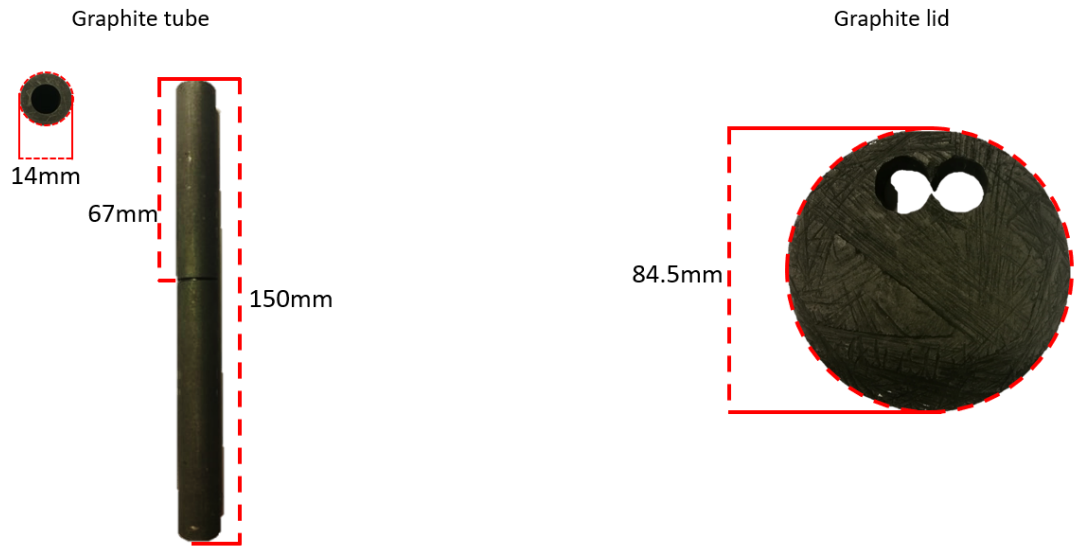

Figure 3.6: Left, the graphite tubes that is used to contain the thermocouples in the graphite crucibles, (the indent 67mm from the top was filed in so it would be possible to fasten the tube 30mm over the bottom of the crucible). Right, the graphite lid used to reduce the amount of fuming (the holes are for the two thermocouples).

3.2.2 Aluminothermic Reduction of SiO_2 in Different CaO-SiO_2-Slags

The goal of the experiments was to investigate the effect different concentrations of input materials have on the end-product in the SisAl process. The slag used was the slag provided from REC with a presumed CaO/SiO_2 mass faction of 1, as well as the acidic- and basic slags with a presumed CaO/SiO_2 mass faction of 0.7 and 1.2 respectively, produced in section 3.1.2. The effect different amount of reductant (Al) has on the end product, was also investigated. This was done by adding Al so that it was stoichiometric and 0.9 times the stoichiometric amount, in relation to eq. (3.1 and the presumed slag compositions. Two parallels with the acidic slag and an Al amount corresponding to 1.1 times the stoichiometric amount, was also investigated.

$$4Al + 3SiO_2 = 3Si + 2Al_2O_3 \tag{3.1}$$

The input mass of SiO_2 was held constant for all the of the experiments (under the assumption of CaO/SiO_2 mass fraction of 0.7, 1, and 1.2). This means that the input slag mass for each slag type was held constant for all of the parallels regardless of the Al content. The input slag mass was varied depending on the slag type due to the different SiO_2 concentrations, see Table 3-2. (N.B! Later analysis indicates that the SiO_2 content was lower for all slags, see section 4.1, meaning that the CaO/SiO_2 fractions as well as the stoichiometries is not as intended. It was found that the CaO/SiO_2 mass fraction was closer to 0.79, 1.1, and 1.26. The reduction amount will still be referred to as 0.9*stoichiometric, stoichiometric, and 1.1*stoichiometric)

Table 3-2: Input mass of metal and slag for the different aluminothermic reduction experiments.

		Mass of input material			
		Slag [g]	*0.9*Stoichiometric Al [g]*	*Stoichiometric Al [g]*	*1.1*Stoichiometric Al [g]*
Master Slags	*Acidic Slag*	249.9	79.2	88.0	96.8
	REC Slag	300.0	79.2	88.0	-
	Basic Slag	323.4	79.2	88.0	-

The aluminium used came from a large bar that was cut into smaller pieces with a Labotom-5 cutting machine. The pieces were then paired up so that their combined mass was as close to the correct input mass as possible. The excess mass was removed with a file.

The graphite tubes used to encapsulate the thermocouples was attached on the inside of the crucibles. This was done by drilling four holes in the side of each of the crucibles and then tie the tubes to the side with a tungsten-rhenium wire (tungsten-rhenium was used as it does not melt on the operating temperature). One of the tubes touched the bottom of the crucible while the other had a 30mm gap between the crucibles and its bottom. This was done to investigate the possible temperature gradient in the samples during the experiments. The crucible was then ready to be charged. The reductant (Al-pieces) was placed in the bottom of the crucible, followed by the slag (see Figure 3.7). The crucibles were placed on a 15mm thick quartz disc that would isolate the bottom of the crucible from the Cu coil as well as keep it straight. Two discs of graphite wool was placed between the crucible and the quarts disc for further isolation. The crucible was then encapsulated with a sheet of graphite wool to isolate its sides. A sheet of mica was the paced on the outside of this again so that it would not be any contact between the graphite wool and coil. A lid consisting of two graphite wool discs similar to the ones used on the bottom, as well as the solid graphite disk depicted in Figure 3.6 were placed on the top to reduce possible fuming.

Figure 3.7: Illustrate the charging process with empty crucible (left), charged with the Al used as reductant (middle), and charged with slag on top of the reductant (right). (NB! The graphite paper observed inside the crucible was tested out, but not used for the experiments described here due to problems that arose when used)

The experiments were conducted by heating up the crucibles and their content to 1650˚C, where it was assumed that all content was melted and then hold it there for 60 minutes. (The holding times for the three parallels using REC slag and stoichiometric reductant amount were: 40 minutes, 60 minutes, and 180 minutes) An Ar-atmosphere with a pressure between 1045-1050mbar was kept in the furnace throughout the experiments. The power input was set to 2kW for the first minute and the increased to 5kW where it was held to the temperature reached 1650˚C. The ramping-time up to the T=1650˚C varied somewhat form sample to sample but had a duration of approximately 30 minutes. The power input was then reduced to keep the temperature stable at 1650˚C. The power input necessary to keep the holding temperature stable varied from sample to sample. Both because of different mass and concentration, but also because of the exothermic reaction that often occurred as soon as the holding temperature at 1650˚C was reached. Regardless, the power input used for the majority of the holding time for all of the experiments, lay on an interval between 3.5-4.8 kW. Table 3-3 shows the number parallels conducted per slag type and stoichiometry.

Table 3-3: Experimental matrix, showing number of experiments conducted for the different slags and different reductant amounts.

		# Experiments per Slag type and amount reductant		
		*0.9*Stoichiometric*	*Stoichiometric*	*1.1*Stoichiometric*
Master Slags	*Acidic Slag*	3x	3x	2x
	REC Slag	3x	3x	-
	Basic Slag	3x	3x	-

3.3 Characterisation

3.3.1 Sample Preparation

The crucibles containing the samples was cracked open with a hammer. The slag and metal were separated and crushed down to more manageable pieces with a hammer. This was the fastest and easiest way as both metal and slag were quite brittle and had a good separation, where the metal lay on top of the slag.

Slag and metal samples were prepared for EPMA analysis as they were cast in epoxy and then polished. The polishing process were as follows:

1. MD-Piano 220, water as lubricant. Speed was set to 300rpm, and the force to 35N. The time was set to 2 minutes.
2. MD-Piano 1200, water as lubricant. Speed was set to 150rpm, and the force to 35N. The time was set to 2 minutes.
3. MD-Largo, with the abrasive DiaPro Allegro/Largo 9µm. The Speed was set to 150rpm, and the force was 35N. The time was set to 8 minutes.
4. MD-Dac, with the abrasive type DiaPro Dac 3µm. The speed was set to 150rpm, and the force to 35N. The time was set to 6 minutes.
5. MD-Nap, with the abrasive type DiaPro Nap B 1µm. The speed was set to 150rpm, and the force to 35N. The time was set to 2 minutes.

Samples was also prepared for ICP-MS and XRF-analysis. The samples were crushed to powder using Retsch RS 200 Disc Mill, the disc material was tungsten carbide. 20 second was enough to crush them down to powder, as both metal and slag were brittle.

3.3.2 Composition analysis

The chemical analysis that was conducted to characterise the products and master slags are presented in the following sub-sections.

3.3.3 Electron Probe Microanalysis (EPMA)

Electron Probe Microanalysis (EPMA) was used to investigate the slag and metal from all of the experiments conducted in section 3.2. The analysis was conducted by Senior Engineer Morten Peder Raanes (NTNU) using the JXA-8500F Field Emission Electron Probe Microanalyzer at NTNU, Trondheim. The metal and slag samples were imaged with a backscatter detector, visualising the different phases in them. Wavelength dispersive X-ray spectrometer (WDS) was used to perform an elemental analysis of the different phases in both slag end metal. Energy dispersive X-ray spectroscopy (EDS) was used over an and area on the samples. This was done to find an approximation of the element distribution in the metal- and slag-bulk materials (focus on the Si, Al, and Ca distribution). For metal was three EDS-scans performed at 40x magnification, while three EDS-scans was performed on 40x and on 600x for the slag.

3.3.4 X-Ray Fluorescence (XRF)

The master slag provided by REC (CaO/SiO_2=1) together the two new master slag, acidic and basic, that was manufactures by adding SiO_2 or CaO to the former (se section 3.1.2), was analysed by XRF. Small amount of the three different slags was crushed down to a powder by a disc mill with a tungsten carbide chamber. The samples were analysed using a PANalytical Zetium 4 kW X-ray spectrometer. The sample was preheated to 1000˚C to remove impurities. 0.5g grams of a given preheated sample was mixed with 5.0g flux of (66/34) lithium tetraborate ($Li_2B_4O_7$)/lithium metaborate ($LiBO_2$) and then melted. The results from the analysis were calculated back to the sample before preheating. The concentrations of the main elements were calculated semi-quantitatively using the software package GEO-QUANT Basic. Three parallels were analysed REC slag, while two parallels was analysed for the acidic- and basic slag.

Analysis of slags and some of the metal samples was also tested out with a handheld XRF machine. The only sample prepping needed before the samples was scanned was to crush them down to powder. If these handheld XRF analysis method could give good results, would this be a great advantage as the previous mentioned method only could analyse oxides with no traces of metal. (Metal would damage the platinum crucible used for the sample metaling). The results from the handheld XRF, were shown to deviate from certain control samples. As this kind of machines are mainly used in the field for qualitative analysis was it decided not to go any further with this type of XRF testes.

3.3.5 Inductive Coupled Plasma Mass Spectrometry (ICP-MS)

Inductive Coupled Plasma Mass Spectrometry was done on metal- and slag samples, from the experiments using the slag provided by REC (CaO/SiO_2=1) and Al input that was stoichiometric to the relation in eq. (3.1. The Chemical analysis was performed by ALS Scandinavia. Metal and slag were separated to the best of my ability. The samples were then crushed to powder in a disc mill and sent in to get an analysis for the main elements Si, Al, and Ca, as well as other impurities. The analysis was performed by the following method:

1. The samples were prepared in steel barrels.
2. ICP-MS as performed according to ASTM D3682: 2013 and ASTM D4502: 2008, by melting lithium metaborate ($LiBO_2$) and dissolving with HNO_3.
3. Dissolution has taken place with HNO_3/HCl/HF according to SS EN 13656: 2003.
4. Analysis with ICP-SFMS has been doen according to SS EN ISO 17294-2: 2016 and the EPA method 200.8: 1994

3.4 Thermodynamic Modelling with FactSage

Thermodynamic modelling was implemented to have a good understanding of what to expect from the experimental results. The modelling of the equilibrium compositions expected was done by Harald Philipson. Thermodynamical data was acquired from the software FactSage.

The calculations of the systems are done in FactSage with the databases used: FToxid 7.3, NTNU 7.0, and FactPS 7.3. The temperature was set to 1650˚C for all calculations, in a 1 atm Ar-atmosphere.

4 Results

This section will present the results and observations from the experiments and analysis described in the experimental section 3. The XRF results of the three master slags used in the aluminothermic reduction experiments will be presented first, as they have implications on the following results.

This will then be followed by observations like temperature date recorded during the experiments, the yield of the metal produced, general cross-section observations, BSE-images of metal and slag coupled with phase identification from the WDS analysis.

The chemical composition of slag and metal found with EPMA will be presented. This is the average of the parallels for each slag and stoichiometry, while the error bares are the standard deviation. These data were used to calculate the mass balance of the main elements I the system.

The simulated equilibrium compositions will then be presented. The simulations were done in FactSage 7.3 by PhD candidate Harald Philipson.

4.1 XRF-analysis of master slag

The average results from the XRF analysis of the three master slags are found in Table 4-1. All parallels are found in appendix A. The difference between parallels was insignificant. The results show that the CaO/SiO_2 mass ratio for the acidic slag is 0.79 rather than the intended 0.7, the REC slag 1.1 rather than previously assumed 1.04, and the basic slag 1.26 for the intended 1.2. The values assumed during the experiments are compared to the XRF results in Figure 4.1. It shows that the CaO concentrations are higher than what was expected, while SiO_2 concentrations are lower.

Table 4-1: XRF results of the three master slags.

	Acidic Slag [wt%]	*REC Slag [wt%]*	*Basic Slag [wt%]*
K_2O	0.014	0.013	0.005
MgO	0.208	0.252	0.273
Mn_3O_4	0.004	0.004	0.004
Na_2O	<LLD	<LLD	<LLD
Fe_2O_3	0.077	0.112	0.027
P_2O_5	<LLD	<LLD	<LLD
SiO_2	55.000	46.667	43.850
TiO_2	<LLD	<LLD	<LLD
Al_2O_3	0.133	0.159	0.149
CaO	43.500	51.333	55.100
SrO	0.007	0.014	0.012
V_2O_5	0.002	<LLD	0.002
ZnO	0.001	0.001	<LLD
ZrO_2	0.008	0.007	0.011
PbO	<LLD	<LLD	<LLD
BaO	0.003	<LLD	0.001
Cr_2O_3	0.003	0.003	0.003
CuO	0.002	0.001	0.002
NiO	<LLD	<LLD	<LLD
HfO_2	<LLD	<LLD	<LLD
LOI 1000˚C	0.055	0.663	-0.010
Sum	99.012	99.229	99.425

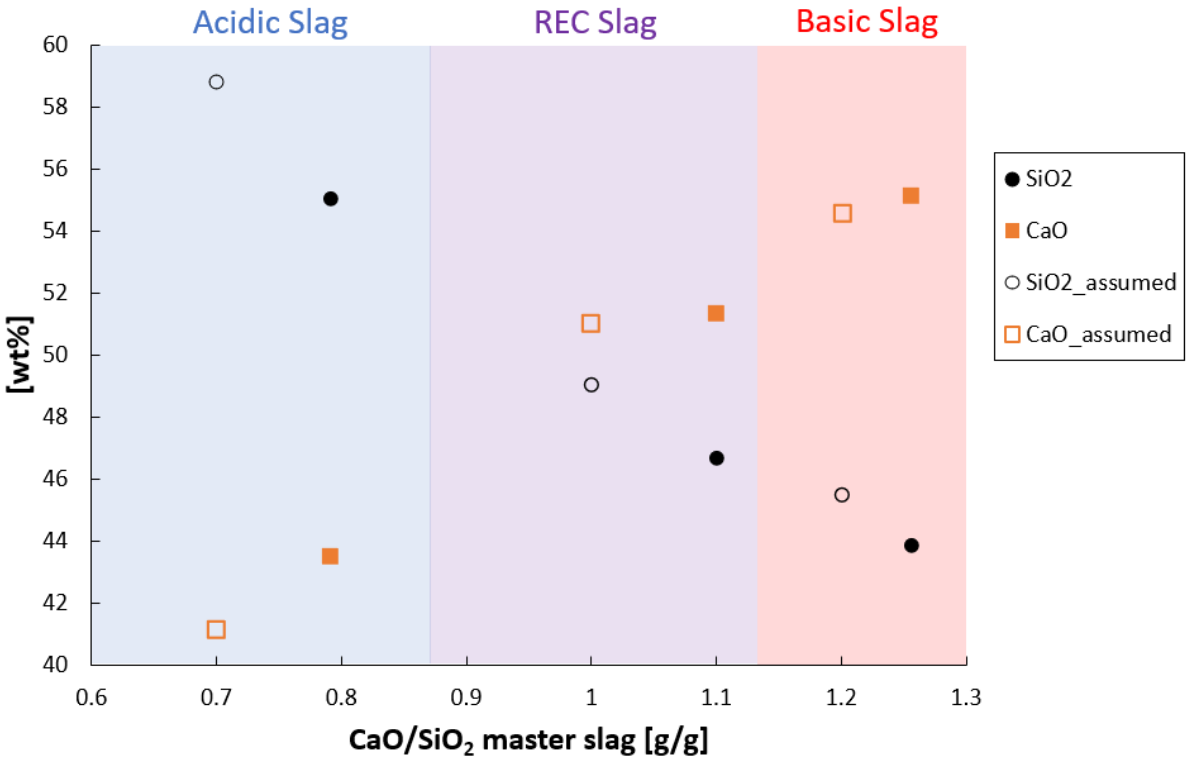

Figure 4.1: Illustrate the CaO (square) and SiO_2 (circle) concentrations of the three master slags assumed during the experiments (solid masks), and the results from XRF analysis (outline).

The aluminothermic reduction experiments was carried out with a presumed SiO_2 content different from the results of the XRF analysis. The stoichiometric relation between the reductants and SiO_2 will therefore be different than the intended. The stoichiometric relations for the experiments, calculated from the analysed values of the master slags can be found in Table 4-2. It is observed that the added Al content is higher than intended for all experiments, where the acidic slag have the largest difference.

Table 4-2: Stoichiometry for the different aluminothermic reduction experiments, calculated form XRF-analyses of the master slags.

		Calculated stoichiometry from XRF results		
		*0.9*Stoichiometric*	*Stoichiometric*	*1.1*Stoichiometric*
Master Slags	*Acidic Slag*	0.96	1.07	1.18
	REC Slag	0.94	1.05	
	Basic Slag	0.93	1.04	

4.2 Temperature observations

The temperatures were measured at the bottom (control thermocouple) of the crucible and near the surface of the metal (30mm over the bottom). To illustrate how the temperature developed when the main reactions occurred are data from each parallel picked out and plotted, from 1500˚C to it stabilised at 1650˚C. Temperatures, as well as the temperature change per second (for the control thermocouples) from each experiment will be presented as a function of time, starting at 1500˚C.

Do remember that the time it took to reach 1500˚C varied for each experiment, and that the chosen start time of 0 minutes at 1500˚C in the plots below was chosen to better compare the temperature data.

4.2.1 Acidic Slag

For acidic slag and 0.9*stoichiometry are the temperature and temperature change plotted in Figure 4.2 and Figure 4.3 respectively. The power input is reduced when the control temperature is close to the holding temperature of 1650˚C. which explains the flattening of the cure in Figure 4.2. The sudden peak observed in both graphs is due to the exothermic reduction. This reaction occurs 5 and 7 minutes after holding temperature is reached, for parallel 2 and 3. There is no notable peak for parallel 1. (The top thermocouple for parallel 1 malfunctioned, which is why it is not present in the plots).

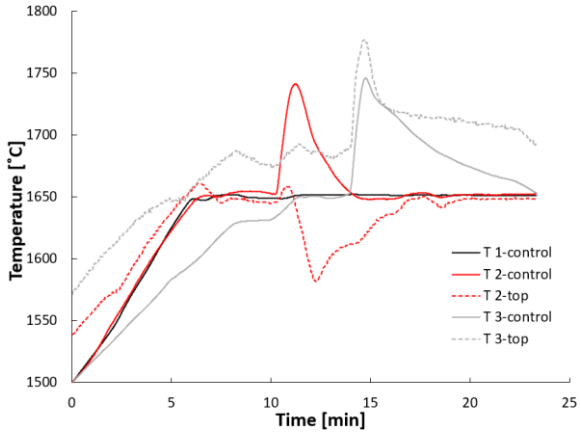

*Figure 4.2: Temperature over time for acidic slag and 0.9*stoichiometric reductant amount. Solid lines are control thermocouple, and dashed line are from top thermocouple. Parallel: 1. (black), 2. (red), and 3. (grey).*

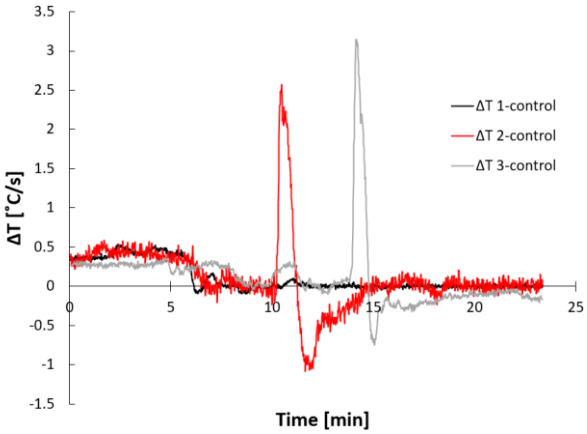

*Figure 4.3: Temperature change per second over time for control thermocouple. Acidic slag and 0.9*stoichiometric reductant amount. Parallel: 1. (black), 2. (red), and 3. (grey).*

The temperature and temperature change for acidic slag and stoichiometric reduction amount are plotted in Figure 4.4 and Figure 4.5. No large differences are observed between the parallels. The exothermic reduction occurs as the temperature reaches 1650˚C. The temperature increase is larger in comparison with the previously mentioned experiments.

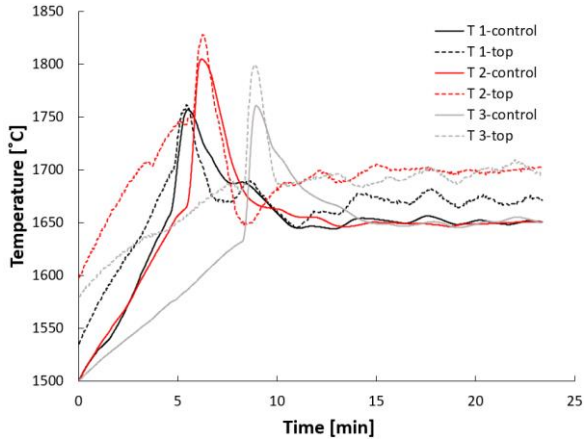

Figure 4.4: Temperature over time for acidic slag and stoichiometric reductant amount. Solid lines are control thermocouple, and dashed line are from top thermocouple. Parallel: 1. (black), 2. (red), and 3. (grey).

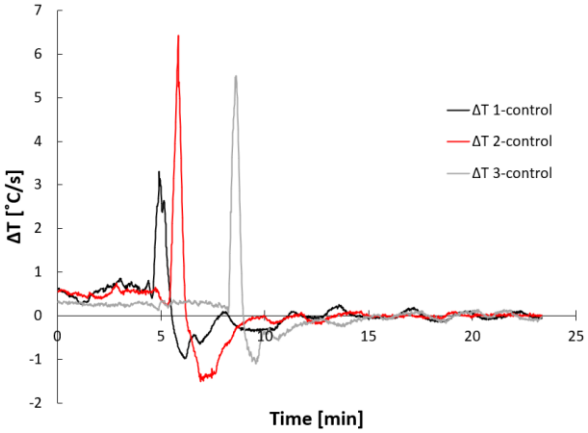

Figure 4.5: Temperature change per second over time for control thermocouple. Acidic slag and stoichiometric reductant amount. Parallel: 1. (black), 2. (red), and 3. (grey).

The temperature and temperature change for acidic slag and 1.1*stoichiometric reduction amount are found in Figure 4.6 and Figure 4.7. There is no significant temperature spike for the parallel 1, while parallel 2 has a clear spike as the temperature reaches 1625˚C. Another notable observation is that the temperature difference between top- and control-thermocouple for parallel 1 is 30˚C too parallel 2 that have a difference around 75˚C.

N.B. It was noted that the control-thermocouple used for both parallel 1 and 2, seemed to go further down in the alumina tube (see section 3.2.1) for parallel 2 than for 1. If this observation is correct do this imply that the control thermocouple was placed higher in the crucible for parallel 1. The temperature is observed to be higher for the top-thermocouple, which then implies that the temperature would as a whole be lower for parallel 1. The fact that the temperature different between top and bottom are much larger for parallel 2 than 1, due further support this observation.

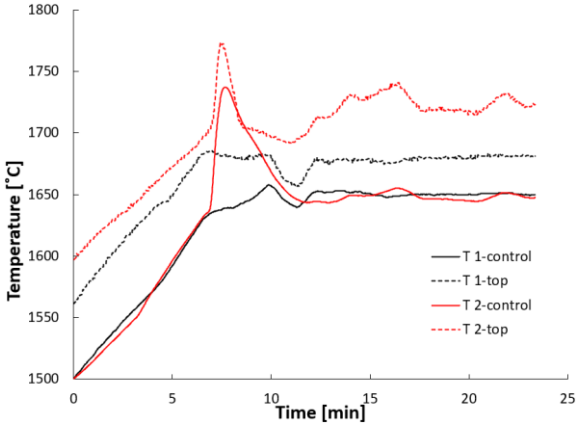

*Figure 4.6: Temperature over time for acidic slag and 1.1*stoichiometric reductant amount. Solid lines are control thermocouple, and dashed line are from top thermocouple. Parallel: 1. (black) and 2. (red)).*

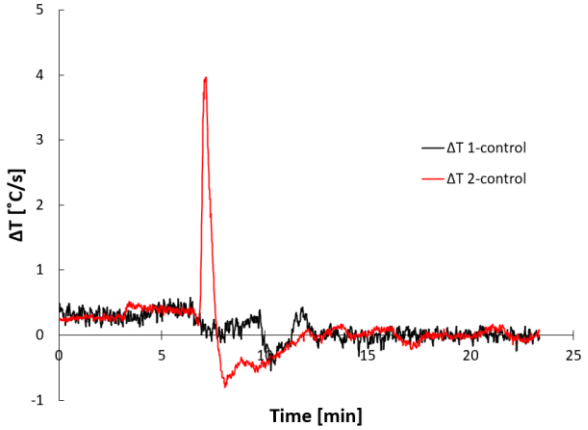

*Figure 4.7: Temperature change per second over time for control thermocouple. Acidic slag and 1.1*stoichiometric reductant amount. Parallel: 1. (black), and 2. (red).*

4.2.2 REC Slag

The temperature and temperature change for REC slag and 0.9*stoichiometric reduction amount are found in Figure 4.8 and Figure 4.9. No significant differences are found between the parallels, and the general trend of a temperature spike at around 1600˚C that rises to around 1700˚C, are observed for all parallels.

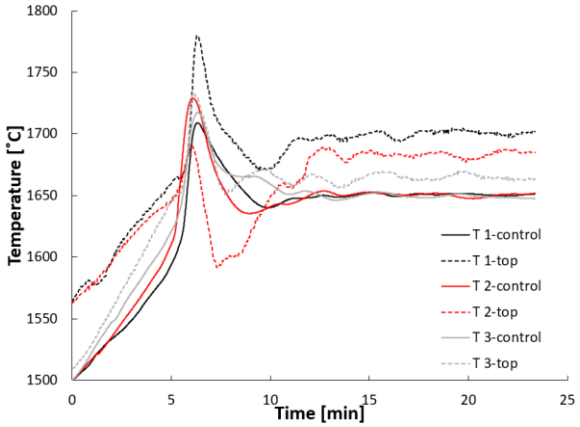

*Figure 4.8: Temperature over time for REC slag and 0.9*stoichiometric reductant amount. Solid lines are control thermocouple, and dashed line are from top thermocouple. Parallel: 1. (black), 2. (red), and 3. (grey).*

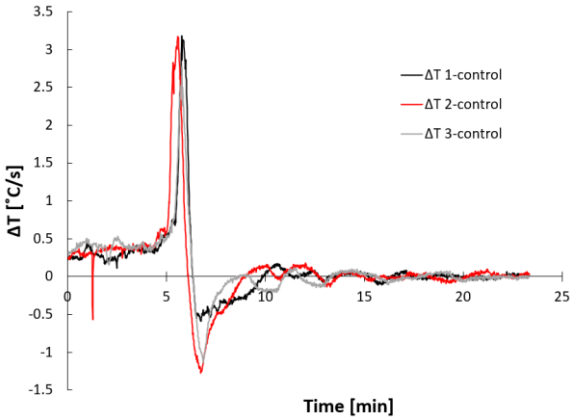

*Figure 4.9: Temperature change per second over time for control thermocouple. REC slag and 0.9*stoichiometric reductant amount. Parallel: 1. (black), 2. (red), and 3. (grey).*

The temperature and temperature change for REC slag and stoichiometric reduction amount are found in Figure 4.10 and Figure 4.11. The trends are the same for all parallels, thought there are some differences in the intensities of the temperature spikes. NB, there were no top thermocouples used in these experiments.

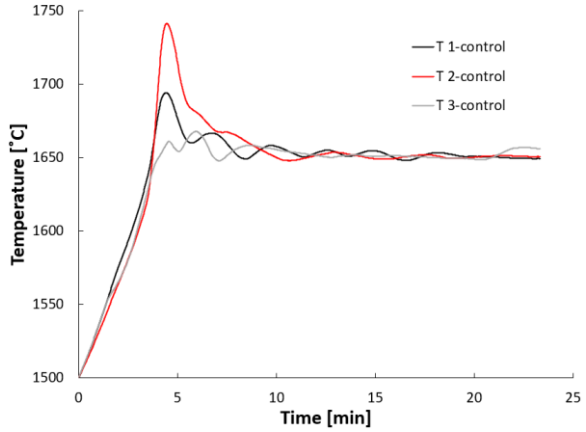

Figure 4.10: Temperature over time for REC slag and stoichiometric reductant amount. No top thermocouple was used in these experiments. Parallel: 1. (black), 2. (red), and 3. (grey).

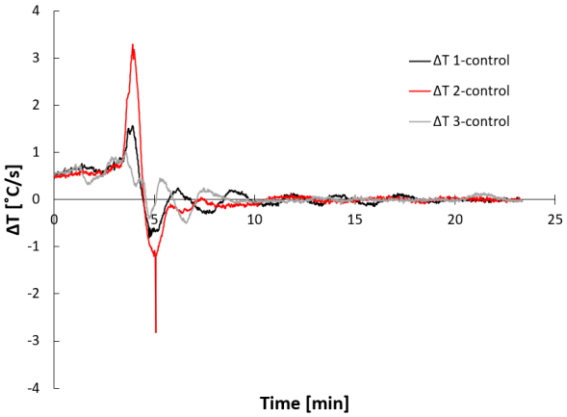

Figure 4.11: Temperature change per second over time for control thermocouple. REC slag and stoichiometric reductant amount. Parallel: 1. (black), 2. (red), and 3. (grey).

4.2.3 Basic Slag

The temperature and temperature change for basic slag and 0.9*stoichiometric reduction amount are found in Figure 4.12 and Figure 4.13. The control-thermocouple for parallel 1 malfunctioned as the holding temperature was reached. The top-thermocouple was used as a control thermocouple for the remaining of the holding time. The temperature spikes are more irregular and comes at later times when compared with experiments conducted with REC/acidic slags.

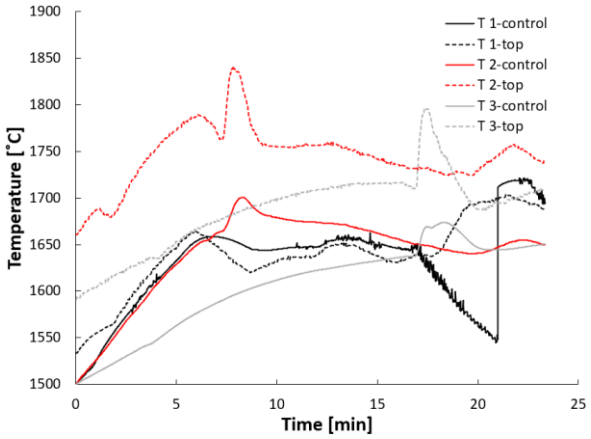

*Figure 4.12: Temperature over time for basic slag and 0.9*stoichiometric reductant amount. Solid lines are control thermocouple, and dashed line are from top thermocouple. Parallel: 1. (black), 2. (red), and 3. (grey).*

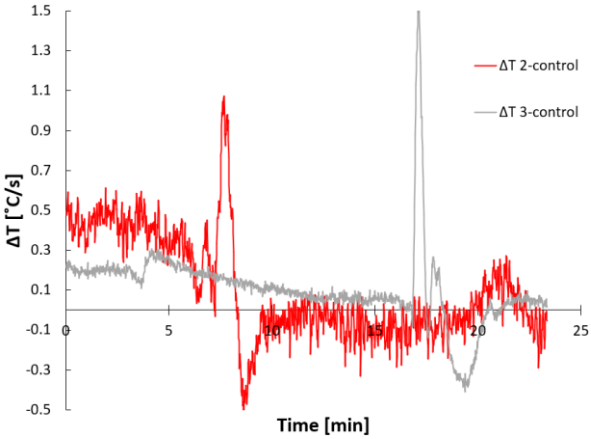

*Figure 4.13: Temperature change per second over time for control thermocouple. Basic slag and 0.9*stoichiometric reductant amount. Parallel: 2. (red), and 3. (grey).*

The temperature and temperature change for basic slag and stoichiometric reduction amount are found in Figure 4.12 and Figure 4.13. In similarity to the under stoichiometric are the temperature spices more irregular and comes later when compared, to experiments conducted with REC/acidic slags. Parallel 2 have several temperature spikes while parallel 1 only have one clear spike late into the holding time.

NB! Parallel 3 failed (see section 4.4.2 for observed sample) where the power was cut as short as 1650˚C was reached and then again 11 minutes after that, as there were problems with the furnace. Due to time constraints as well as lack of material was this parallel not repeated.

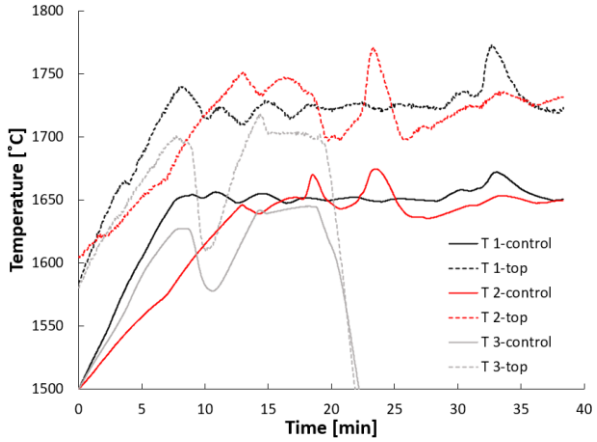

Figure 4.14: Temperature over time for basic slag and stoichiometric reductant amount. Solid lines are control thermocouple, and dashed line are from top thermocouple. Parallel: 1. (black), 2. (red), and 3. (grey).

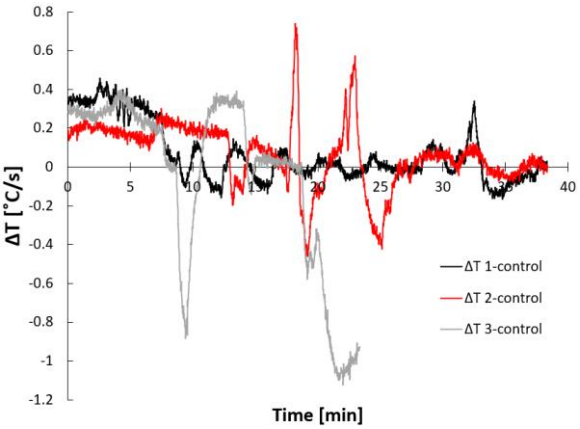

Figure 4.15: Temperature change per second over time for control thermocouple. Basic slag and stoichiometric reductant amount. Parallel: 1. (black), 2. (red), and 3. (grey).

4.3 Metal-yield

The mass loss samples had during the experiments are found in Table 4-3. There are no values for basic slag, as all crucibles cracked during cooling. This led to large losses from the powdered slag that was found in all of these samples, (see Figure 4.19). The losses were so great that they would overshadow actual losses from fuming. There are also some values that are marked with "*". These had pieces of the alumina tubes used to encapsulate the thermocouples stuck in the graphite tubes. This is the reason for the weight gain. There are no significant trends from these values.

Table 4-3: Mass lost during furnace run (mass of crucible in – mass of crucible out). There is no values for basic slag as losses when the crucible was too large to use. Values marked with "" are samples where pieces of alumina tubes were stuck in the graphite tubes.*

		Mass loss from sample after experiment [g]							
		*0.9*Stoichiometric*			*Stoichiometric*			*1.1*Stoichiometric*	
	Parallel #:	*1.*	*2.*	*3.*	*1.*	*2.*	*3.*	*1.*	*2.*
Master Slags	*Acidic Slag*	3.20	3.35	-8.70*	1.85	-9.35*	-7.90*	2.80	-8.30*
	REC Slag	3.30	0.45	2.55	0.95	0.85*	3.05		
	Basic Slag	-	-	-	-	-	-		

The metal that had coalesced on the top of the slag was separated by hammering it out from the slag. This was easy as both metal and slag was brittle and had separated well. The weight of the metal that was hammered out can be found in Table 4-4. Note that the separation process has a substantial room for error due as some metal was crushed and fell away as small pieces/dust.

*Table 4-4: Mass of metal separated from the different experiments. Note: 1. basic slag and stoichiometric do not have a value as the metal was to brittle/flaky to be separated without too large loss. 1. acidic slag and 1.1*stoichiometric do not have a value as the metal did not coalesce*

		Mass metal separated from the experiments [g]							
		*0.9*Stoichiometric*			*Stoichiometric*			*1.1*Stoichiometric*	
	Parallel #:	*1.*	*2.*	*3.*	*1.*	*2.*	*3.*	*1.*	*2.*
Master Slags	*Acidic Slag*	20.80	58.88	56.63	69.78	65.30	64.82	-	64.73
	REC Slag	60.67	56.53	57.52	65.83	65.17	67.30		
	Basic Slag	62.70	56.99	59.81	-	61.37	59.77		

The average coalesced metal mass divided by the input Al reductant, are plotted Figure 4.16. This illustrates how the different input parameters affects the metal yield. It is observed that there is a general trend of higher metal yield for stoichiometric than for 0.9*stoichiometric. This trend is not that present for the basic slag, though it is important to remember that there was larger danger of metal loss as the crucibles as well as the slag/metal cracked during cooling (see Figure 4.19). It was therefore a danger of metal loss before the mechanical separation process was started. To illustrate the point, Figure 4.17 illustrates the coalesced metal from acidic slag (one main lump), and the separated metal from an experiment using basic slag. Note also that the metal yield for over stoichiometric reduction amount is low.

Note that the weight from experiments: (parallel 1) acidic slag and 0.9*stoichiometric reductant amount, (parallel 1) acidic slag and 1.1 stoichiometric reductant amount, and (parallel 3) basic slag

and stoichiometric reductant amount, are not used in the creation of Figure 4.16 as their metal yield is not representative (see section 4.4.2).

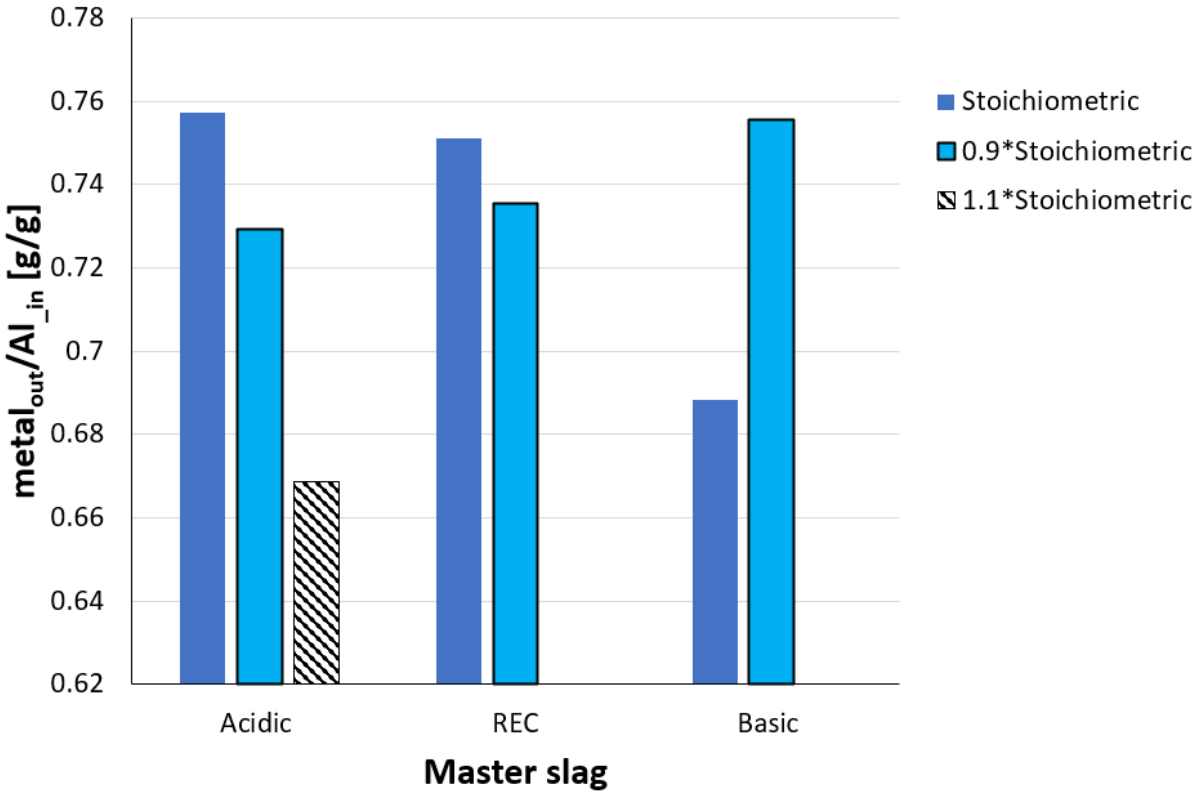

Figure 4.16: The average metal yield separated from the slag for each slag and input reductant divided by the input Al in the reductant addition .

Figure 4.17: Main metal lump separated form (parallel 3) acidic slag and stoichiometric reduction amount (left). Metal pieces comprising the metal yield form (parallel 3) basic slag and stoichiometric reductant amount, after separation (right).

4.4 Observations

This section will contain different observations made from the experiments and resulting samples both on a macro and micro level. It will point out general trends as well as observable deviations from these trends.

4.4.1 Visual inspection, differences between the input slags

In general, the Si-alloy phase will lie on top of the slag phase for all experiments regardless of the starting slag or amount of reductant. Small droplets of metal are observed dispersed throughout the slag (the amount varies somewhat between samples), as well as small amount of metal in the form of thin films. These are visible in all samples, though most of the metal will lie in the main metal phase on top of the slag. General cross sections are found in Figure 4.18, illustrating the separation of metal and slag, as well as the metal film (the samples illustrated are from parallels using the acidic slag, and REC slag).

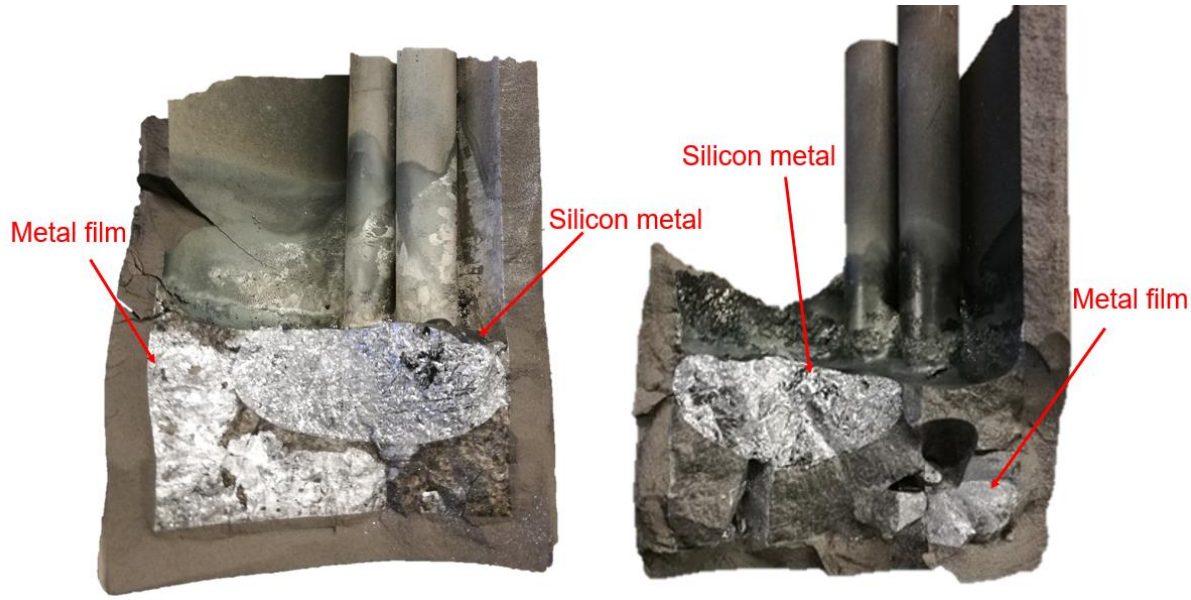

*Figure 4.18: Illustrate cross section of samples with input material: acidic slag and Stochiometric Al (Left), REC slag and 0.9*Stoichiometric Al (Right).*

Initial observations of samples made from acidic- and REC slag were quite similar where the only notable difference was that samples from REC slag had a darker more homogeneous colour on the slag, while samples made with acidic slag had a patchy brown/dark colour scheme, see Figure 4.18.

A trend observed for all experiment conducted with the basic master slag was that the crucibles had cracked in the bottom after cooling. The bottom half of these samples was a grey powder while the top half was metal on top encased in a dark slag (see Figure 4.19).

Figure 4.19: Cacked crucible after experiment conducted with basic master slag. Illustrate grey powder found in bottom off all experiments with basic slag, as well as the cross section of metal and slag form this parallel.

4.4.2 Observable outliers

Three samples deviated from the general trends described in the previous section (section 4.4.1). These samples were: the first parallel with acidic slag and 0.9*stoichiometric reductant addition, the first parallel with acidic slag and 1.1*stoichiometric reductant addition, and the third parallel with basic slag and stoichiometric reductant addition.

The first parallel with acidic slag and 0.9*stoichiometric reductant addition, had a smaller lump of coalesced metal than the other parallels with the same input parameters. Its weight was less than 40 % than that of the metal yield of the two other parallels. Large amount of dispersed metal droplets was visible throughout the slag, see Figure 4.20.

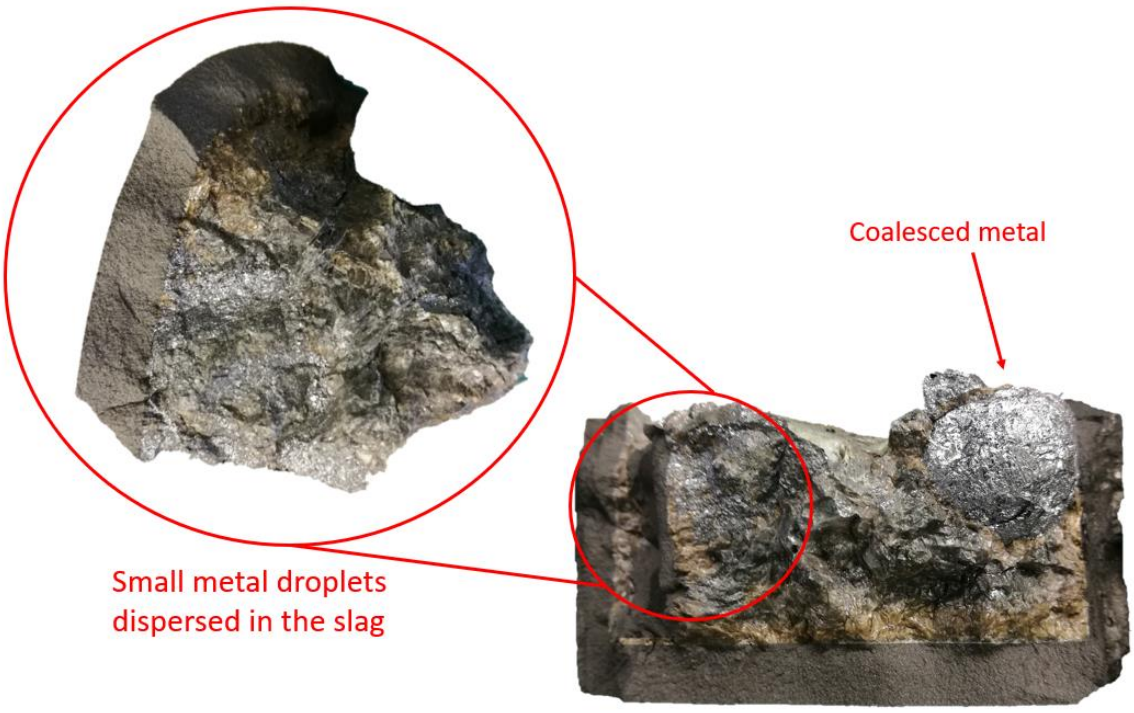

*Figure 4.20: 1. Parallel of acidic slag with 0.9*stoichiometric Al amount: illustrate the cross section of the sample with a small coalesced metal ball, and metal droplets dispersed in the slag.*

The first parallel with acidic slag and 1.1*stoichiometric reductant addition, did not have a larger coalesced metal phase. Instead a divide was observed in the sample where the bottom half was mainly slag (as per usual for all samples), while the top half can be described as a dense cloud of dispersed metal droplets, see Figure 4.21.

*Figure 4.21: 1. Parallel of acidic slag with 1.1*stoichiometric Al amount: illustrate the top (left), and cross section of the sample. The metal had not coalesced in this sample, there were instead a dense dispersion of metal droplets in the top half of the slag.*

Parallel 3 with basic slag and stoichiometric reductant amount, was held for a shorter time on 1650˚C (approximately 11 minutes) than all other experiments due to problems with the furnace. General observations show a larger amount of the grey power (present for all experiments using basic slag) and smaller amount of solid slag lumps, in comparison with other experiments using the basic slag. In contrast to the two previously mentioned outliers had large metal phase coalesced on top of the slag, despite the short running time. Two metal pearls (with a diameter of approximately 10mm) lay on top of the coalesced metal (see Figure 4.22). The coalesced metal was observed to be quite brittle (as usual for silicon metal) and seemed to have a layered structure, as larger flakes fell of when the septation of metal and slag was attempted. This was not the fact for the metal pearls as it was possible to flatten them with a hammer, see Figure 4.22.

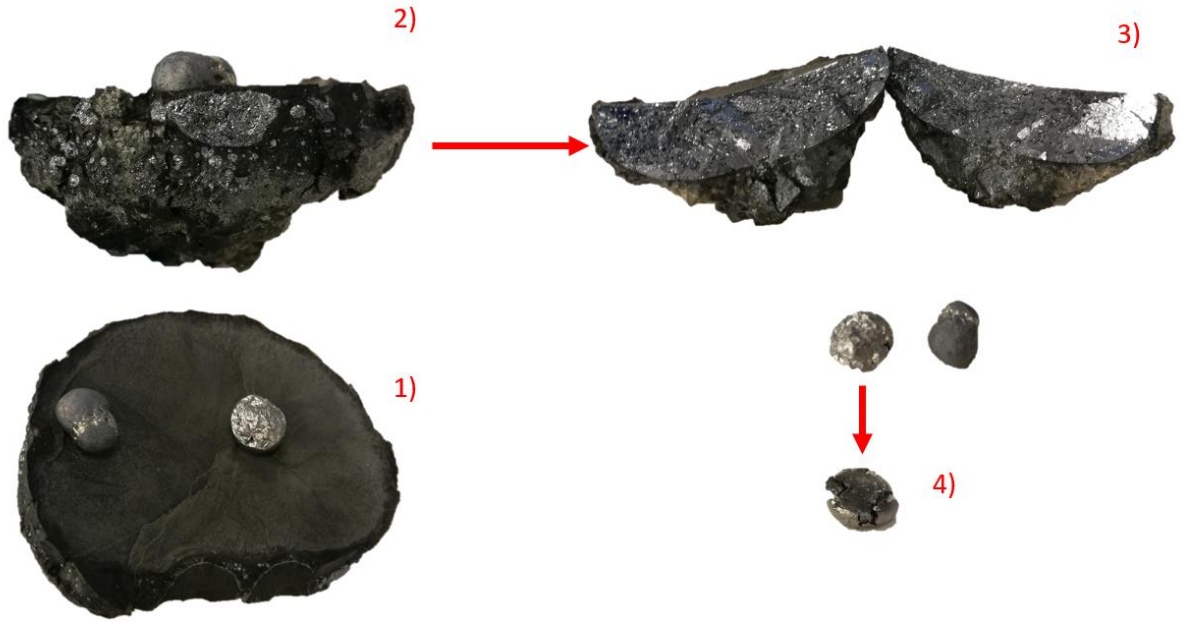

Figure 4.22: 3. Parallel of basic slag with stoichiometric Al amount: 1) illustrate the top of the slag clad coalesced metal (2 metal droplets on top). 2) side view of same lump. 3) said lump cracked in two. 4) illustrate the two metal droplets form the top of the coalesced metal, and the result of one after it was flattened with a hammer.

4.4.3 BSE images and WDS analysis

In this section will the backscatter images be paired with the results from the WDS analysis (to identify the phases) by both slag and metal samples from all input variations. The results will be presented in the order: acidic master slag, REC master slag, and finally the basic master slag. Samples from each slag will be presented with increasing reductant amount. 4 main phases are observed in almost all of the metal samples: a pure Si phase, a Si_2Al_2Ca phase, a Si_2Ca phase, and a Si-Al-Ca phase with the main impurities, like Fe, Mn, and Mg. The slags are much more varied in phase, in which phases that is present and the phase compositions. The markings of each phase are calculated form the WDS. N.B. notable amount of metal was observed in all slag pieces, either in the form of metal droplets with the same phases as the bulk metal, or as dispersed Si_2Ca metal. All WDS results can be found in Appendix B.

The metal and slag from the first parallel with acidic slag and 0.9*stoichiometric amount of reductant (mentioned in section 4.4.2) can be observed in Figure 4.23. A large amount of Si phases was observed in metal. The slag structure varied which is why two images of its slag is presented in Figure 4.23. The metal in parallel 2 and 3 had the same phases as the first parallel, though a smaller area fraction of the Si-phase compared with the first parallel. The slag for these two parallels had relatively the same phase

composition throughout (see Figure 4.24). Note that parallel 1, has an observable larger fraction of the Si rich slag phases than parallel 2 and 3.

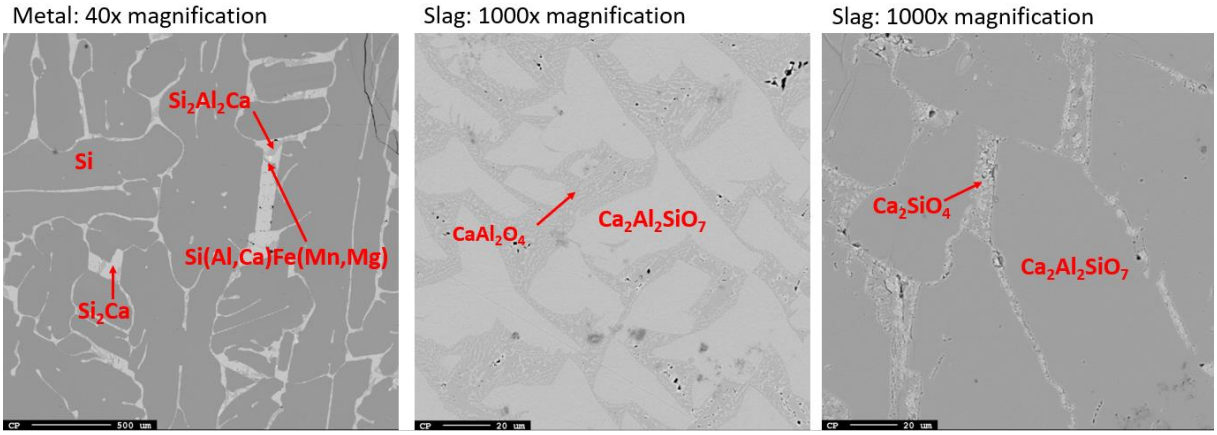

*Figure 4.23: BSE-images; acidic slag and 0.9*stoichiometric reductant, parallel 1. (Left) shows phases in metal sample. (Middle) and (Right) shows phases in slag sample.*

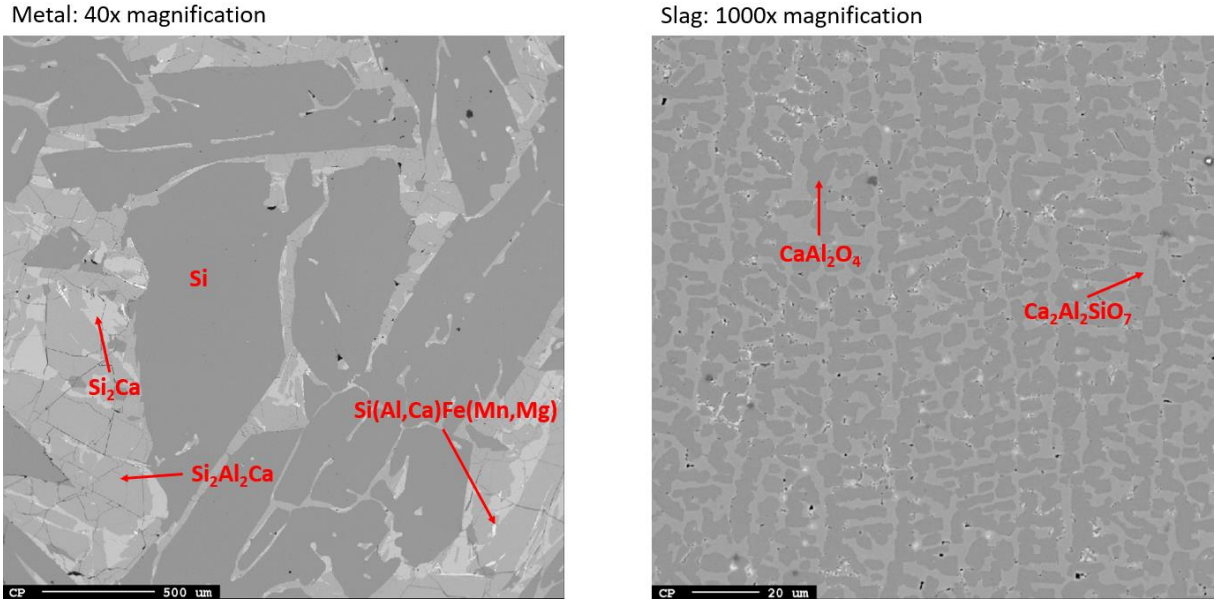

*Figure 4.24: BSE-images; acidic slag and 0.9*stoichiometric reductant, parallel 2 and 3. (Left) shows phases in metal sample for parallel 2. (Right) shows phases in slag sample for parallel 3.*

The metal and slag from acidic slag and stoichiometric amount of reductant can be observed in Figure 4.25. There was a relatively small variation between the parallels. The metal had in general low amounts of the Si_2Ca phase. Small amount of a pure Al phase was also observed in parallel 2 and 3.

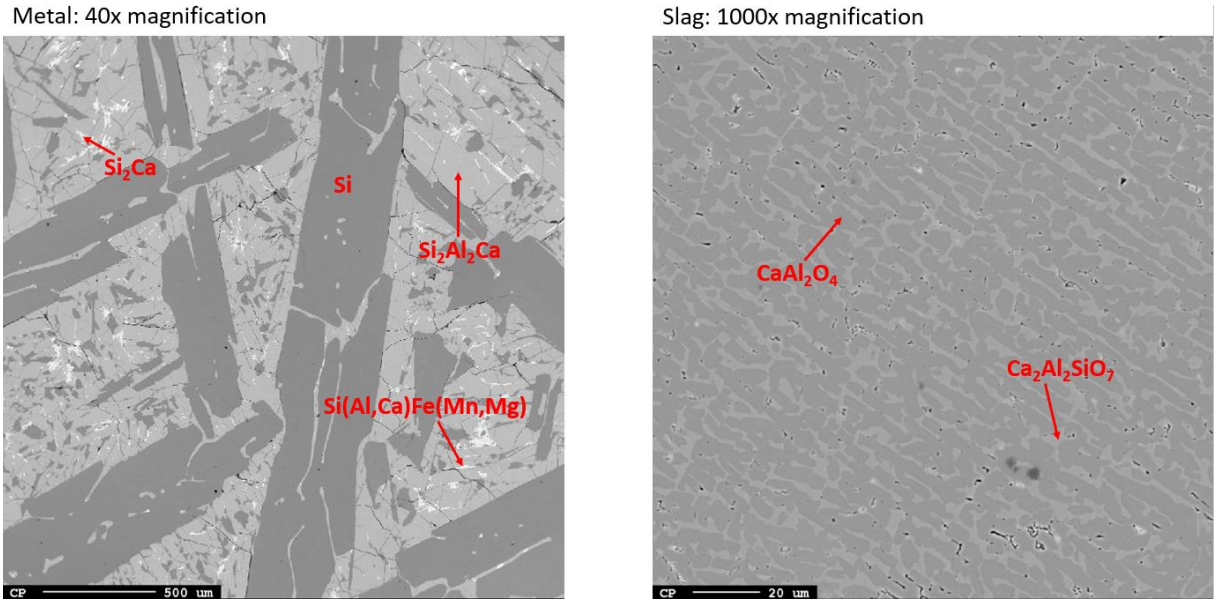

Figure 4.25: BSE-images; acidic slag and stoichiometric reductant. (Left) shows phases in metal sample for parallel 1. (Right) shows phases in slag sample for parallel 3.

The metal droplet dispersion from the first parallel with acidic slag and 1.1*stoichiometric reduction amount (mentioned in section 4.4.2) can be observed in Figure 4.26. WDS analysis of the metal droplets shows that the metal droplets consist of the same phases observed in the bulk metal form the other experiments. BSE-images of the slags form top part of the crucible (where metal droplet density was high) and form the bottom part of the crucible (where there was a purer slag) can be observed in Figure 4.27.

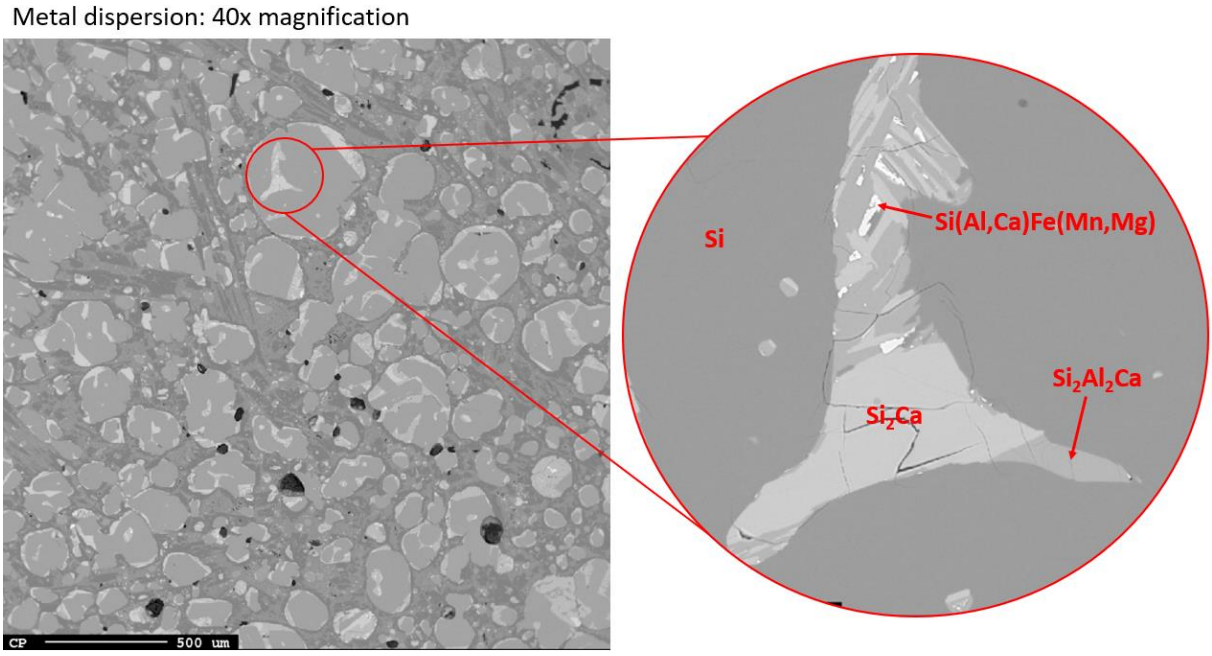

*Figure 4.26: BSE-images; acidic slag and 1.1*stoichiometric reductant, parallel 1. Metal droplets trapped in slag, (top part of the crucible).*

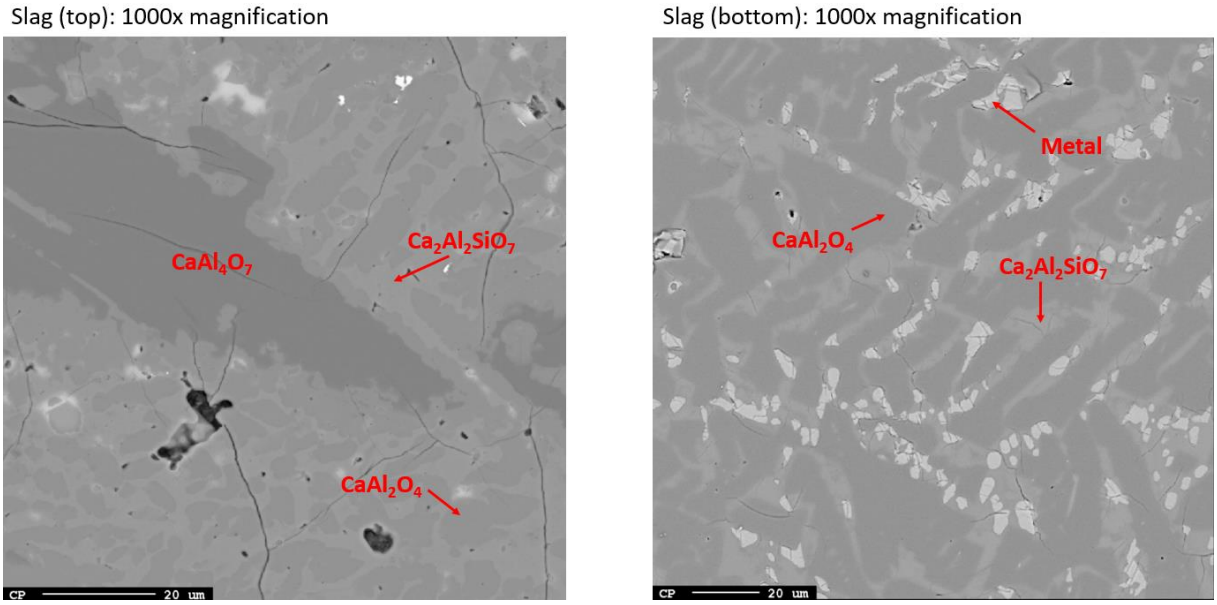

*Figure 4.27: BSE-images; acidic slag and 1.1*stoichiometric reductant, parallel 1. (Left) shows slag form the top part of the crucible (in between the metal droplets. (Right) shows slag from the bottom part of the crucible.*

The metal and slag from the second parallel from acidic slag and 1.1*stoichiometric amount of reductant can be observed in Figure 4.28 and Figure 4.29. One notable observation is that the metal for this sample has no observable Si_2Ca phase. It consisted of two main phases, pure Si- and Si_2Al_2Ca, as well as a small amount of pure Al and the light phase with most of the impurities.

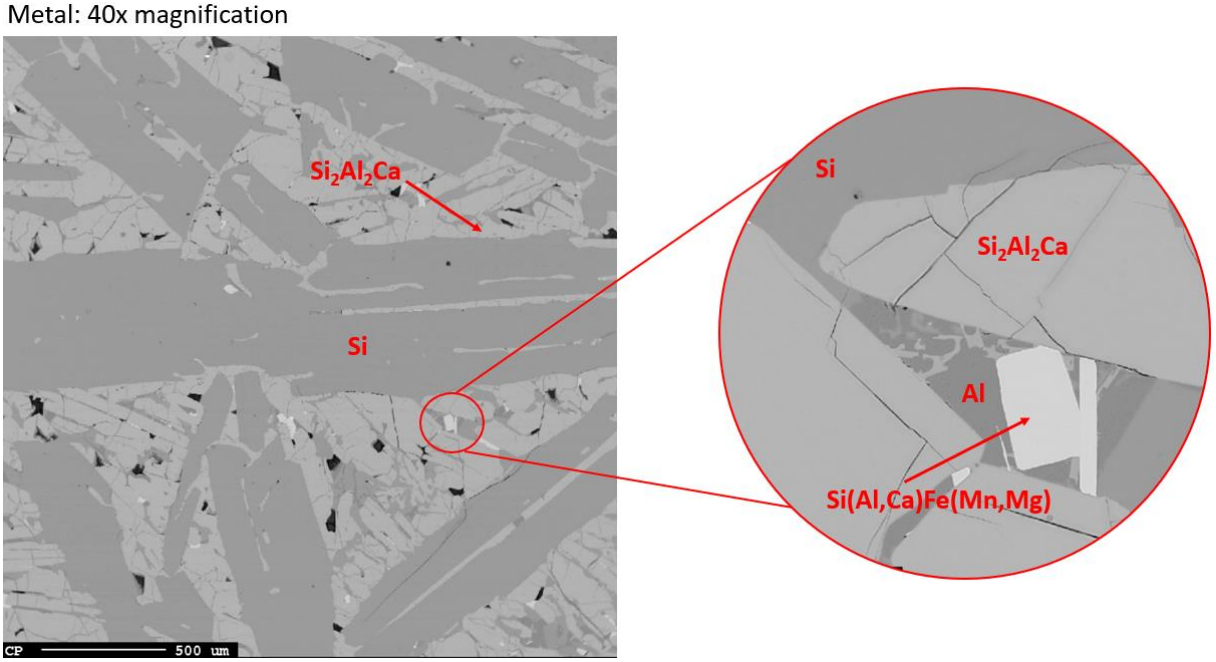

*Figure 4.28: BSE-images; acidic slag and 1.1*stoichiometric reductant, parallel 2. Metal droplets trapped in slag, (top part of the crucible).*

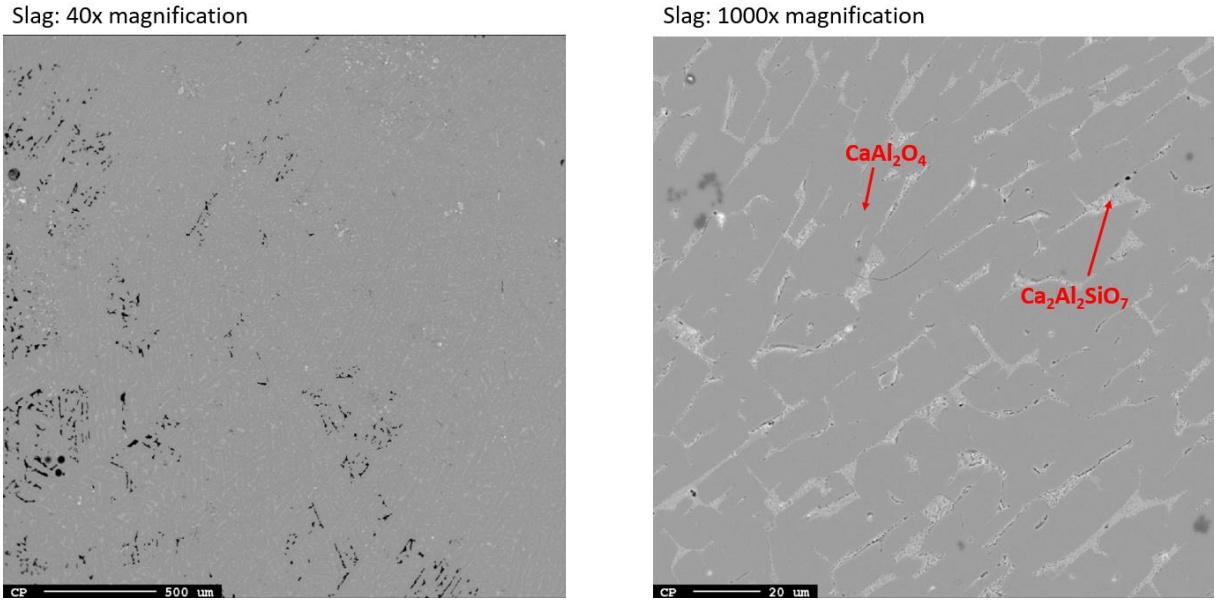

*Figure 4.29: BSE-images; acidic slag and 1.1*stoichiometric reductant, parallel 2. (Left) shows slag with 40x magnification. (Right) shows slag phases at 1000x magnification.*

The metal and slag from REC slag and 0.9*stoichiometric amount of reductant can be observed in Figure 4.30. No large differences were observed between the parallels. There are small phases observed in the slag that is not marked. This is due to their small size making it difficult to analyse with WDS.

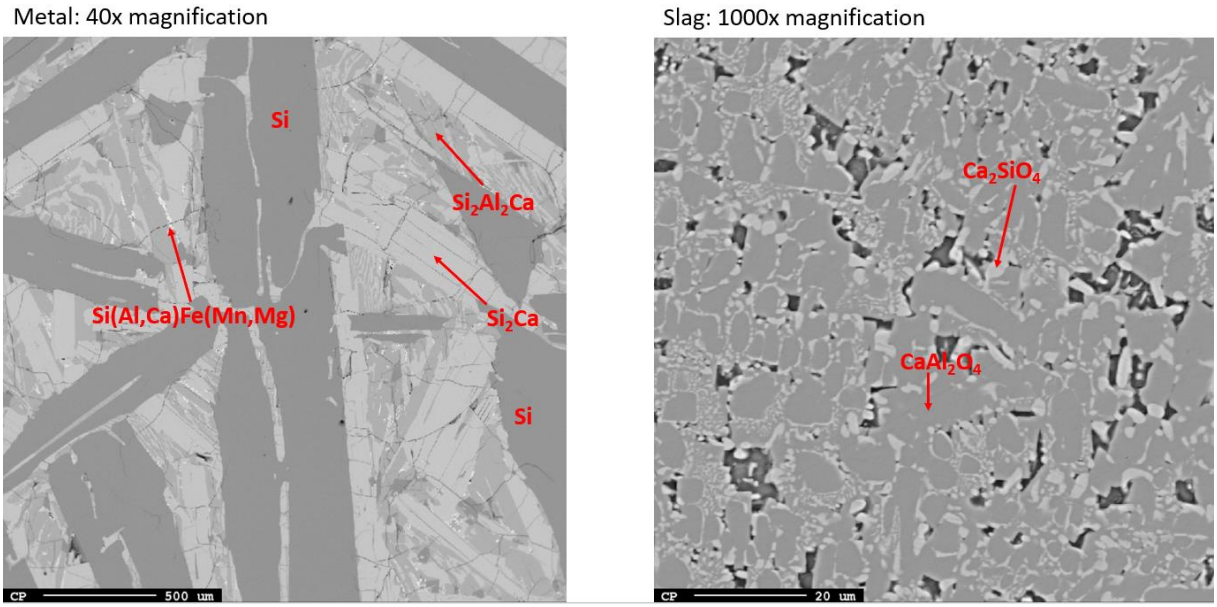

Figure 4.30: BSE-images; REC slag and stoichiometric reductant, parallel 3. (Left) shows metal with 40x magnification. (Right) shows slag phases at 1000x magnification.

The metal and slag from REC slag and stoichiometric amount of reductant can be observed in Figure 4.31. No large differences were observed between the parallels.

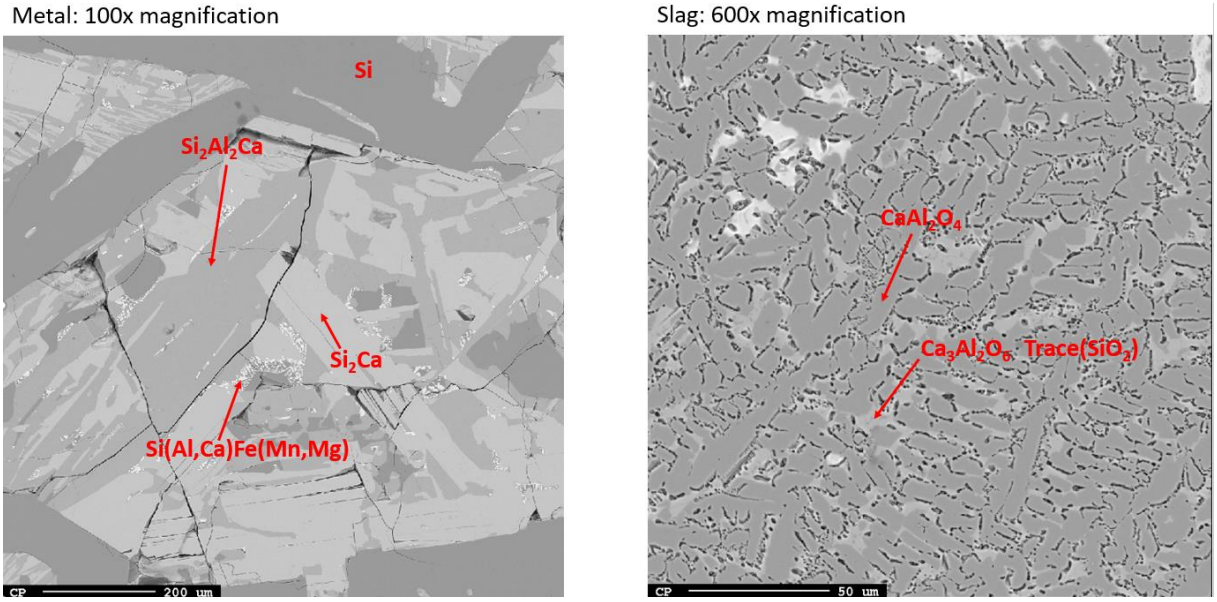

Figure 4.31: BSE-images; REC slag and stoichiometric reductant, parallel 2. (Left) shows metal with 100x magnification. (Right) shows slag phases at 600x magnification.

The metal and slag from basic slag and 0.9*stoichiometric amount of reductant can be observed in Figure 4.32. There were no large observable differences between the metal phase for the different parallels. The slag depicted is slag from the top of the crucible encasing the metal, and not the grey powder from the bottom of the crucible (see Figure 4.19). There were no notable differences in the slags in between the parallels with the exception of areas with SiC found in the first and third parallel.

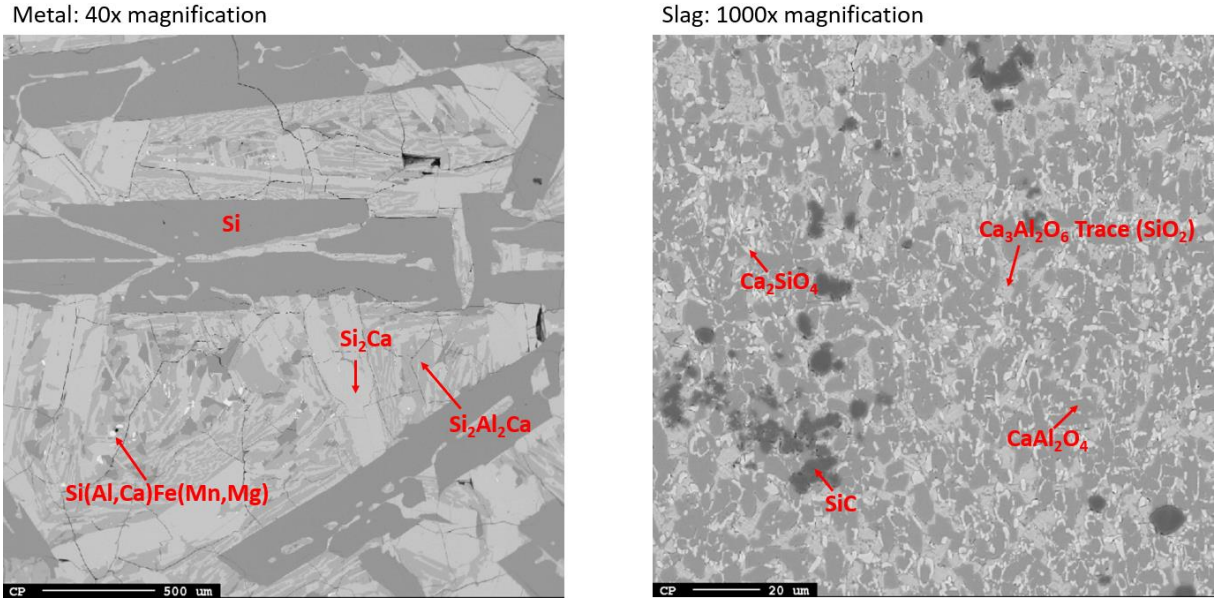

*Figure 4.32: BSE-images; Basic slag and 0.9*stoichiometric reductant. (Left) shows metal with 40x magnification from the first parallel. (Right) shows slag phases at 1000x magnification from the third parallel.*

The metal and slag from basic slag and stoichiometric amount of reductant parallel 1 and 2 can be observed in Figure 4.33 and Figure 4.34 respectively. There are notable differences in the metal structure for the two parallels. Parallel 1 have a much larger area fraction of the Si_2Al_2Ca phase and a much smaller fraction of the Si_2Ca than parallel 2. One notable commonality is metal from both parallels had small areas with visible SiC. There are visible differences in the slags as well. Parallel 1 have larger grains with less pores than parallel 2. It should be mentioned that a there was tested out a different policing technic for parallel 1, where the last steps described section 3.3.1 was skipped. The

slag here is also the top slag as described in the last paragraph. One notable observation done on the 2. parallel is that piece of metal covered in slag was found on the bottom of the cracked crucible, tant turned out to be mostly Al.

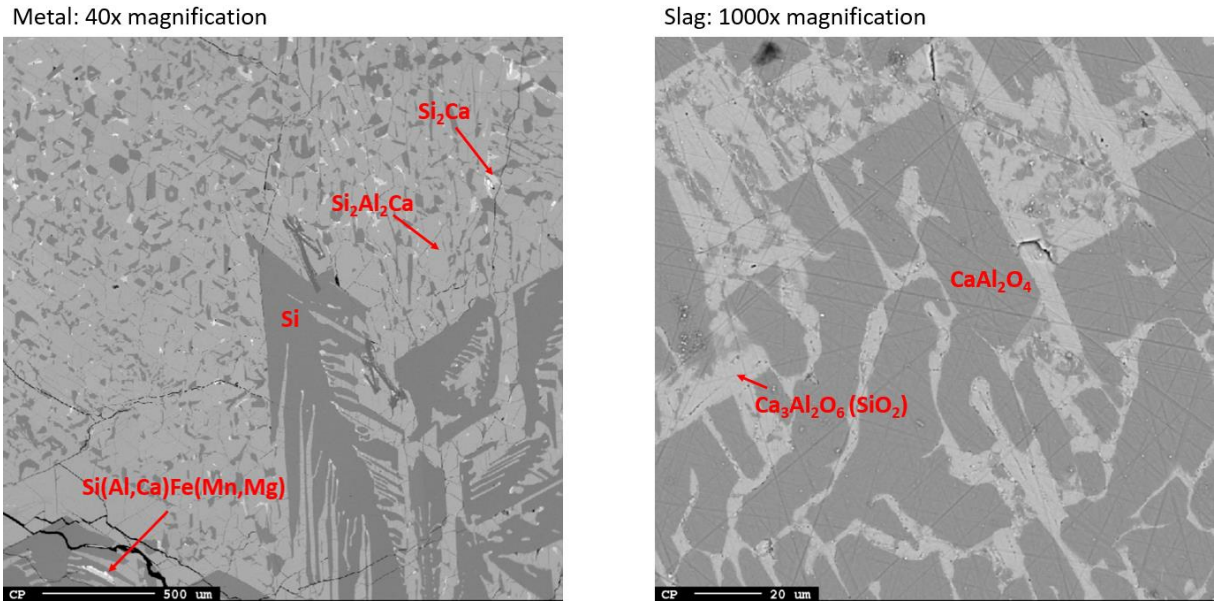

Figure 4.33: BSE-images; Basic slag and stoichiometric reductant, parallel 1. (Left) shows metal with 40x magnification from the first parallel. (Right) shows slag phases at 1000x magnification.

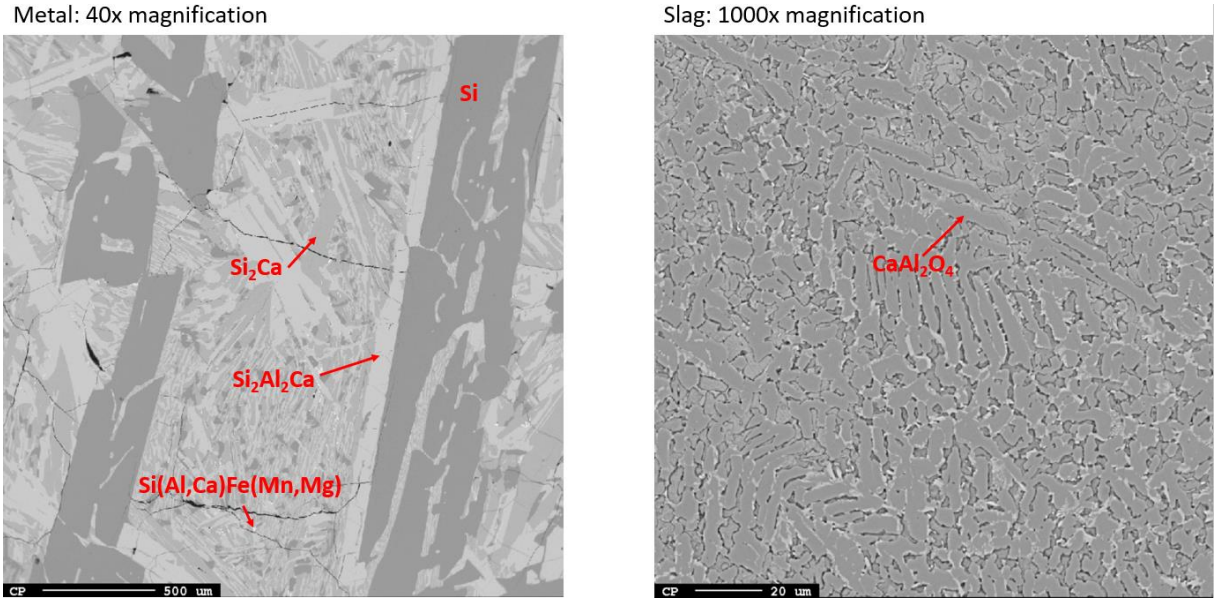

Figure 4.34: BSE-images; Basic slag and stoichiometric reductant, parallel 2. (Left) shows metal with 40x magnification from the first parallel. (Right) shows slag phases at 1000x magnification.

The third parallel with basic slag and stoichiometric amount of reductant is the sample with a to short holding time due to problems with the furnace, described in section 4.4.2. BSE-images of the “flaky” main metal and the encasing slag phase are illustrated in Figure 4.35, while the BSE-images of the metal pearl that was flattened (found on top of the other metal phase) is depicted in Figure 4.36. (For macro images of these see Figure 4.22). The main metal phase is shown to have a laminar structure which is in line with previous observations in section 4.4.2. Its composition differs from the metal the other experiments as it has a large amount Al-phase and a relatively small amount of Si-phase. There is also a large amount of Si_2Al_2Ca-phase. Its solid slag phase does not differ in any particular way from others, with similar input materials. The metal pearl is shown to be an Al-alloy with a main phase

consisting of Al, and two smaller phases consisting of pure Si, and a mixed phase high in Si and other impurities.

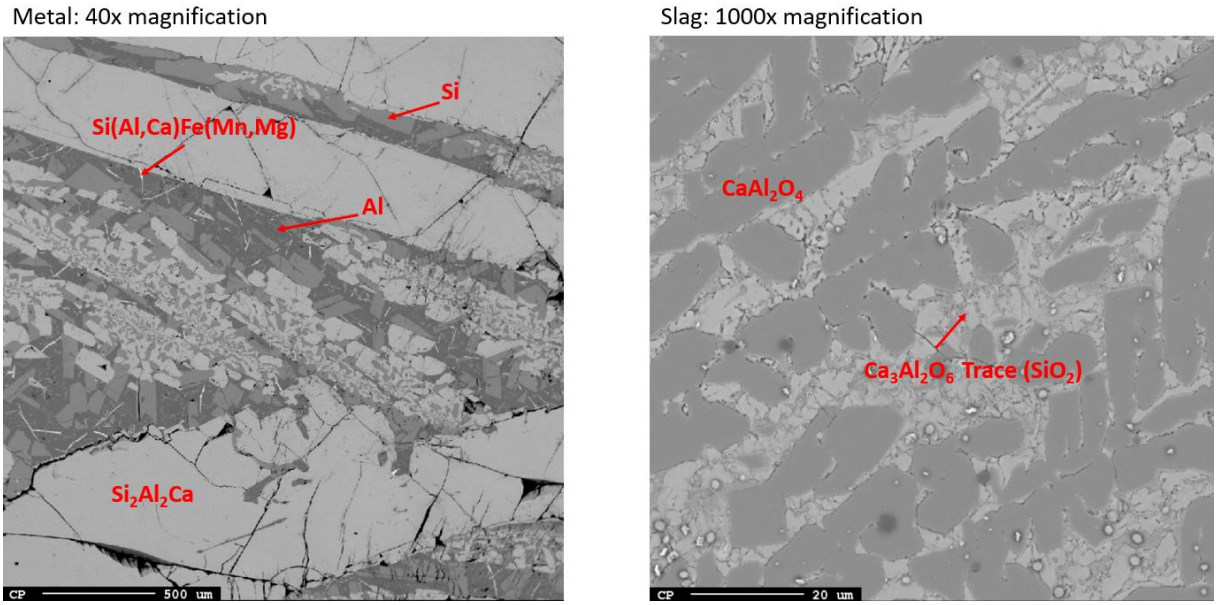

Figure 4.35: BSE-images; Basic slag and stoichiometric reductant, parallel 3. (Left) shows metal with 40x magnification from the first parallel. (Right) shows slag phases at 1000x magnification.

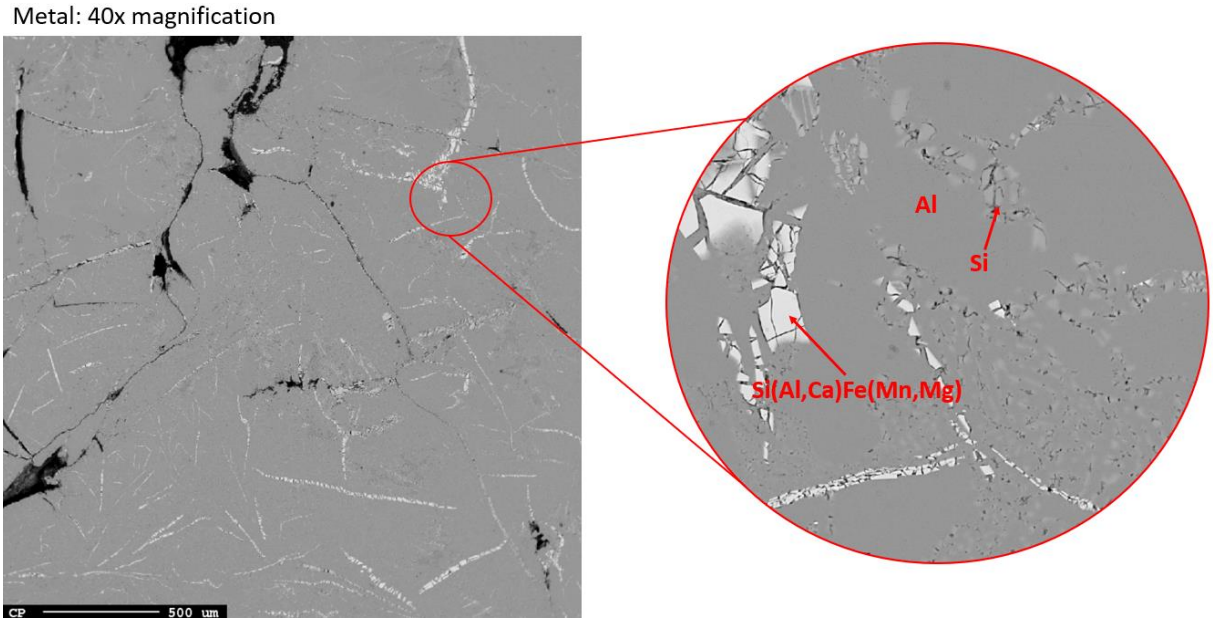

Figure 4.36: BSE-images; Basic slag and stoichiometric reductant, parallel 3. Metal pearl at 40x magnification (left) and 400x magnification (right).

The grey slag powder found in the bottom part of all samples where basic master slag was used, was also investigate (see Figure 4.37). It was shown that it consisted of two types of particles: one compact slag phase, and one cracked consisting of Ca_2SiO_4 and $Ca_2Al_2SiO_7$.

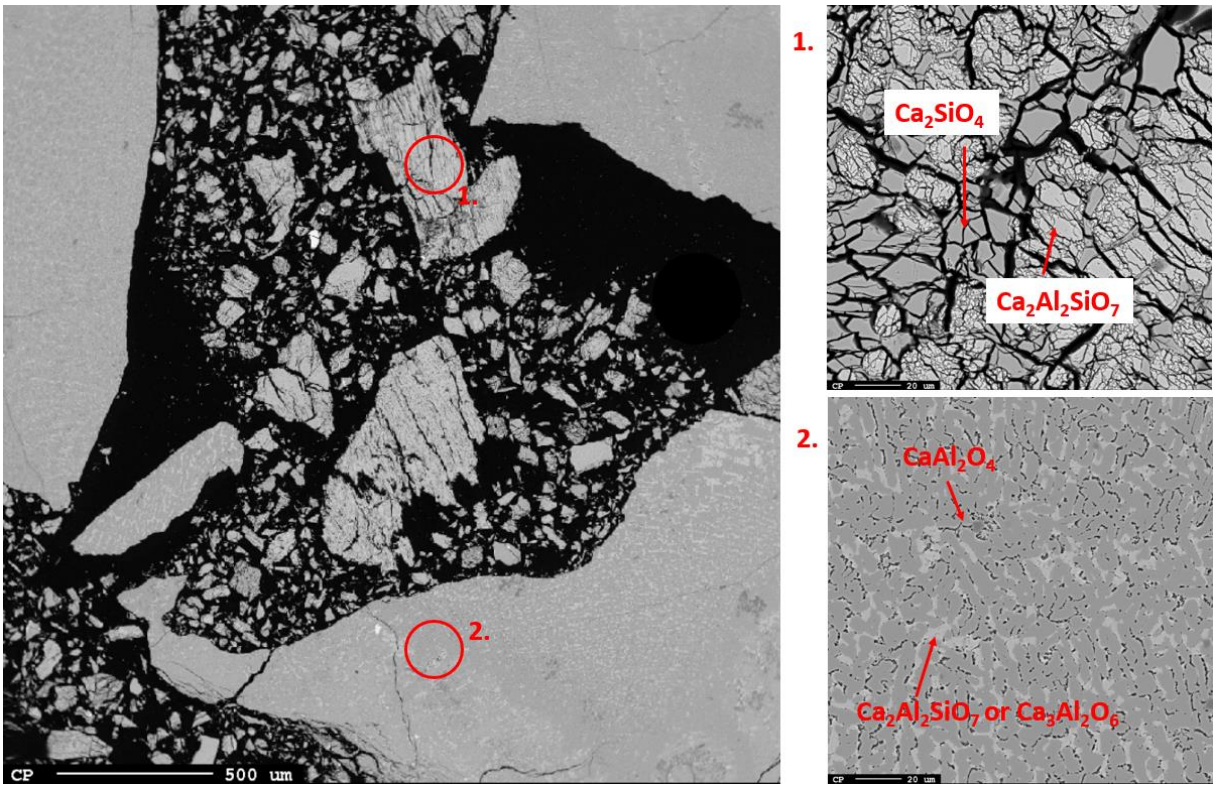

Figure 4.37: BSE-images of grey slag powder from all experiments using basic slag. (Left) show an overview of the powder at 40x magnification, showing a compact slag and cracked particles. (Right) show a 600x magnification of the cracked particles (1.) and the compact particles (2.).

The presence of carbides was found in the slag of several of the samples. Areas close to the crucible wall was inspected, and it, like rest of the slag, varied between small clusters of metal, and areas with pure slags. A metal phase close to the wall had a carbide phase between the wall and metal. Figure 4.38 shows and aluminium carbide phase present between an aluminium phase and the graphite crucible wall, as well as SiC particles dispersed thorough the slag phase. This illustrate that, carbides can be formed close to the wall, as well as being dispersed throughout the slag.

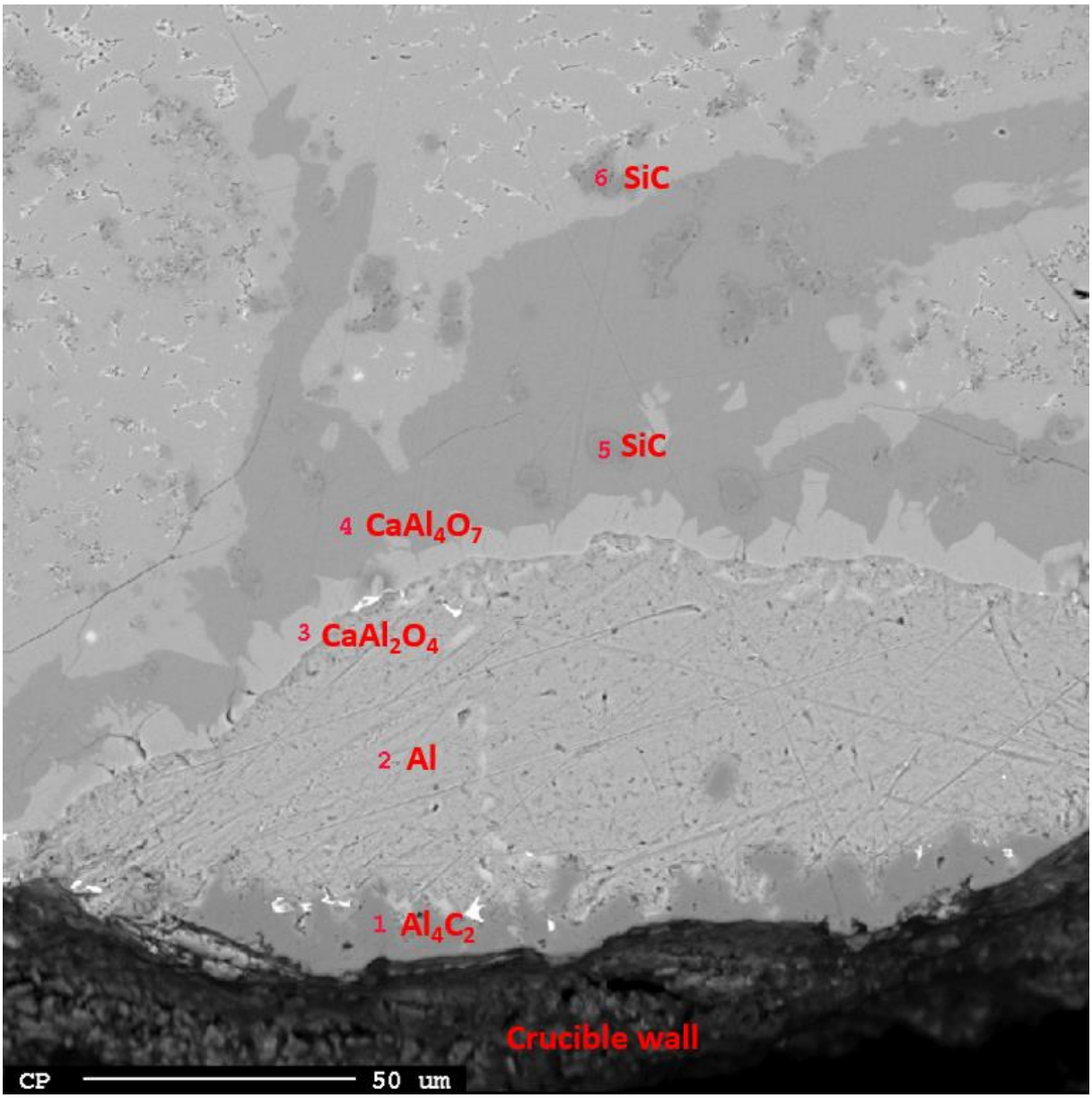

*Figure 4.38: BSE-images; Acidic slag and 1.1*stoichiometric reductant, parallel 2. Shows: Al metal close to the crucible wall (2), an aluminium carbide phase in between the wall and Al phase (1), two slag phases (3) and (4), as well as SiC particles dispersed throw-out the slag phase (5) and (6).*

4.5 Chemical composition

The results from the energy dispersive X-ray spectroscopy (EDS) will be presented in this section. For the metal were three scans (40x magnification) done over an area of the samples for each parallel. Six scans were carried out; three at 40x magnification, and three at 600X magnification. The slag analysed with EDS with the basic start slag is only solid pieces from the top of the crucible, as the slag in the bottom was crushed into powder (see section 4.4.1) and not possible to analyse with any sort of precision.

The Inductive Coupled Plasma Mass Spectrometry (ICP-MS) results conducted on samples from REC with stoichiometric reductant addition are found in appendix C. The results from this analysis were close to the results found with EPMA. It was therefore decided to not conduct any more analysis by this method, as it was expensive and time consuming. The similarities between ICP-MS and the EPMA result has been seen previously in a specialisation project conducted by the author [34]. This was further backed by Hassan [33] that did the same analysis an similar samples.

4.5.1 EDS area analyses of metal and slag

The following diagrams will show the composition for metal and slags. The three main elements (Si, Al, and Ca) in the metal will be presented alongside their respected oxides (SiO_2, Al_2O_3, and CaO) in the slags. The error bares are the standard deviation for all scans over all parallels for each master slag and stoichiometry. The red "x"s marks results from experiments with 0.9*stoichiometric reduction amount, the black diamonds marks results from experiments with stoichiometric reduction amount, and the blue square outline marks results from the experiment with 1.1*stoichiometric reduction amount. The y-axis represents the wt% of the element/oxide in the metal/slag, while the x-axis represents the CaO/SiO_2 weight fraction of the original input master slags. Note that the data from acidic slag and 1.1*stoichiometric reduction amount (parallel 1), and basic slag and stoichiometric reduction amount (parallel 3) are not part of these data sets as they were not representative. This was due to the nature of the experimental in- and output (see section 4.4.2). Note that the slag data is a combined measurement of the analysis done on both high and low magnification described in section 3.3.2. (Data from analysis on high magnification, and on low magnification separated are found in appendix D)

The Si content in metal products and the SiO_2 content in the slags can be found in Figure 4.39 and Figure 4.40 respectively. Looking at the metal (see Figure 4.39), there are two trends regarding the Si content that becomes clear. The first is that the concentration increases with the concentration of SiO_2 in the master slag, and the second is that the Si concentration in the metal will be higher for 0.9*stoichiometric reduction amount that for higher reduction amount. Looking at the slag (Figure 4.40) is it clear that the SiO_2 concentration in the slag will decrease with increasing reductant addition for all master slags.

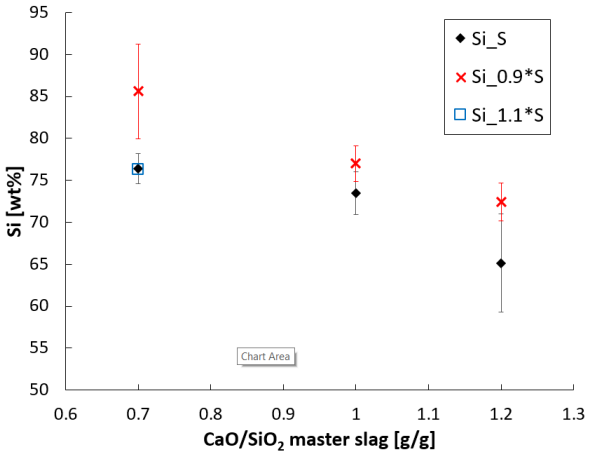

Figure 4.39: Average wt% Si in metal for the different input slags and reductant amount. (Red x) under stoichiometric, (black diamantes) stoichiometric, and (blue square) over stoichiometric. The error bars are the standard deviation between the parallels.

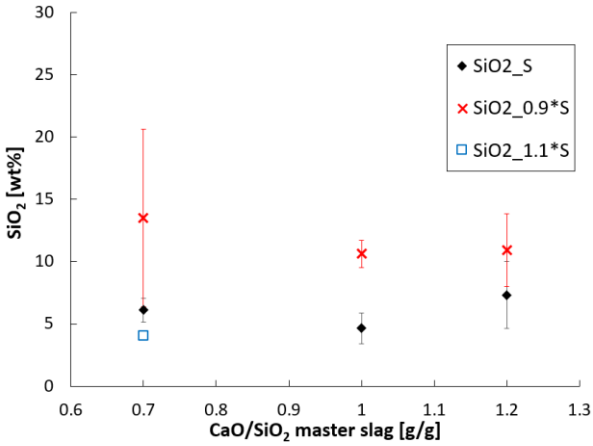

Figure 4.40: Average wt% SiO_2 in slag for the different input slags and reductant amount. (Red x) under stoichiometric, (black diamantes) stoichiometric, and (blue square) over stoichiometric. The error bars are the standard deviation between the parallels.

The Al content of the metal produced, and the Al_2O_3 content in the slags can be found in Figure 4.41 and Figure 4.42 respectively. Looking at the metal (Figure 4.41) it becomes clear that a higher reduction amount will lead to a higher Al concentration in the metal. The case will be the same looking at the slag (Figure 4.42). The Al_2O_3 concentration will also here increase with increasing reduction amount.

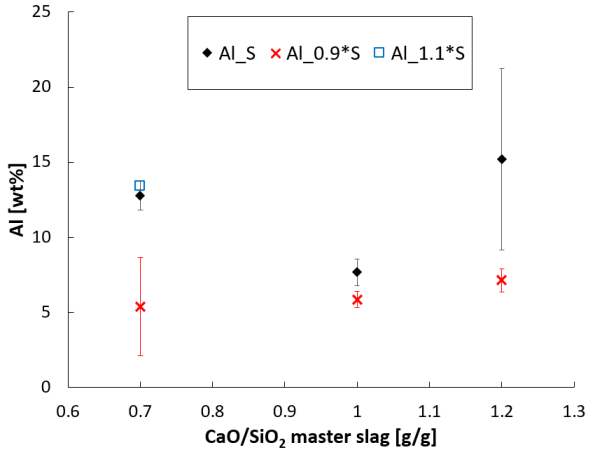

Figure 4.41: Average wt% Al in metal for the different input slags and reductant amount. (Red x) under stoichiometric, (black diamantes) stoichiometric, and (blue square) over stoichiometric. The error bars are the standard deviation between the parallels.

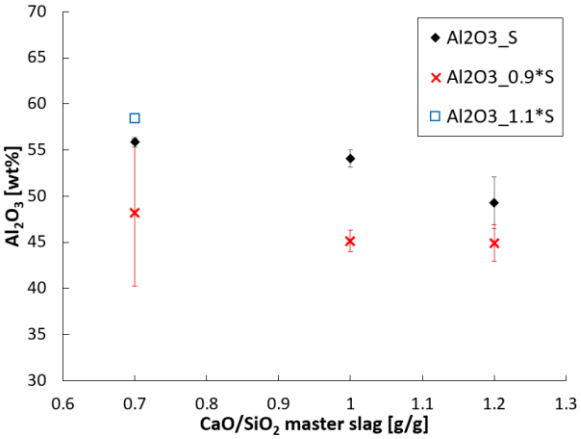

Figure 4.42: Average wt% Al_2O_3 in slag for the different input slags and reductant amount. (Red x) under stoichiometric, (black diamantes) stoichiometric, and (blue square) over stoichiometric. The error bars are the standard deviation between the parallels.

The Ca content in the metal produced, and the CaO content in the slags can be found in Figure 4.43 and Figure 4.44 respectively. Looking at the metal (see Figure 4.43) it becomes clear that the Ca concentration increases with increasing CaO/SiO_2 mass ratio in the start slag. There are no clear trends related to the reduction addition. For the slag (see Figure 4.44) there will also here be a trend of increasing CaO with increasing CaO/SiO_2 mass fraction of the master slags. There seems to be a trend of increasing CaO with decreasing reduction amount, but this is not that clear.

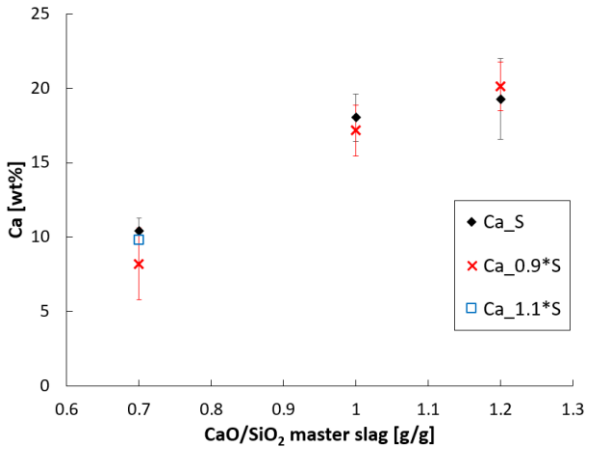

Figure 4.43: Average wt% Ca in metal for the different input slags and reductant amount. (Red x) under stoichiometric, (black diamantes) stoichiometric, and (blue square) over stoichiometric. The error bars are the standard deviation between the parallels.

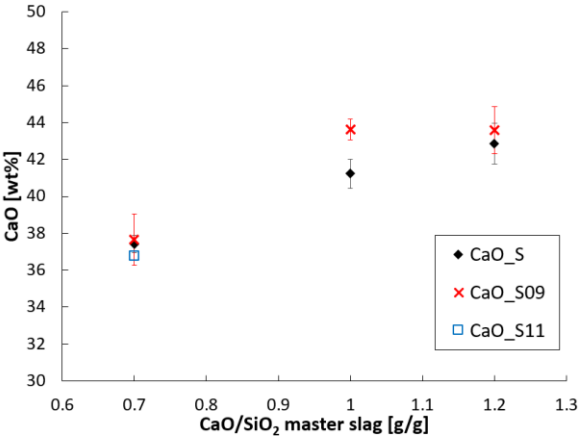

Figure 4.44: Average wt% CaO in slag for the different input slags and reductant amount. (Red x) under stoichiometric, (black diamantes) stoichiometric, and (blue square) over stoichiometric. The error bars are the standard deviation between the parallels.

The results from the EDS area scan analysis for the third parallel with basic slag and stoichiometric reduction amount (see Figure 4.22) can be found in Table 4-5

Table 4-5: The EDS analysis of the third parallel with basic slag and stoichiometric reduction amount. The error are the standard deviation between the 3 measurements done.

	EDS analysis of Parallel 3: basic slag with stoichiometric reduction amount [wt%]		
Sample material:	*Si*	*Al*	*Ca*
Metal Pearls	21±1.8	76±1.7	0.5±0.15
Coalesced metal	49.8±0.75	33.4±0.82	17±1.2
	SiO_2	*Al_2O_3*	*CaO*
Slag	5.3±0.9	50.4±0.9	43.7±0.5

4.5.2 Metal dispersed in Slag

As mentioned, the area scanners of the slag were done on two different magnifications, 40x and 600x. The wt% of species in the area scanned will be analysed by EPMA-analysis. A software will calculate the analysed species to their respective oxides wt%. This means that metal scanned will be assumed to be oxides by the software. The scan on 600x magnification makes it easier to only analyse "pure" slag, but there is also the problem of local differences in the slag composition, having a large effect on the analysed composition. These data were therefore combined with the area scans on 40x magnification. This gets a more representative analysis of the overall composition; though it will also include metal and carbide particles dispersed throughout all of the slag. Figure 4.45 illustrate the amount of metal that can be observed in slag at 40x magnification, compared to slag at 600x magnification. To investigate if there were large differences in analysed composition on 40x- and 600x magnification, were the average value from the 40x magnification scans subtracted with the value of the 600x magnification scans. The results are plotted for the SiO_2-, Al_2O_3-, and CaO concentrations in Figure 4.46, Figure 4.47, and Figure 4.48 respectively. It becomes clear that the concentration of Si is higher at 40x magnification than for 600x, while the opposite is true for Al and Ca. This is just a semi-quantitative analysis that gives an idea of trends with regards to the quantity of metal/carbides that is trapped in the slag. It is in no way statistically valid to draw actual numbers from due to the complexity of the heterogeneous slag produced.

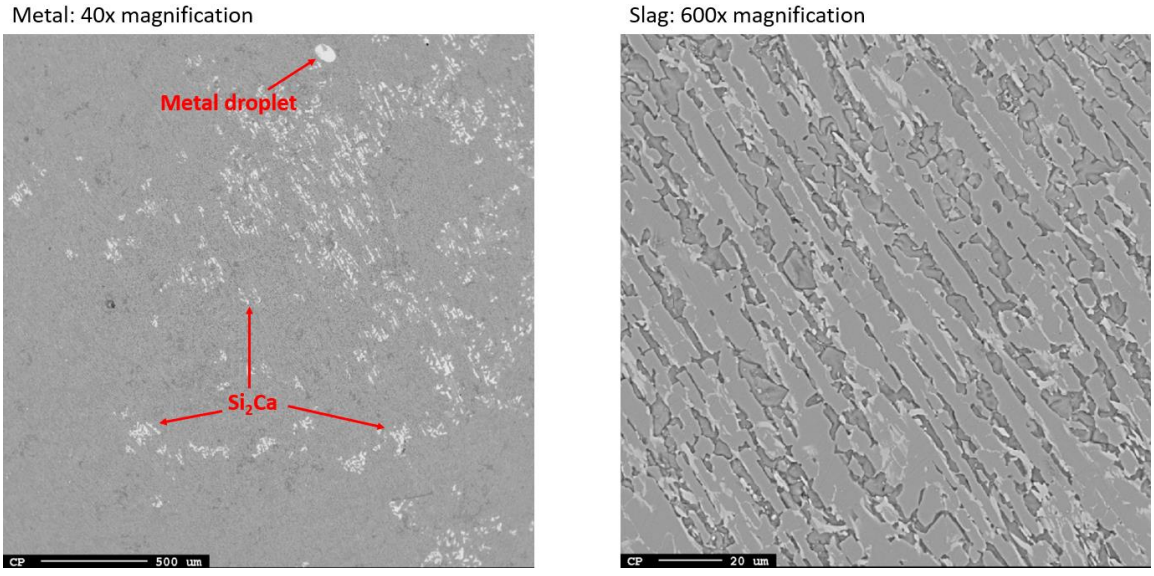

Figure 4.45: Illustrate the difference between how much metal that can be in a area scan of a slag sample at 40x magnification (left), and 600x magnification (right). The slag are the second parallel with basic slag and stoichiometric reduction addition.

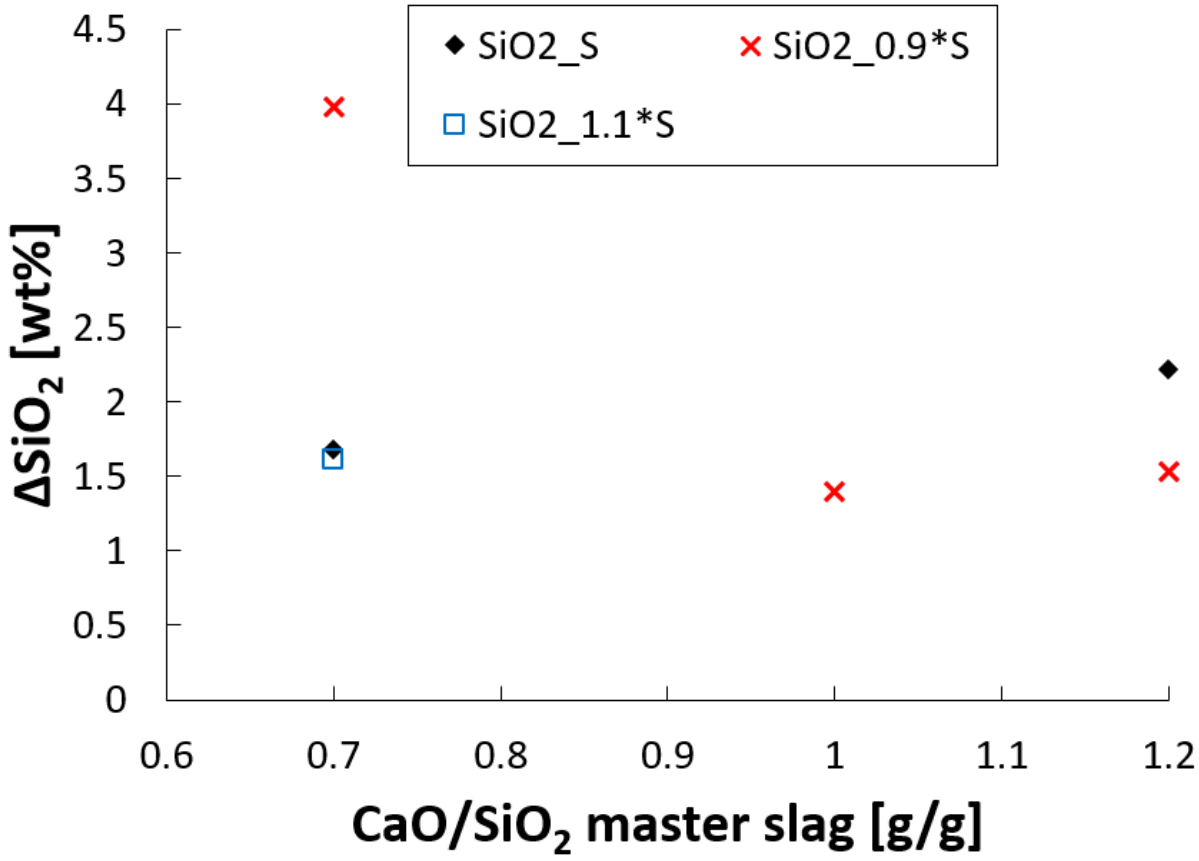

Figure 4.46: Difference in analysed SiO_2 with EPMA EDS area scan between 40x and 600x magnification

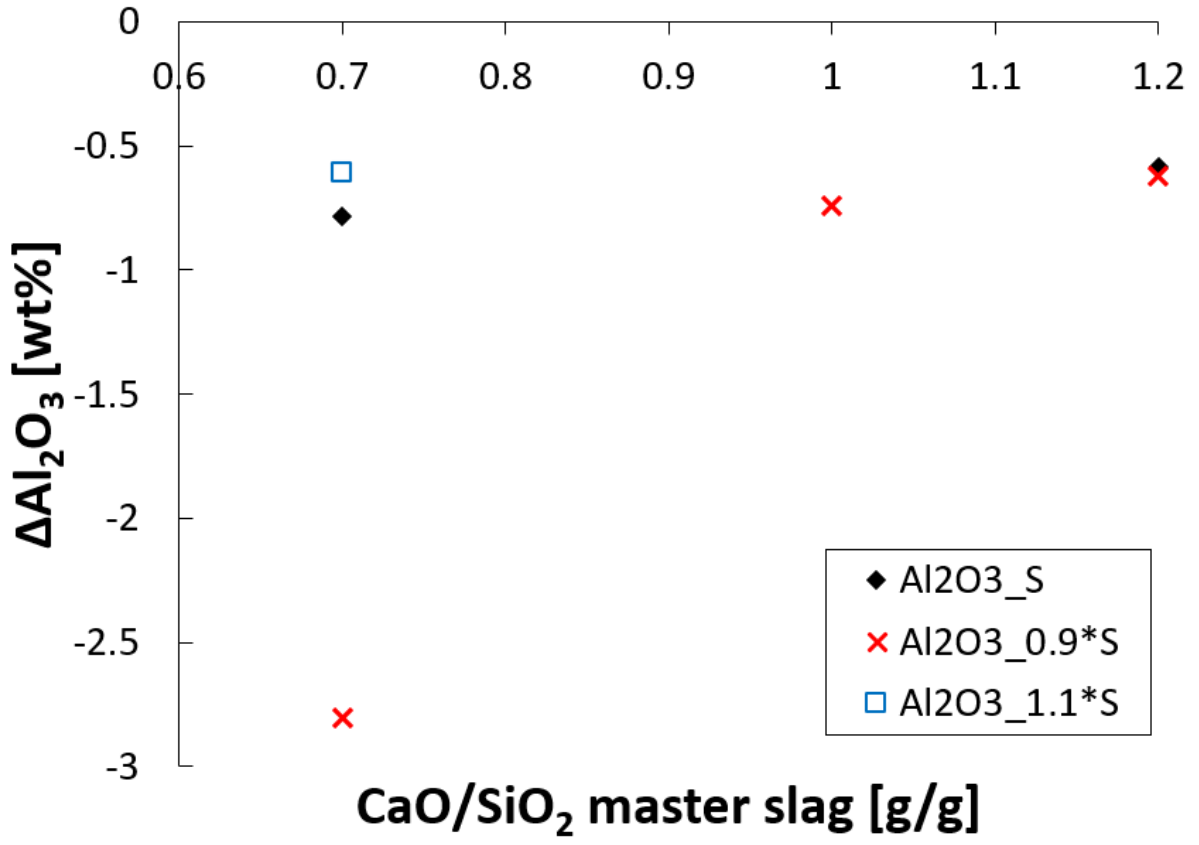

Figure 4.47: Difference in analysed Al_2O_3 with EPMA EDS area scan between 40x and 600x magnification

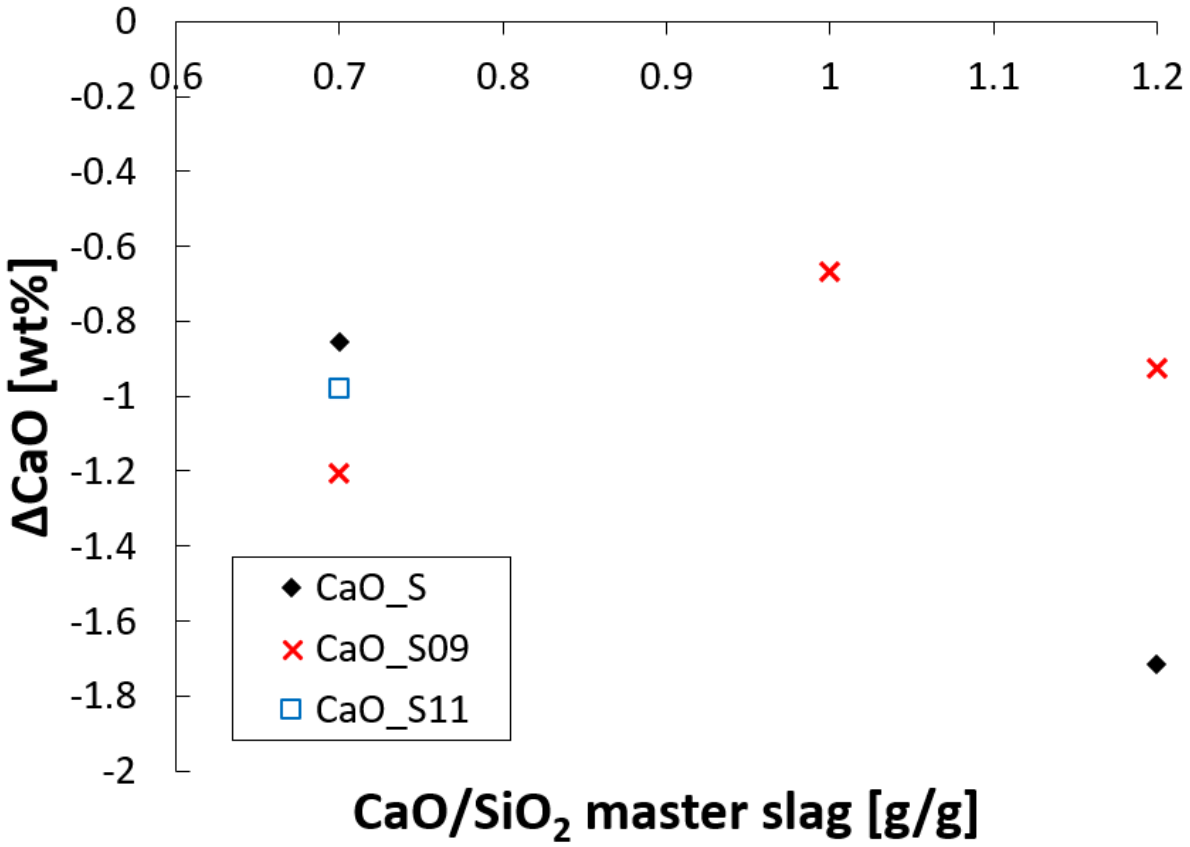

Figure 4.48: Difference in analysed CaO with EPMA EDS area scan between 40x and 600x magnification

4.5.3 Mass balance

A simple mass balance was calculated to find out where the three main species put in to the system ended up in the after the experiments. This was done by finding the elements going in to the system: mass Al and slag into the system are found Table 3-2. Mass of each specie in the slag was calculated from the mass in coupled with the XRF results of the master slags (see Table 4-1). The mass of metal and slag out of the system were found by taking the metal yields from Table 4-3 (assuming that this was all metal), subtracting the losses noted in Table 4-4 (Basic slags, and samples with weight gains due to alumina tubes that was stuck in crucible, was noted with no loss), and assuming that rest of the mass are slag. These results are plotted in Figure 4.49. The balance of elements out of the system was found by using the results for the chemical analysis for both metal and slag (see appendix E for each sample). These results were multiplied with the metal and slag yield to find the mass of each element out of the system. These results were then divided with the calculated input mass of each specie. The results of the three main elements (Si, Al, and Ca) are plotted underneath.

Note that this is not a perfect method as the room for errors are large. Mass losses (from Table 4-3) don't necessarily need to be silica fume (or other input from slag and metal), but can be mass from the crucible that has fumed off. The potential source of error from the mechanical metal/slag separation are huge. There is also the fact that there were metal droplets observed in the slag that is not necessarily reflected in the analysed slag composition. There are of course uncertainties connected to the analysed results themselves. All of this said though, will the mass balance give an indication of the overall trends in the experiments.

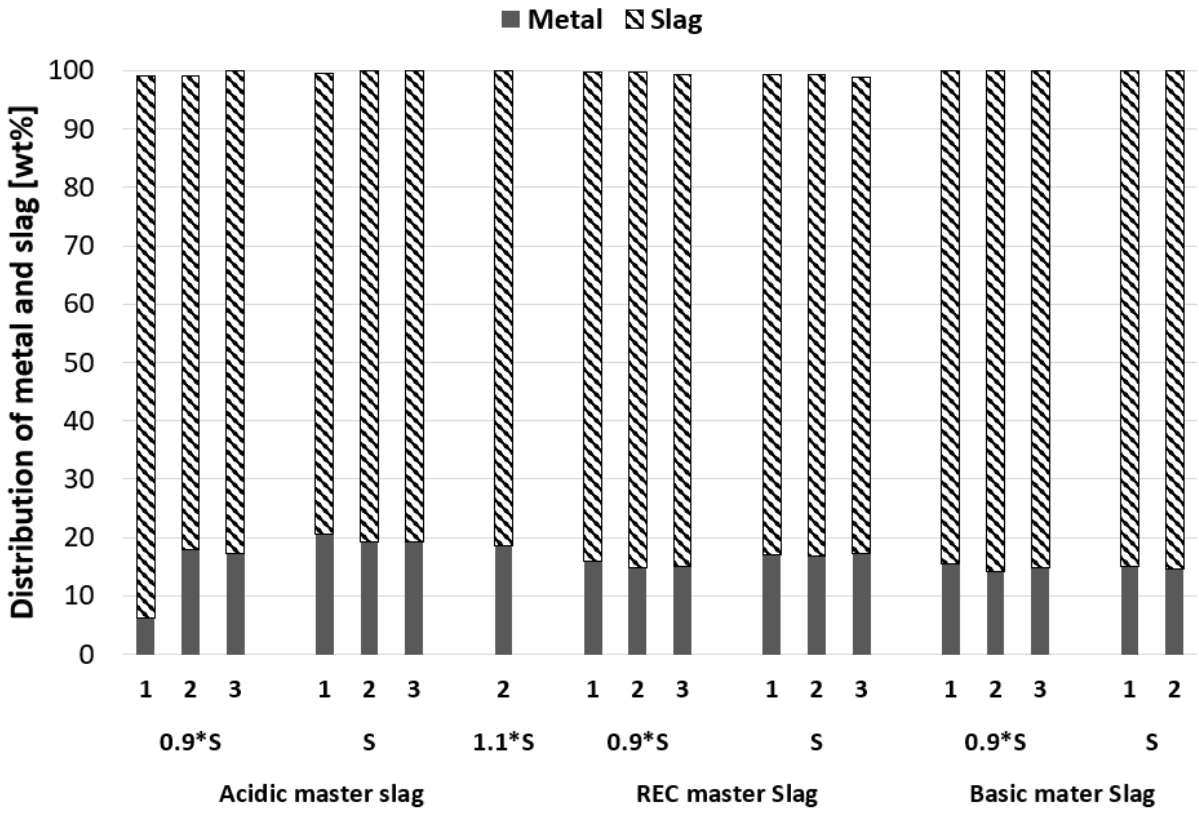

Figure 4.49: Illustrate the distribution between extracted metal yield and the presumed slag for all experiments. (S stands for stoichiometric)

The distribution of Si between metal and slag are found in Figure 4.50. It can be observed that there is a loss of analysed Si in the output material for all experiments.

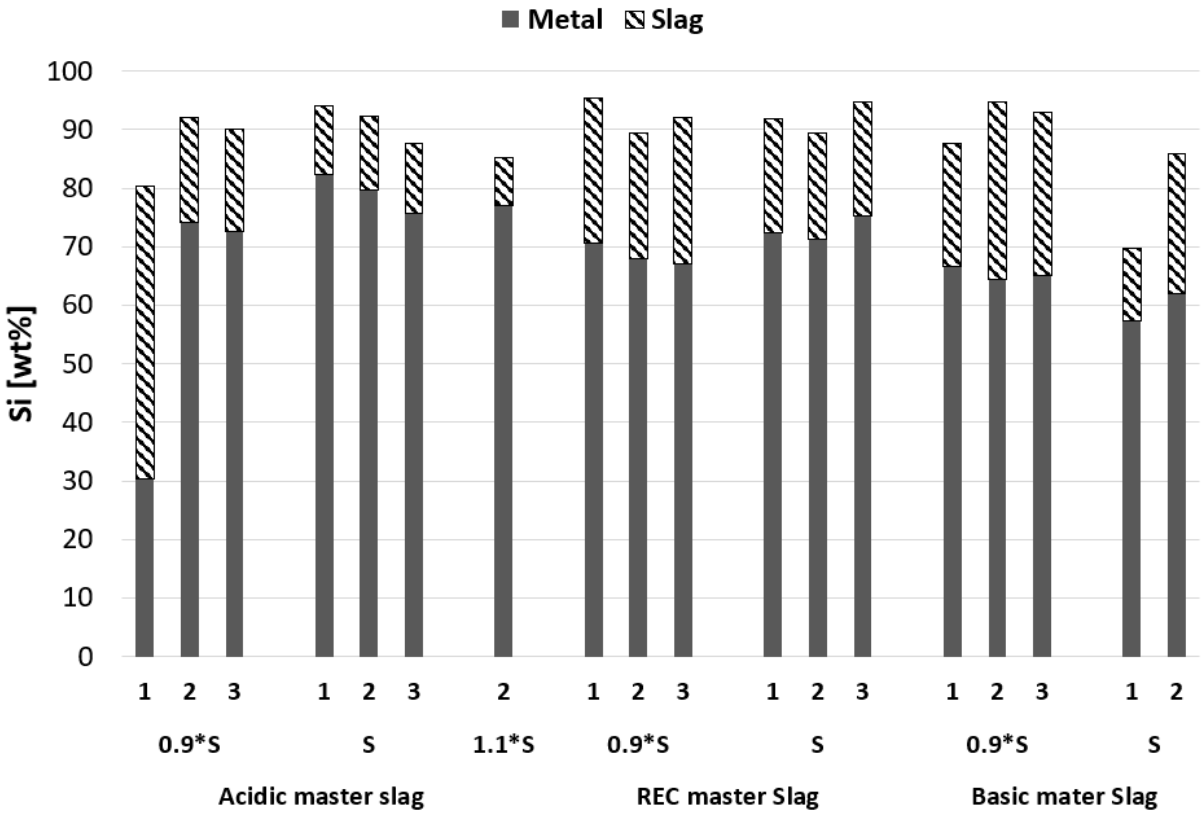

Figure 4.50: Illustrate the distribution of input Si in the output metal and slag for all experiments. (S stands for stoichiometric)

The distribution of Al between the metal and slag are found in Figure 4.51. Here it can be observed that there are several experiments that has an overall higher analysed Al output than the input. The Al output from the slag alone, were higher than the input for some of the experiments.

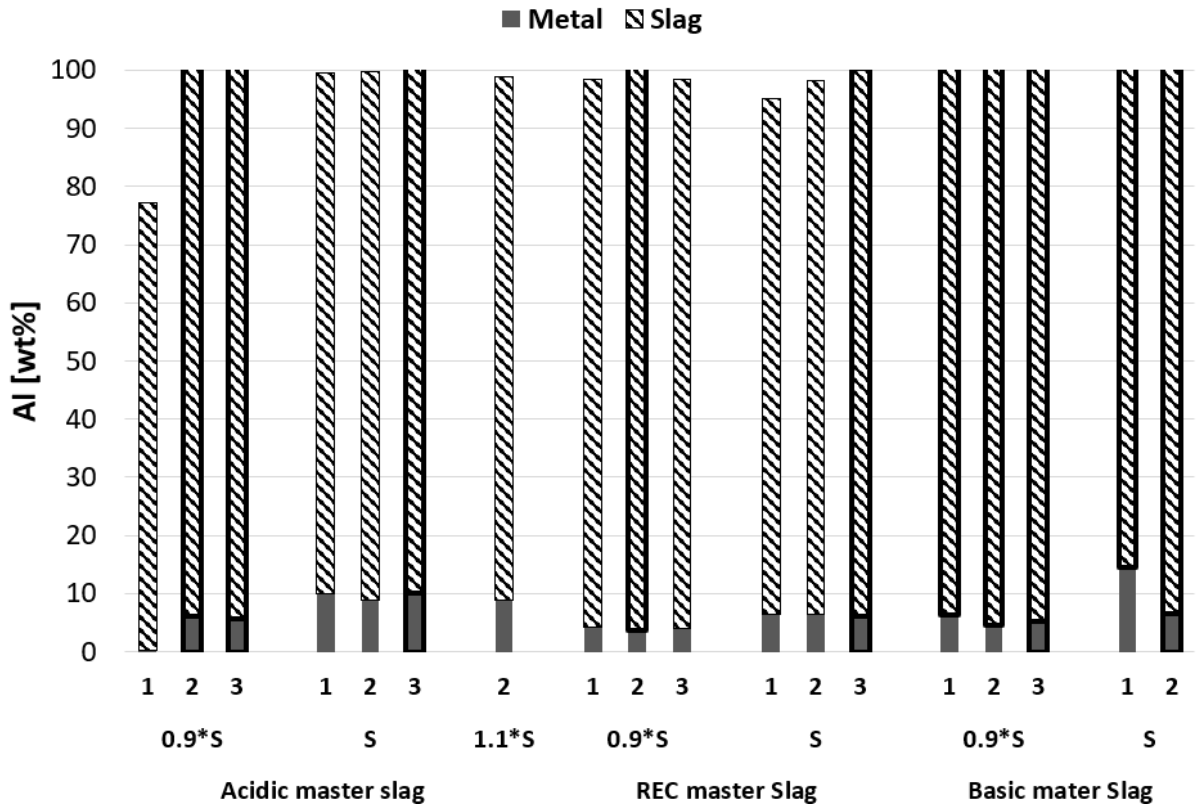

Figure 4.51: Illustrate the distribution of input Al in the output metal and slag for all experiments. The samples that had a combined higher Al content in output slag and metal than the input, has a thicker outline around the bar. The samples where only the slag had a higher Al content than the output has a thick outline around the slag bar. (S stands for stoichiometric)

The distribution of Ca between the metal and slag are found in Figure 4.51. Also, here it can be observed that there are several experiments that has an overall higher analysed Ca output than the input. For some of the experiments are the Ca output from the slag alone, higher than the input.

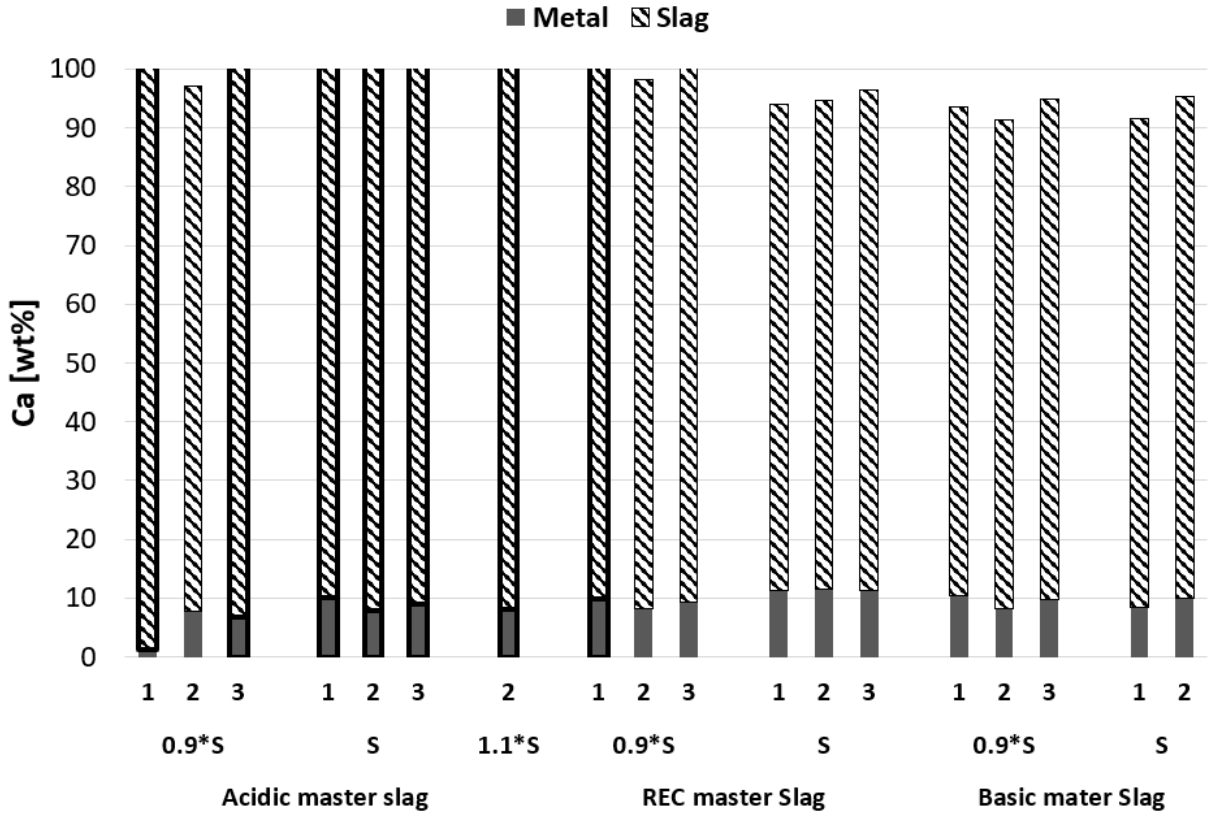

Figure 4.52: Illustrate the distribution of input Ca in the output metal and slag for all experiments. The samples that had a combined higher Ca content in output slag and metal than the input, has a thicker outline around the bar. The samples where only the slag had a higher Ca content than the output has a thick outline around the slag bar. (S stands for stoichiometric)

4.6 Simulated equilibrium values

4.6.1 Metal yield

Thermodynamical equilibrium simulations of the systems from the different experiments were performed in FactSage by Harald Philipson. The databases used FToxid 7.3, NTNU 7.0, and FactPS 7.3. The only input materials were the slags with compositions gathered from Table 4-1, aluminium reductant, and a 1 atm Ar-atmosphere, at a temperature of 1650˚C (amount of Al reductant and slag was the same mass as for each experiment, Table 3-2). The metal yield from these simulations can be found in Table 4-6. These values are higher than the metal yield from the experiments, see Table 4-3.

Table 4-6: Simulated metal yield in for the different input materials with no carbon in the system.

		Simulated metal out [g]		
		*0.9*Stoichiometric*	*Stoichiometric*	*1.1*Stoichiometric*
Master Slags	*Acidic Slag*	69.23	78.00	87.14
	REC Slag	73.37	82.30	
	Basic Slag	74.95	83.96	

Simulations was also conducted introducing carbon to the system. The amount of carbon necessary, as well as the amount SiC produced, so that the simulated metal yield matches the average metal yield for each experimental series, are found in Table 4-7. This means that the simulated values were a pure metal phase, one pure slag phase, and lastly one pure SiC phase. The reason for the large variations and large amount of C input are that C only reacted with Si in the simulation, forming only SiC. When some of the experimental series had a large metal loss (like, losses from mechanical separation, fuming, metal

lost in slag, and metal lost to carbides), would this need to be corrected with losses of Si through SiC formation.

Table 4-7: Amount of input C and output SiC for the simulated metal yield to match the experimental metal yield.

		C in to system/SiC out of system so simulated metal yield to match experimental metal yield [g]					
		*0.9*Stoichiometric*		*Stoichiometric*		*1.1*Stoichiometric*	
		C in	*SiC out*	*C in*	*SiC out*	*C in*	*SiC out*
Master Slags	*Acidic Slag*	4.5	15.02	4.5	15.2	8.7	29.04
	REC Slag	5.6	18.70	6.0	20.03		
	Basic Slag	5.6	18.70	9.7	32.38		

4.6.2 Simulated composition of metal and slag

The simulated chemical compositions for metal and slag can be found in Table 4-8. The table include values for all experiments both with and without carbon introduced into the system. The general trend is that the Si content in metal and slag decreases, as a part of the input Si reacted with carbon to form SiC.

Table 4-8: Simulated compositions for metal and slag, both for system with, and without carbon introduced. Values are the 3 main elements and impurities.

		Simulated wt% elements/oxides in metal/slag [wt%]							
		Metal (no C in system)				*Slag (no C in system)*			
		Si	*Al*	*Ca*	*Fe*	*SiO_2*	*Al_2O_3*	*CaO*	*FeO/MgO*
Acidic Slag	*0.9*Stoichiometric*	78.01	6.27	15.56	0.16	8.83	54.44	36.53	0.20
	Stoichiometric	75.11	7.80	16.95	0.14	5.03	59.56	35.21	0.20
	*1.1*Stoichiometric*	71.05	11.03	17.80	0.12	2.27	63.52	34.01	0.21
REC Slag	*0.9*Stoichiometric*	70.71	5.71	23.27	0.32	9.65	46.81	43.28	0.25
	Stoichiometric	68.88	6.62	24.22	0.29	6.23	51.53	41.98	0.25
Basic Slag	*0.9*Stoichiometric*	68.18	5.45	26.34	0.04	10.07	43.35	46.32	0.27
	Stoichiometric	66.67	6.17	27.12	0.04	6.86	47.82	45.05	0.27
		Metal (C in system)				*Slag (C in system)*			
Acidic Slag	*0.9*Stoichiometric*	76.60	6.4	16.77	0.19	8.10	54.71	36.99	0.20
	Stoichiometric	73.41	8.23	18.20	0.16	4.31	59.81	35.68	0.20
	*1.1*Stoichiometric*	65.76	14.15	19.92	0.17	1.25	63.39	35.16	0.20
REC Slag	*0.9*Stoichiometric*	68.82	5.84	24.94	0.40	8.55	47.02	44.18	0.25
	Stoichiometric	66.66	6.96	26.03	0.36	5.08	51.73	42.95	0.25
Basic Slag	*0.9*Stoichiometric*	66.36	5.55	28.04	0.05	8.93	43.51	47.30	0.27
	Stoichiometric	63.07	6.66	30.22	0.05	4.86	48.04	46.83	0.27

5 Discussion

5.1 Master slags and experiments stoichiometries

As mentioned in the experimental work was the aimed for CaO/SiO_2 mass ratio 0.7, 1.04 and 1.2 for the acidic-, the REC-, and the basic slags respectively. Later XRF analysis showed that the mass ratios were closer to 0.79, 1.1, and 1.26 (see section 4.1). The analysis showed that the there was a smaller amount of SiO_2 than expected in all of the slag compositions. The REC slag was provided from the REC Silicon with an in-house analysis 51wt% CaO and 49wt% SiO_2. The XRF showed that the CaO concentration was the same but that the SiO_2 was diluted by other impurities in the slag. This can be the reason for the difference in expected and later measured results.

The acidic- and basic master slags was produced by adding SiO_2 or CaO to the REC slag. The added SiO_2 amount was too low for the targeted acidic composition, and the CaO amount was too high for the targeted basic composition, as the calculations for the input SiO_2- and CaO amounts were made using the assumed REC composition. Fuming was observed during fusing of the two new master slags (see section 3.1.2). It is a well-known fact from the silicon industry that Si exits the furnace in the form of SiO fume (see eq. (2.2)). These two effects could therefore explain why the deviations of assumed to measured SiO_2 content, are larger for the basic and acidic slags, than for the REC slag. The fact that the deviations of assumed to measured SiO_2 content are higher for acidic- than for basic slag matches the observation as well. The fuming would affect the slag high in SiO_2 more than the one low in SiO_2. All of these observations help to validate the analysed XRF results.

It can be observed from Figure 2.11 that the higher CaO concentration in the basic slag means that the melting temperature are at almost the exact same as the holding temperature, (T=1650˚C). This is important to keep in mind as small changes in concentration, or too low temperature, means the system no longer will be a pure liquid system. It should also be said that the high CaO content means that a Ca_2SiO_4 phase can be formed. This phase has a self-deprecating effect due to a 12vol% increase that occur in a phase transition during cooling [37]. This phase was later confirmed to be present in the bottom slag powder of the basic slags (see Figure 4.37), through EPMA analysis.

The lower SiO_2 content means that relation between the reductant and SiO_2 will be different from what was intended. This will not be a large problem for the simulated values, as the correct slag compositions were used. The effect an increasing reduction amount have on the system will be correct looking at each slag. A direct comparison of the same stoichiometry for different slags, will not be entirely correct however, as the stoichiometries varies somewhat between each of the three slags (see Table 4-2). Acidic slag has 0.96*stoichiometric reduction amount, while the basic slag has 0.93*stoichiometric reduction amount for the experiments using under stoichiometric reduction amount. This is important to keep in mind for the rest of the discussion.

5.2 Composition of metal and slag

The simulated trends in metal- and slag concentrations between the different experiments are the same the for the system with, and without carbon introduced. When carbon is introduced will the Si concentration in both metal and slag decrease, while Al and Ca concentrations will increase in both slag and metal. This is due to the fact that all carbon goes to form SiC, as mentioned in section 4.6..

This section will discuss the analysed concentrations in metal and slag for the different experiments conducted. The results will be compared to the simulated equilibrium concentrations. This data will only be from the system without carbon, as the simulated concentrations and trends are so similar between the two systems (with/without carbon). The simulated values with carbon are plotted with the experimental values in appendix F.

5.2.1 Effect of reduction amount

Simulations show a decrease in Si-concentration, and an increase in Al- and Ca- concentrations in the metal phase when more reductant is added to the system. This is a general trend for all of the master slags. Simulated values for the slag product unsurprisingly show that the SiO_2- and CaO-concentration will decrease, while the Al_2O_3-concentration will increase. The simulated values without carbon are plotted with the experimental results in the following figures.

Figure 5.1 illustrate that the experimental Si-concentration in the produced metal is higher than the simulated values (exception: basic slag with stoichiometric reduction amount. Will be discussed later). The expected trend of increasing Si with decreasing reduction amount is true for all master slags however. Showing that the purity of the Si metal product will be higher when the reductant addition is lower., as was expected. (Note: that the difference between stoichiometric and over stoichiometric with acidic slag are lower than expected. The data from over stoichiometric are only from one parallel, which makes this less representative, however.).

The SiO_2 concentrations in the slag are plotted in Figure 5.2. It can be observed that it is a corelation between the simulated and the experimental values with regards to the increasing SiO_2 amount with a decreasing reduction amount. The experimental values are close to the simulated values, where most simulated values lie within the error bars of the experimental values. (The experiments with acidic slag and stochiometric, and over stochiometric reductant addition had more notable difference in the experimental SiO_2 concentrations, than in the Si concentrations in the metal. This was more as expected as a higher reductant addition would lead to more SiO_2 being consumed.)

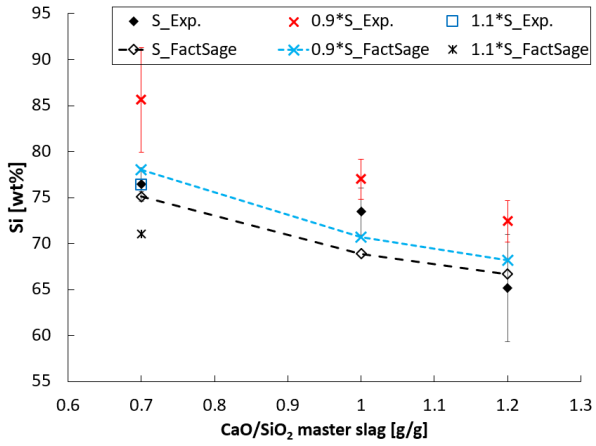

Figure 5.1: Simulated and experimental Si concentration in metal.

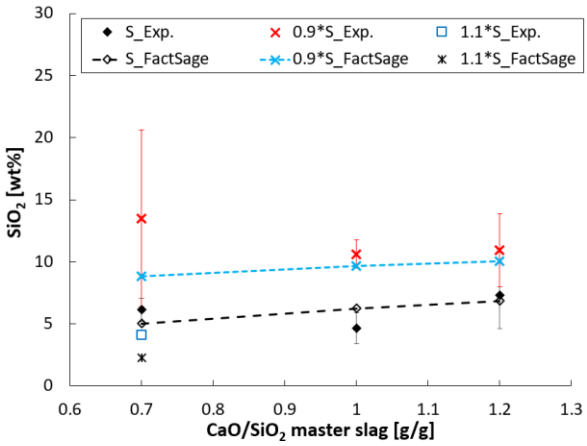

Figure 5.2: Simulated and experimental SiO_2 concentration in slag.

When it comes to the Al content in the metal are the trends from the simulations ones again supported by experimental data. Contrary to the trend observed for Si, did an increase in the reductant addition led to an increase in Al concentration (seen in Figure 5.3). As was the case for Si concentrations, the Al concentrations were generally higher than the simulated values (the exception of this is the acidic slag with 0.9*stoichiometric reductant addition. This will be discussed further later). Note: the experimental differences between acidic slag with over stochiometric reductant addition and stoichiometric reductant addition was small when compared to their respective simulated values.

The trend observed in the metal was the same for the slags: Increasing the reductant addition, increases the Al_2O_3 concentration in the slag, see Figure 5.4.

Note that the experimental Al value in metal is higher (though with how much varies) than the simulated, coupled with a lower experimental Al_2O_3 value than the simulated in the slag, would imply that the system has not reached equilibrium. Note that REC also here is close to the simulated values.

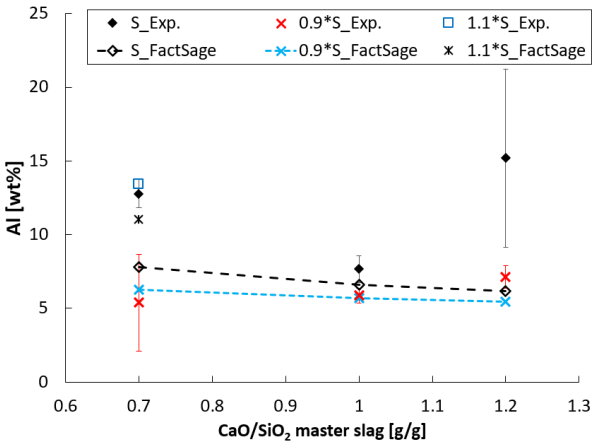

Figure 5.3: Simulated and experimental Al concentration in metal.

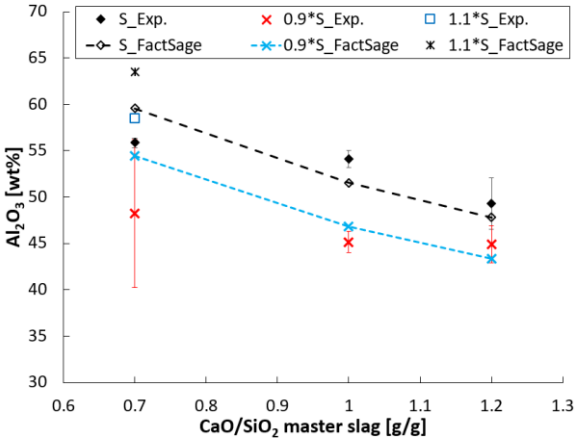

Figure 5.4: simulated and experimental Al_2O_3 concentration in slag.

The simulated Ca concentrations increase with increasing reductant addition, though this difference is small (see Figure 5.5). The small differences between the reductant additions are reflected in the experimental values, as they overlap each other. What is clear is that there is a systematic gap between the simulated values and the experimental values, where the experimental values are lower that the simulated ones.

The simulated trend of higher CaO concentration in the slag with lower reductant addition are present in the experimental values (see Figure 5.6), though the differences are small.

That Si and/or Al are high higher than the simulated values, while the Ca are lower can imply that equilibrium is not reached. Theory seam to imply that there is no problem with transport of CaO in slag, but rather SiO_2. This then imply that the there are some errors in the simulated values instead.

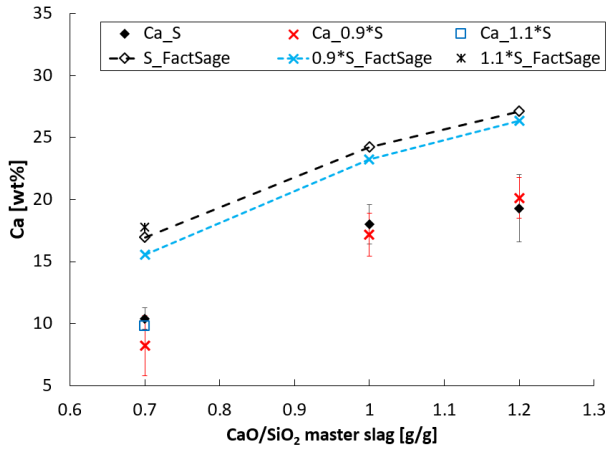

Figure 5.5: Simulated and experimental Ca concentration in metal.

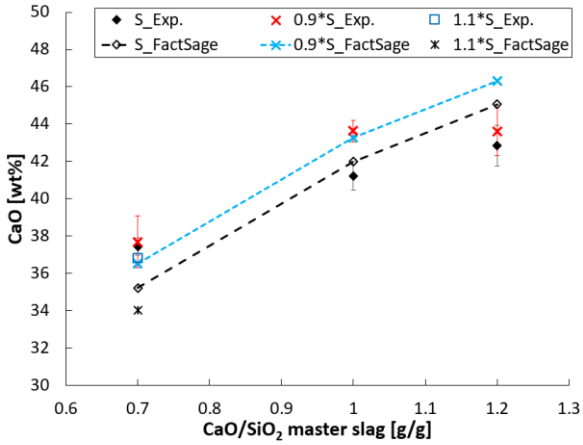

Figure 5.6: Simulated and experimental CaO concentration in slag.

What was observed was that an increase in added reductant led to an increase in the Al concentration, a decrease in the Si concentration, while the Ca concentration was relatively unaffected in the produced metal. An interesting observation was that the experimental metal values for acidic slag with stochiometric, and over stoichiometric reductant addition was so similar, despite the difference in their respective simulated values, as well as for the difference in measured slag concentrations. The system with over stoichiometric reductant addition has one effect on the slag, and another on the metal.

5.2.2 Effect of slag composition

Figure 5.1 show that an increase in CaO/SiO_2 ratio for the master slag would mean a decrease in Si concentration in the produced metal. This trend was apparent for both equilibrium simulations and experimental results. It was however observed that the experimental values were higher than the simulated, with the only exception being the basic slag with stoichiometric reduction amount. This had an average that was somewhat lower than the simulated value. Its corresponding data was collected from only two parallels, as the third failed due to problems with the furnace. There was large difference in both slag and metal composition for the two parallels. The reason for these differences is not fully understood, but it is important to note as it explains the spread in the data. When it comes to the SiO_2 concentration of the product slag did the simulated values show small increase in with increasing CaO/SiO_2 ratio (see Figure 5.2). This trend was not so clear, though all of the experimental values (with the exception of REC slag and stoichiometric reduction amount) are higher than the simulated ones. This was most prominent for the acidic slag. These results are counter intuitive as less Si should be available to form oxides in the slag when a higher-than-expected concentration is found in the metal. The reason for the higher-than-expected Si in the metal can simply be that the system has not reached equilibrium or that the databases used in the simulations are in need of updating. This does not explain the high SiO_2 content in the slag however. The most likely explanation to this is that the slag had both metal droplets as well as SiC particles that would be part of the analysed slag. Si from metal droplets and in SiC would mistakenly be measured as SiO_2 in the EPMA analysis of the slag. (This will be discussed further later, when mass balance is taken into account).

The simulated concentration for Al in metal has only a slight decrease in value with an increasing CaO/SiO_2 concentration. (NB: it is important to remember that the input Al/SiO_2 ratio decreased with the CaO/SiO_2 ratio, as the master slag analysis was done after the experiments was conducted (see Table 4-2). This is probably the largest reason for the decrease). The experimental values for the REC slag are close to the simulated values, while the data from the acidic and basic slags deviate more form the simulated values. The difference between the different reduction amounts deviate from each other as the values for 0.9*stoichiometric reduction amount are close to the simulated values, but the stoichiometric are higher with about 5 wt% difference for both acidic- and basic master slag (see Figure 5.3). These two had a smaller deviation in simulated and experimental Si concentration, where the rest had in general higher experimental values than the simulated ones (see Figure 5.1). This means that it is reasonable to believe that Al was not finished reacting for these two, implying that equilibrium was not yet reached. It is previously explained that the basic slag had high uncertainties, and large variations between parallels. This makes it hard to say anything for certain. The acidic slag did not vary much between parallels, implying that it is a systematic trend for this slag and stoichiometry to have a higher than simulated Al value after 60 minutes. Park et al. [29] found that it was the transport in of SiO_2 in a SiO_2-CaO-Al_2O_3 that was the rate determining step during aluminothermic reduction of SiO_2. This could explain the difference the high Al and low Si concentration as the reaction would slow down when most of the SiO_2 in the slag was used due to the slow transport of SiO_2. When a smaller reduction amount is introduced (as with under stoichiometric) would the SiO_2 be more abundant compared to the Al, meaning that transport would not be an issue before the system reached equilibrium. If more Al need to react to form more Si doe this imply that: the equilibrium calculations are wrong and that the reactions are still going and have not reached equilibrium, or that Si are SiC/trapped in slag. Both of these explanations are dependent on the fact that the simulated values are wrong and that there is expected a higher Si concentration. Bjørnstad and Tranell [32] wrote that the presence of Ca in slags was necessary as it, would allow the amphoteric Al to act as a network former which is its lowest energy level in oxides melts. This could help to explain the reason for the high deviations on over stoichiometric reductant addition on the acidic slag (as the slag is low in Ca). It is unclear to the author if the simulation database takes this into account. The simulation software does not give a perfect representation of reality. This is proven as it assumes that all C added to the system forms SiC, yet it is observed experimentally (see Figure 4.38) and in theory[39], that C also reacts with Al to form carbides. The simulated values for

Al_2O_3 concentration are decreasing with CaO/SiO_2 concentrations (see Figure 5.4). This trend is not that clear in the experimental values. How the experimental deviate from their respective simulated value varies for each master slag. The experimental values are lower than the simulated, for the acidic slag. This makes perfect sense from the previous observations, as mor than simulated Al are left in metal and that there is a higher SiO_2 (most probably due to metal in slag) that dilutes the analysed Al_2O_3. The simulated value is lower for high reductant addition and higher for the low reduction amount, for the REC slag, though these values are close to their simulated value. The experimental values are higher than their respected simulated values, for the basic slag. Though also these deviates little from each other, when compared to the acidic slag.

The simulated concentration of Ca in metal is increasing with increasing CaO/SiO_2 ratio in the start slag. This is reflected in the experimental values as they also have an increasing trend (see Figure 5.5). Earlier it was mention that the simulated values were systematically higher than the experimental. This explains the overall higher value for Si, Al, or both, for all slags and stoichiometries mentioned above. As mentioned earlier is it theorised that the equilibrium simulations simply can be wrong and that the measured values are the actual stable values. There is of course the possibility that it is the transport of the Ca specie that is the rate determining step, though it is found that it is the transport of SiO_2 in slag that is that is the rate determine step due to its structural forming abilities [29]. If it was transport that was the problem, would it therefore be reasonable to assume that the Si convention in metal would be lower and that the Ca concentration would be corrected continuously. It should also be mentioned that there was observed large amount of Si_2Ca phase throughout the slags during the EPMA analysis. If this phase is stable in the slag could large amount of Ca and Si be trapped, as if would not be a driving force for it to react as it already is metal. (This will be discussed further later). The experimental concentration of CaO is general higher than the simulated, for the acidic slag. For the REC slag are they quite close to simulated but under stoichiometric are higher, and stoichiometric are lower. Basic slag has experimental values generally lower than the simulated values. It is important to remember that the analysed basic slag only is from the top of the crucible as the bottom slag were crushed to powder (see Figure 4.22). As mentioned earlier was this powder identified as, slag similar to the top slag, as well as a large amount of the Ca_2SiO_4 phase. This can help to explain the lower-than-expected amount of CaO.

5.3 Metal yield/mass balance

In this section will the experimental composition data, be discussed in light of metal yield to get a better understanding of where the different elements put into the system ended up.

5.3.1 Metal losses

Metal loss can be calculated by subtracting the metal yield (see Table 4-4) with the theoretical metal yield from the simulations. As discussed previously do the simulated metal composition not match the experimental values. A new theoretical metal yield can then be calculated by assuming that the measured composition is representative as a whole for the metal. This metal yield is calculated by using the input mass of the aluminium with these values (see appendix G for calculations). The losses in grams and weight percent from both theoretical masses can be found in Table 5-1. It is observed that the losses are higher when the difference between simulated metal yield and actual metal yield are considered, rather than when the differences between calculated metal yield and actual metal yield are considered. This can be explained by the fact that the Ca concentration was lower for the analysis values than the simulated ones. An increase in Ca will increase the mass of the output material, as the molar mass of Ca is higher, while the oxidation number is lower than both Si and Al.

Table 5-1: The metal loss of theoretical metal mass in g and wt%. Theoretical mass calculated from analysed metal composition, and theoretical mass form the FactSage simulation.

			Mass loss from theoretical mass (calculated/simulated)			
			Calculated mass (analysis)		*Simulated mass (FactSage)*	
		Parallels:	*Mass loss [g]*	*Mass loss [wt%]*	*Mass loss [g]*	*Mass loss [wt%]*
Acidic Slag	*0.9*Stoichiometric*	*1*	43.28	67.54	48.43	69.96
		2	8.73	12.91	10.35	14.95
		3	10.49	15.62	12.60	18.20
	Stoichiometric	*1*	6.61	8.65	8.22	10.54
		2	9.98	13.26	12.70	16.28
		3	11.53	15.10	13.18	16.89
	*1.1*Stoichiometric*	*1*	-	100	-	100
		2	18.63	22.36	22.41	25.72
REC Slag	*0.9*Stoichiometric*	*1*	10.32	14.53	12.70	17.30
		2	13.30	19.04	16.84	22.95
		3	13.42	18.92	15.85	21.60
	Stoichiometric	*1*	14.62	18.17	16.47	20.02
		2	13.67	17.34	17.13	20.82
		3	11.73	14.84	15.00	18.23
Basic Slag	*0.9*Stoichiometric*	*1*	10.58	14.44	12.25	16.34
		2	14.41	20.19	17.96	23.96
		3	12.97	17.82	15.14	20.20
	Stoichiometric	*1*	20.37	24.92	22.59	26.91
		2	21.92	26.83	24.19	28.81

There are 4 main factors that can explain the metal loss. The first is fuming, as it is a well-known fact from the silicon industry that material exits the furnace in the form of SiO- and CO-gass, (see eq.(2.2)) [7]. The losses noted from the experiments are found in Table 4-3, though these alone are not enough mass to explain the large metal losses, as the maximum loss from fume was 3.35g, corresponding to 1.0 wt% of the input charge. Losses can also be due to reactions between metal and carbon, as they form carbides. Both silicon carbides, as well as some aluminium carbides were found in the slag (see Figure

4.38). Hoseinpur and Safarian [39] studied the rection between Si and Si20wt%Al-alloys with graphite crucibles. They found that both silicon carbides, aluminium carbides, as well as aluminium silicon carbides was created on det surface and in the pores in the crucible. It was also discovered that SiC particles loosened from the walls and ended up in the melt at temperature of 1800˚C. This can explain the SiC particles observed throughout the slags. There is also the fact that metal was lost during the separation prosses, which can explain the metal losses (The mechanical separation gives a relatively large uncertainties as the reason for this is simply due to human error). Lastly is the fact that there is metal still entrapped in the slag. Droplets and veins of metal with roughly the same phase composition as the bulk metal, together with dispersed Si_2Ca was found in all slag samples. This is furthered backed as subtracting the analysis results from the area scan of the slag with a low magnification (large area of slag with more metal droplets), with analysis done on a high magnification (smaller area of the slag with less metal droplets), end up with a positive value for SiO_2-consentration and negative results for Al_2O_3- and CaO concentrations for all experiments (see section **Error! Reference source not found.**). This is not a good quantitative measurement of metal concentration in the slag, though it does show qualitatively a trend which implies that there are metal droplets dispersed throughout all slags and all experiments (this is also true for SiC, which was found in clusters throughout the slag).

In a specialisation project conducted by the author [34], kinetic experiments were conducted using dross and pure aluminium as reductant in combination with the REC slag. Si-alloy droplets together with Si_2Ca metal was found disperse throughout the slag. Analysis done later of these slag pieces showed that metallic Si content were between 2-3%. J. F. White[31] studied the kinetics between a Si-alloy and SiO_2-CaO slags with mechanical stirring, at 1550˚C. There was formed an emulation with metal dispersed in the slag. The amount of metal dispersed throughout the slag was reduced over time as the composition got closer to equilibrium and the interfacial tension between metal and slag became higher than the energy from the reactions between the metal and slag, and stabilized at about 2%. Even though White did not have Al in his system, and used mechanical stirring, is it reasonable to assume that the system works in a similar way, as experiments conducted in this thesis will have some stirring from the induction. These results imply that there are hard to get all the metal out of the slag. Calculated metal loss from Table 5-1 was compared to the slag mass (slag mass are assumed to be rest after mass from fume losses (see Table 4-3) and separated metal (see Table 4-4) was subtracted from input mass) to find a potential wt% of slag that was entrapped metal. There are assumed no losses during separation. The result of the maximum entrapped concentration metal in slag are fund in Table 5-2.

Table 5-2: Show the maximum calculated wt% of slag that is entrapped metal. There are here assumed no losses during separation, nor to carbides.

		Slag weight that is metal, assuming no losses during separation [wt%]							
		*0.9*Stoichiometric*			*Stoichiometric*			*1.1*Stoichiometric*	
	Parallel #:	*1.*	*2.*	*3.*	*1.*	*2.*	*3.*	*1.*	*2.*
Master Slags	*Acidic Slag*	14.2	3.3	3.8	2.5	3.7	4.2	-	6.6
	REC Slag	3.2	4.2	3.7	4.6	4.3	3.7		
	Basic Slag	3.1	4.2	3.8	7.1	7.6	-		

5.3.2 Elemental balance for Acidic Slag

The calculated Si recovery (see section 4.5.3 for all) for the acidic master slags, together with the theoretical simulated values are plotted in Figure 5.7. (Note that parallel 1 with 1.1*stoichiometric reductant addition is not plotted as it did not have coalesced metal, see section 4.4.2). A general trend for all stoichiometries is that the Si recovery are too low. The combined Si recovery is between 80.4-90.0 wt% of the total input. Note also, Si recovery in metal is between the simulated values for systems

with no C (higher than experimental), and those with C (lower than experimental). The only exception to this is parallel 1 with 0.9*stoichiometric reduction amount, which was one of the experimental outliers with a small metal yield, (see section 4.4.2). For 0.9*stoichiometric reduction amount was the Si recovered to metal between 30-74 wt%, while the Si recovered in slag was between 17-50wt%. The simulated Si recovery without/with C, were; 83.5-68.6 wt% in metal, 16.5-15.1 wt% in slag, and 0-16.3 wt% in SiC. The first parallel with 0.9*stoichiometric reductant addition is one of the outliers described in the section 4.4.2, which is the reason for the low Si recovery in the metal despite having a high Si concentration in the metal. It has over all a low Si recovery, though it has the highest Si recovery in the slag. EPMA showed that a high SiO_2 content in the slag (slag phases high in Si seen in section 4.4.3), but did it also have an unusual high amount of metal droplets. The overall low Si recovery in this therefore concluded to be due to metal being trapped in the slag. The other two parallels had a Si recovery to slag between 17-18 wt%, and 73-74 wt% to the metal. The somewhat higher Si in slag can be explained by metal droplets and while the metal recovery lies between the two simulated values. This indicate that there are some losses to metal droplets/SiC formation not analysed in the slag, while the reason for the for the overall losses is probably due to losses during the metal separation and some from fuming.

For stoichiometric reduction amount was the Si recovery in metal between 76-82 wt%, while the Si recovery in the slag was between 12-13 wt%. The simulated Si recovery without/with C, were; 90.6-75.7 wt% in metal, 9.4-8.0 wt% in slag, and 0-16.3 wt% in SiC. These samples are close to the two previously mentioned 0.9*stoichiometric parallels. The high Si recovery is probably due to SiC and metal droplets in the slag. This is supported as Table 5-2 show that the potential metal lost in slag are relatively low. As it was observed metal in slag, combined with the fact that some metal are expected to form a stable dispersed with the slag [31], does it indicate that there was little metal that was lost in separation.

For 1.1*stoichiometric reduction amount was it only one parallel with coalesced metal. The Si recovery in metal was 77 wt%, while the Si recovery in the slag was 8 wt%. The simulated Si recovery without/with C, are; 95.8-66-2 wt% in metal, 4.2-2.3 wt% in slag, and 0-31.5 wt% in SiC. This parallel has a relatively high Si recovery into the in the slag, and a low Si recovery to metal (despite having a higher-than-expected Si concentration in its metal product (mentioned in section 5.2.1)) compared to simulated values, (see Figure 5.1). It also a larger metal loss (Table 5-1). The high Si recovery in slag could be explained by the metal droplets, while the low recovery to metal could simply be due to unusually high metal losses from the separation. However, there is also the possibility off losses of Al, either to carbide or in droplets in the slag. Figure 4.38 illustrate an Al metal droplet between the crucible wall (forming carbides) and Ca/Al slag, for this sample. The formation of Al carbides and how it seeps into the pores of graphite are described by Hoseinpur and Safarian [39]. If the transport of SiO_2 is slow, and there are no available SiO_2 in the slag is it possible that patches of Al simply react with the graphite wall and seps in to its pores creating carbides (as mentioned previously) instead of contributing to the aluminothermic reduction. If enough Al are “lost” in local pockets like this, will the practical Al amount in the system be closer to that of on with less Al, explaining the similarities in metal concentration between stoichiometric and 1.1*stoichiometric reduction amount discussed in section 5.2.1. This could also explain where a large portion of the metal went, as chemical analysis was conducted on slag samples that was taken from more central areas of the crucible and not from the edges. This should be investigated further at a later date. The truth of the matter is probably a combination of all of the points mentioned above.

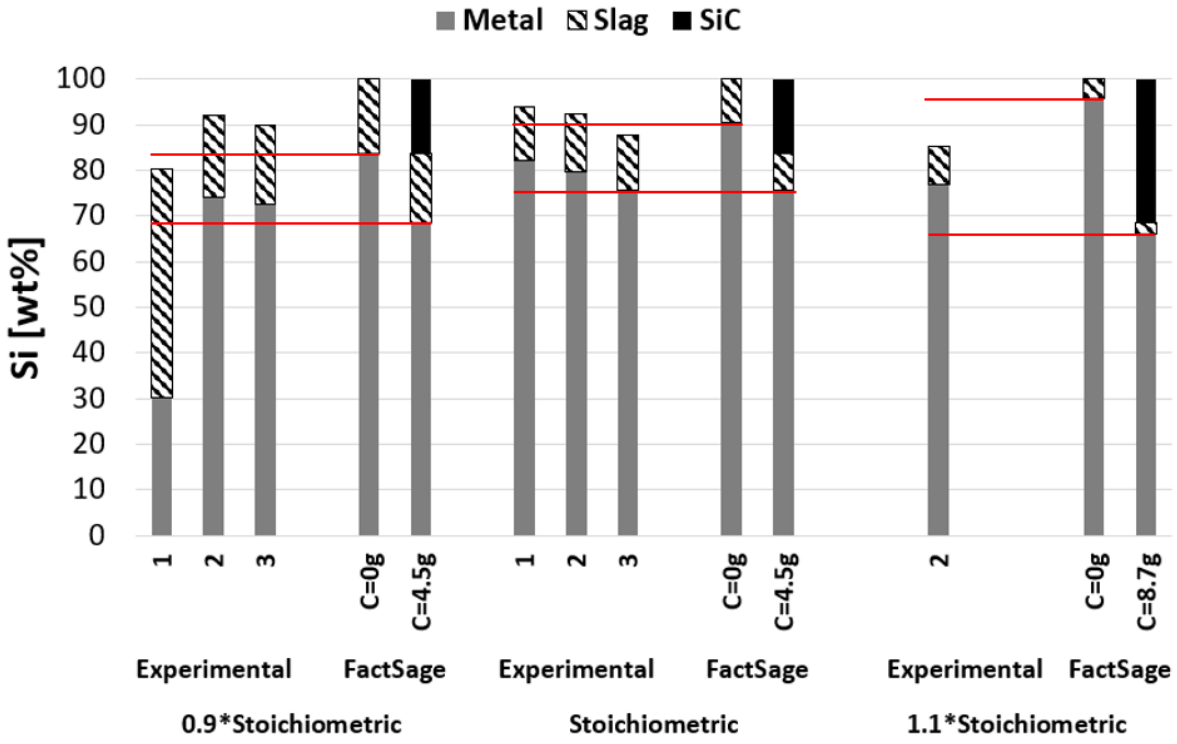

Figure 5.7: Calculated Si recovery for Acidic slag, compared with the simulated values with and without C.

The total Al recovery varied between 77.3-102 wt%, for acidic slag (see Figure 5.8). For 0.9*stoichiometric reduction amount was the Al recovery in metal between 0-6 wt%, while it in slag was between 77-96 wt%. The simulated values without/with C were; 5.3-4-3 wt% for metal, and 94.7-95.7 wt% for slag. With the exception of the first parallel (already discussed), is the Al recovery close to the simulated.

For stoichiometric reduction amount was the Al recovery in metal between 9-10 wt%, while it for slag was between 89-92 wt%. The simulated values without/with C were; 7.0-6.3 wt% for metal, and 93.0-93.7 wt% for slag. The recovery is close to the simulated, though with more in metal and less in slag than simulated. As the metal losses are relatively small (see Table 5-1) and the chemical analysis is skewed in the same way was the Al recovery as expected.

For 1.1*stoichiometric reduction amount was the Al recovery in metal 9 wt%, while it for slag was 90 wt%. The simulated values without/with C were; 10.0-9.6 wt% for metal, and 90.0-90.4 wt% for slag. The small difference in Al recovery in metal and over all Al loss, can be explained by the higher metal loss from separation (see Table 5-1) and to slog, as the Al concentration in metal was higher than simulated. This may be explained by the lost pockets explained in the previous when discussing Si, though more data is needed to say anything conclusive.

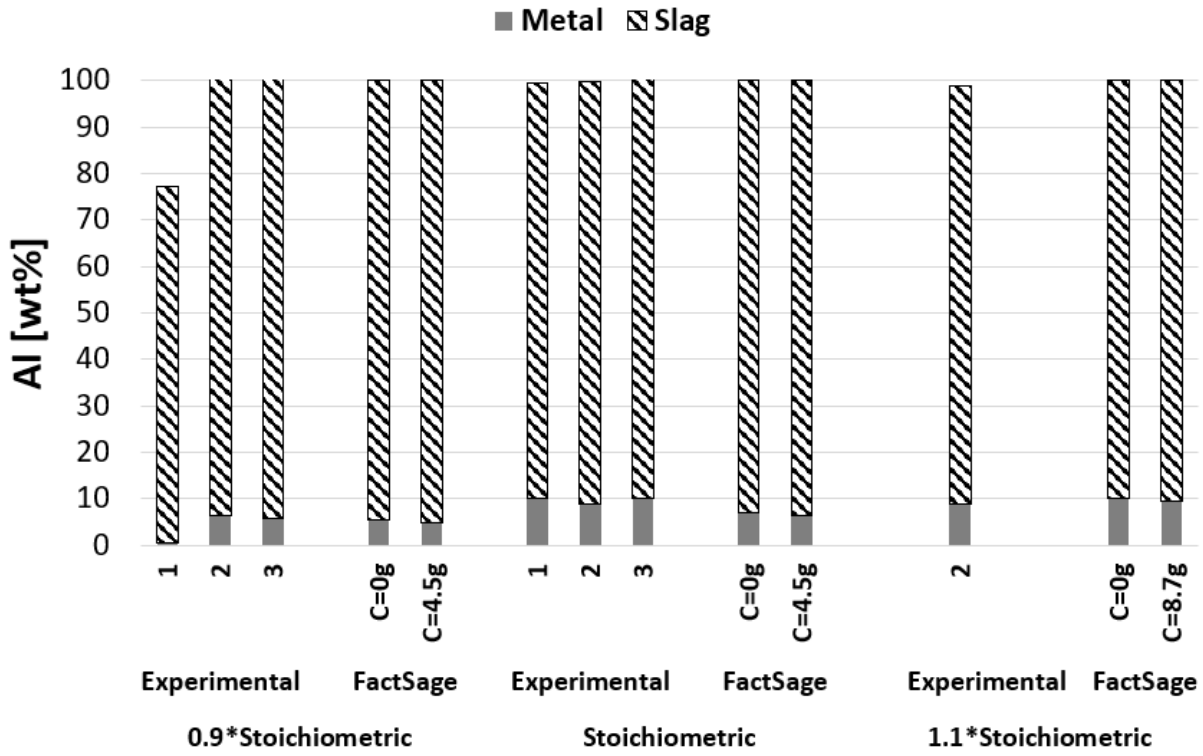

Figure 5.8: Calculated Al recovery for Acidic slag, compared with the simulated values with and without C.

The total Ca recovery in for the acidic slags, both experimental and simulated are plotted in Figure 5.9. The total calculated Ca recovery for the experimental values varied between 97.1-111.1 wt%. For 0.9*stoichiometric reduction amount was the Ca recovery in metal between 1.3-7.8 wt%, while it for slag was between 94.1-109.8 wt%. The simulated values without/with C were; 13.8-12.4 wt% for metal, and 86.2-87.6 wt% for slag.

For stoichiometric reduction amount was the Ca recovery in metal between 7.9-10.0 wt%, while it for slag was between 91.7-94.1 wt%. The simulated values without/with C were; 16.9-15.5 wt% for metal, and 83.1-84.5 wt% for slag.

For 1.1*stoichiometric reduction amount was the Ca recovery in metal 8.2 wt%, while it for slag was 95.4 wt%. The simulated values without/with C were; 19.9-16.6 wt% for metal, and 90.0-90.4 wt% for slag.

The general trend for all experiments on with acidic slag was a lower-than-expected Ca recovery in the metal, and a higher Ca recovery in the slag. This is simply because of the overall lower Ca concentration in the metal (see Figure 5.5). The reason for the over 100% recovery is that the slag weight is calculated as all that is left after losses from fume and the metal weight is subtracted. Samples with high metal loss, will get a higher assumed slag mass, which again have a high CaO content. The fact that Si_2Ca metal are found together with metal droplets with same phase composition as bulk metal can explain some of the high CaO content analysed. This effect would not be significantly large enough as the seen in Figure 4.48, as all values are negative. The possible effect Si_2Ca would have on to increasing the analysed CaO is still overshadowed how Si in metal droplets skews the slag composition.

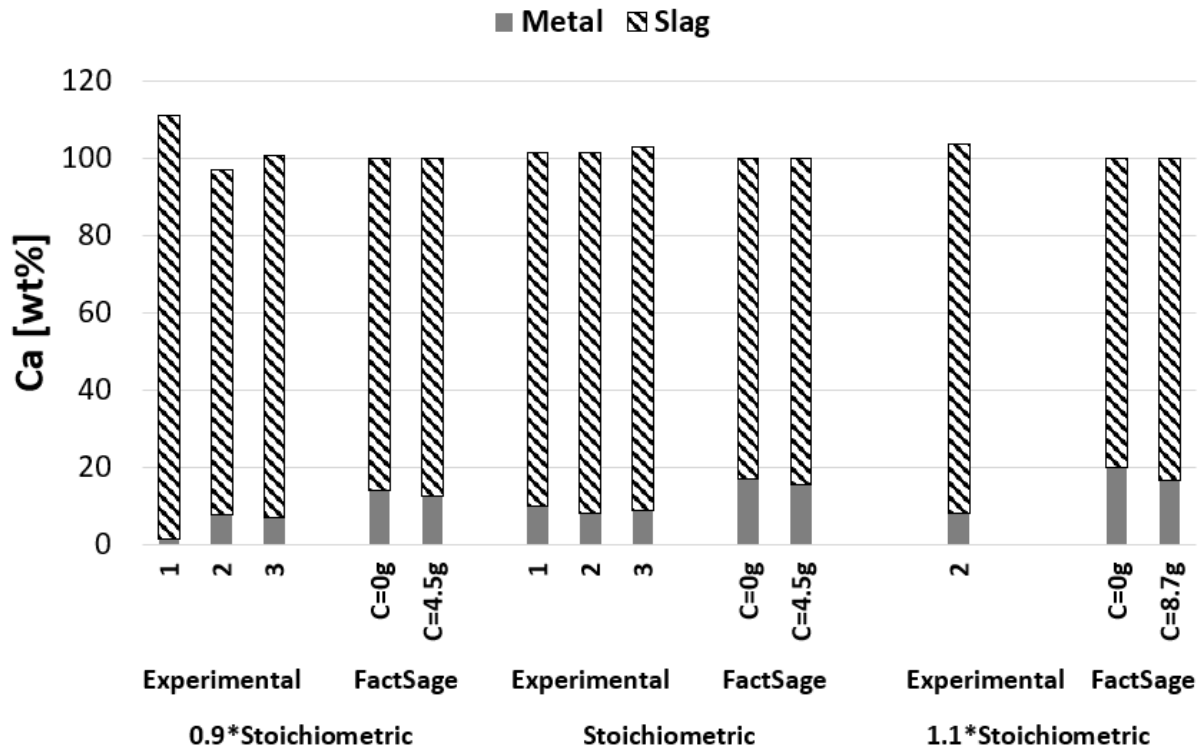

Figure 5.9: Calculated Ca recovery for Acidic slag, compared with the simulated values with and without C.

The trends for the elemental balance for acidic slag is that there is loss in Si, where most are believed to be from metal losses during separation, losses of metal in slag/SiC, and form fuming. Fuming is believed to be part of the problem though it is not enough data to say anything for certain (see Table 4-3), and even with the highest mass loss recorded is it not enough to explain all of the Si loss. It is also observed a low Ca recovery in the metal. This cannot be explained by the metal losses but is probably due to the lower-than-expected Ca concentration in the metal. What is observed is that Acidic slag varies quite a bit for some of its parallels. The Si recovery was quite high, it is important to remember that the Al/SiO_2 was higher for acidic slag than the other two however.

5.3.3 REC Slag

The Si recovery for the REC slag, both experimental and simulated, are plotted in Figure 5.10. The trend where the Si recovery in the metal lies between the two simulated values also observed for acidic slag was also present for REC slag. The calculated total Si recovery for REC slag was between 89.3-95.3 wt%. For 0.9*stoichiometric reduction amount was the Si recovery in metal between 67.0-70.5 wt%, while it for slag was between 21.3-25.1 wt%. The simulated values without/with C were; 79.3 61.5 wt% for metal, 20.7-18.5 wt% for slag, and 0-20.0 wt% for SiC. The higher Si recovery in the slag can be contributed to metal particles and SiC fond throughout the slag. The overall losses in Si are attributed to mainly the metal loss in from separation and losses in the slag that was not analysed.

For stoichiometric reduction amount was the Si recovery in metal between 71.3-75.3 wt%, while it for slag was between 18.2-19.5 wt%. The simulated values without/with C were; 86.6-67.6 wt% for metal, 13.4-11.0 wt% for slag, and 0-21.4 wt% for SiC. The situation is the same for stoichiometric as whit 0.9*stoichiometric, though stoichiometric has a larger Si recovery in the metal.

When comparing the REC to results from acidic slag is it clear that acidic has a higher Si recovery in the metal. REC slag had a general higher metal loss than the acidic slag (see Table 5-1) though these results have large uncertainties, but as mentioned in Table 4-2, do the acidic slag have a larger Al to SiO_2 ratio than the other slags. Both acidic- and REC slag had a general higher Si recovery to the metal for stoichiometric reductant addition than for 0.9*stoichiometric reductant addition.

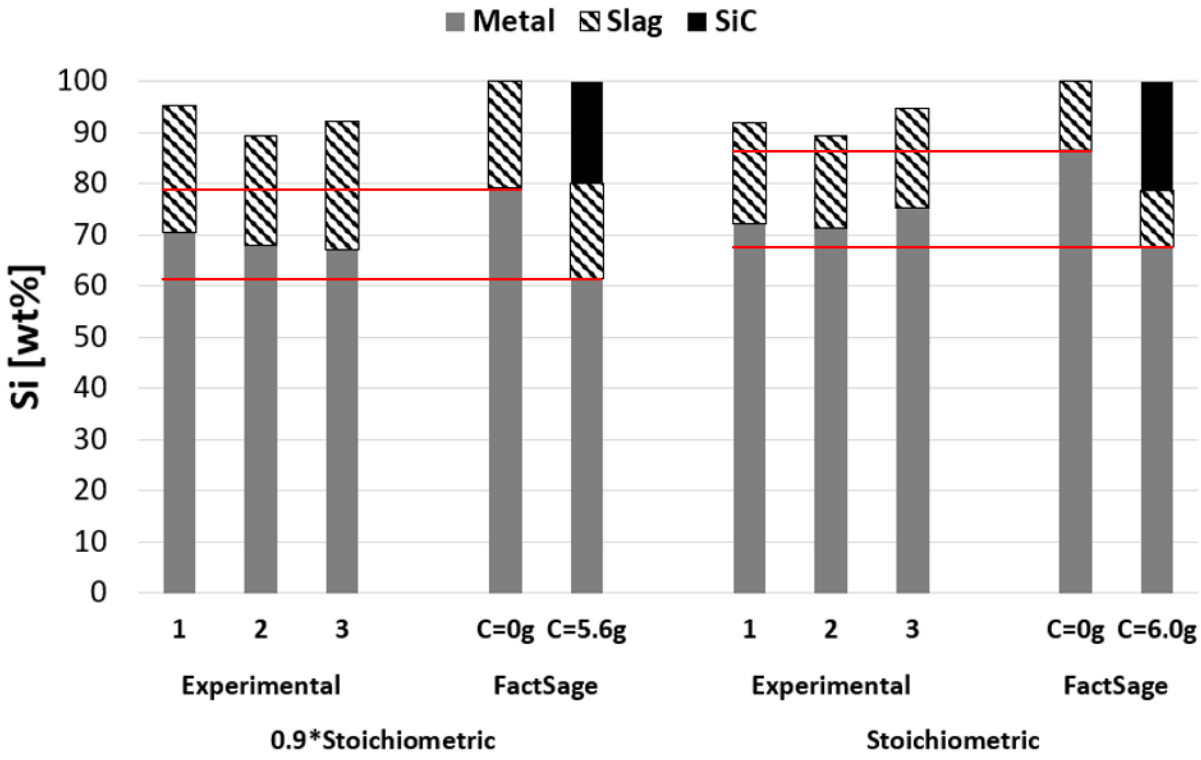

Figure 5.10: Calculated Si recovery for REC slag, compared with the simulated values with and without C.

The calculated total Al recovery for REC slag was between 95.1-104.4 wt% (see Figure 5.11). For 0.9*stoichiometric reduction amount was the Al recovery in metal between 3.6-4.3 wt%, while it for slag was between 94.1-100.8 wt%. The simulated values without/with C were; 5.3-4.3 wt% for metal, and 94.7-95.7 wt% for slag. The results were close to the expected values.

For stoichiometric reduction amount was the Si recovery in metal between 6.1-6.4 wt%, while it for slag was between 88.7-94.2 wt%. The simulated values without/with C were; 6.2-5.3 wt% for metal, and 93.8-94.7 wt% for slag. These results were also close to the expected values, when compared to the analysed composition.

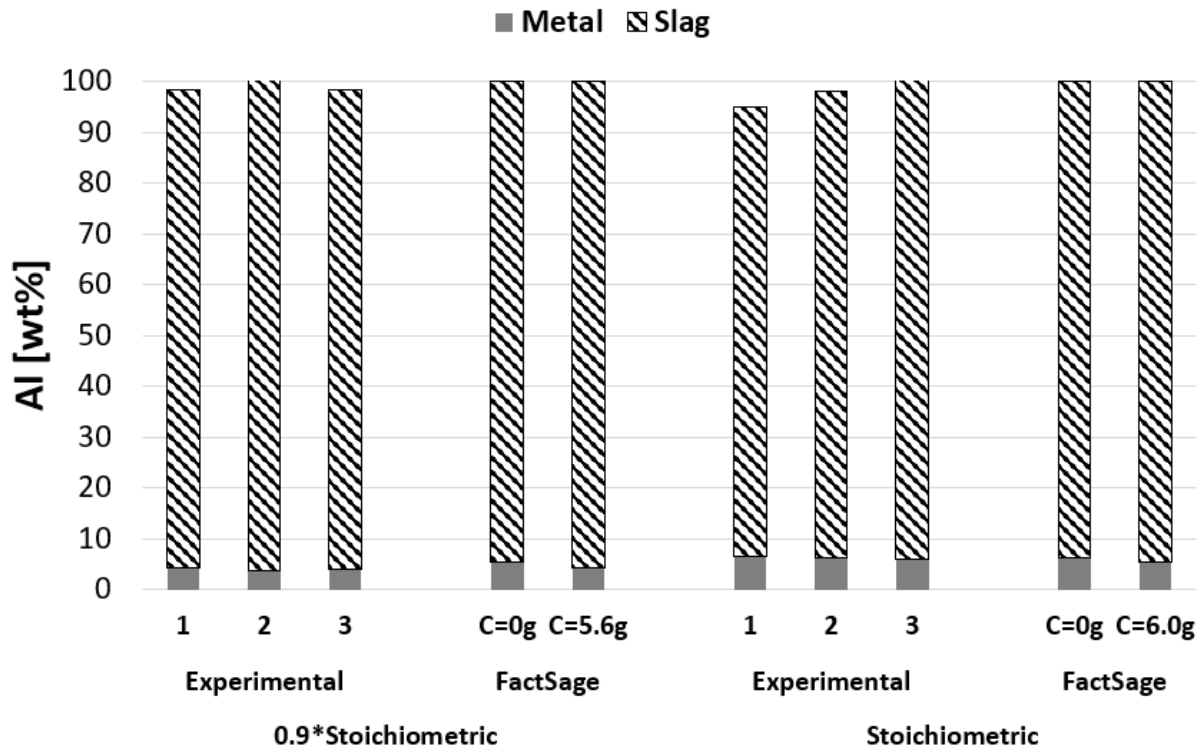

Figure 5.11: Calculated Al recovery for REC slag, compared with the simulated values with and without C.

The calculated total Ca recovery for REC slag was between 94.0-100.8 wt% (see Figure 5.12). For 0.9*stoichiometric reduction amount was the Ca recovery in metal between 8.1-9.9 wt%, while it for slag was between 90.0-90.9 wt%. The simulated values without/with C were; 15.5-13.3 wt% for metal, and 84.5-86.7 wt% for slag.

For stoichiometric reduction amount was the Ca recovery in metal between 11.3-11.4 wt%, while it for slag was between 82.5-85.1 wt%. The simulated values without/with C were; 18.1-15.7 wt% for metal, and 81.9-84.3 wt% for slag.

There were no large surprises in the Ca recovery for neither slag.

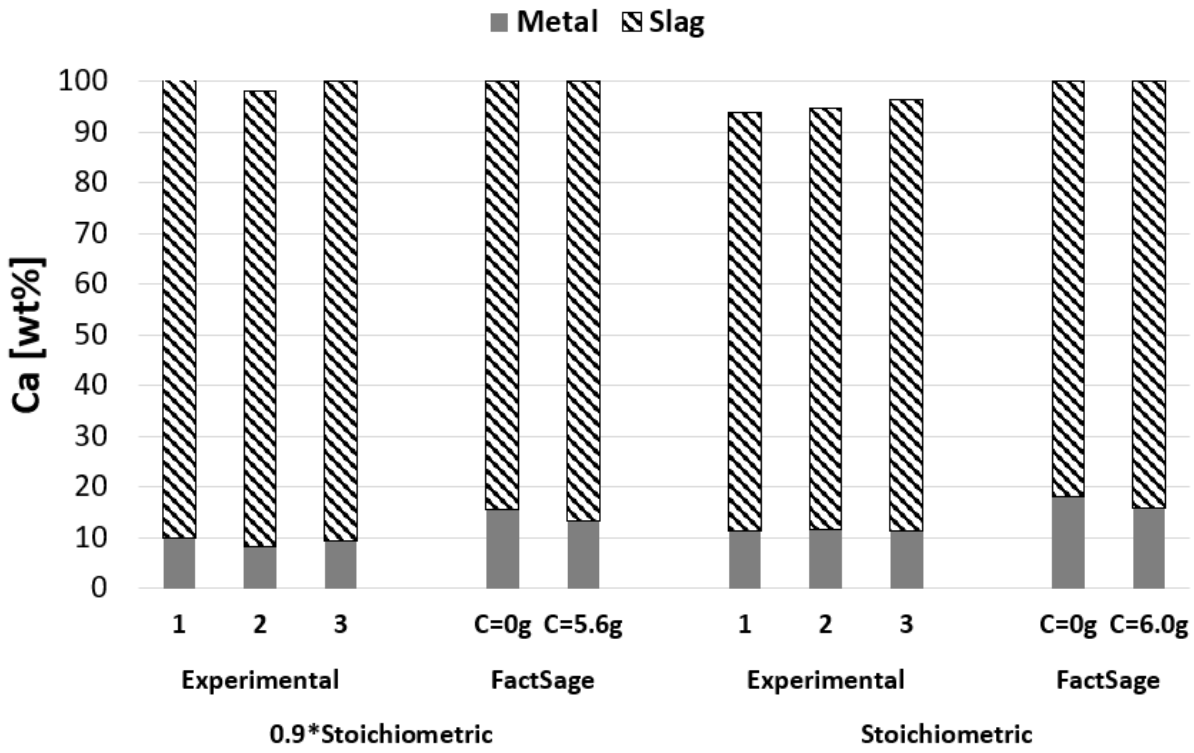

Figure 5.12: Calculated Ca recovery for REC slag, compared with the simulated values with and without C.

5.3.4 Basic Slag

The Si recovery for the basic slag, both experimental and simulated, are plotted in Figure 5.13. The trend where the Si recovery in the metal lies between the two simulated values observed for both acidic- and REC slag was also present for basic slag. The calculated total Si recovery for basic slag was between 69.8-94.6 wt%. For 0.9*stoichiometric reduction amount was the Si recovery in metal between 64.3-66.5 wt%, while it for slag was between 21.1-30.3 wt%. The simulated values without/with C were; 77.0-59.7 wt% for metal, 23.0-20.6 wt% for slag, and 0-19.7 wt% for SiC. As with acidic- and REC slag are the losses contributed to metal loss (this was overall high for basic slag) in separation, fuming, and losses in SiC and metal droplets in slag. The slag on the other hand had a much metal, but also SiC particles distributed throughout the slag, that could raise the overall Si concentration. The largest source of error was that only the top most part of the slag was analysed as the bottom was cracked due to the self-decrepitating Ca_2SiO_4 phase.

For stoichiometric reduction amount was the Si recovery in metal between 57.3-62.0 wt%, while it for slag was between 12.5-23.8 wt%. The simulated values without/with C were; 84.3-54.6 wt% for metal, 15.7-11.2 wt% for slag, and 0-34.2 wt% for SiC. What was interesting for the stoichiometric was that the two parallels analysed varies widely in metal composition and slag composition (as mentioned in section 5.2.2). For when parallel 1 had smaller concentration of Si in the metal did it also have a smaller concentration of Si in the slag. The reason for the low Si in metal is probably due to unreacted Al. The reason for the high Si concentration in the slag of the second parallel is found to be due to a high amount of metal in it. All analysis had metal in it (even on larger magnification), especially the Si_2Ca found throw-out the slag of many slag samples. The large variations are most probably due to the high melting point of the start slag, as it is around the operation temperature. The large overall losses will here most probably be due to unreacted metal and losses in the separation process. See Table 5-1.

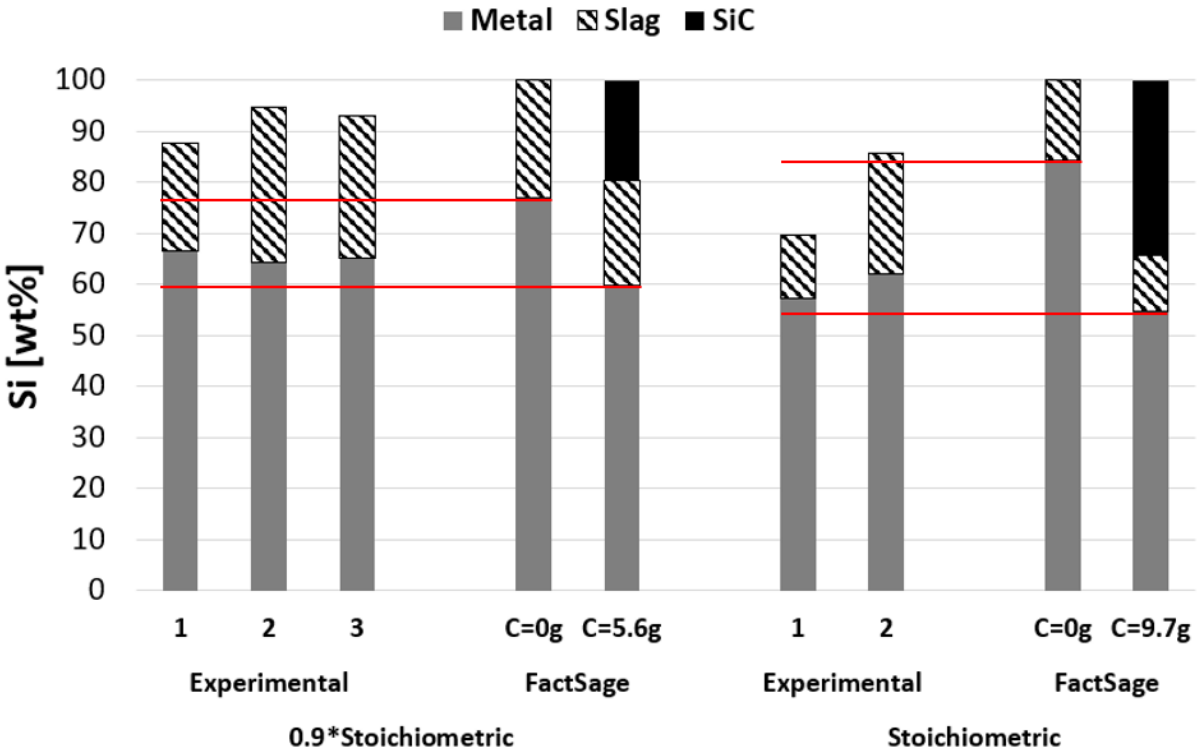

Figure 5.13: Calculated Si recovery for Basic slag, compared with the simulated values with and without C.

The calculated total Al recovery for basic slag was between 104.8-123.5 wt% (see Figure 5.14). For 0.9*stoichiometric reduction amount was the Al recovery in metal between 4.6-6.4 wt%, while it for slag was between 99.6-106.4 wt%. The simulated values without/with C were; 5.2-4.2 wt% for metal, and 94.8-95.8 wt% for slag. The high Al recovery to the slag can probably be explained by the tu uncertainties due to the self-decrepitating phase described earlier.

For stoichiometric reduction amount was the Al recovery in metal between 6.6-14.5 wt%, while it for slag was between 98.2-109.0 wt%. The simulated values without/with C were; 5.9-4.4 wt% for metal, and 94.1-95.6 wt% for slag. As mentioned for the Si recovery did the first parallel have a high concentration of Al in the metal. This coupled together with the lower metal/SiC concentrations in the slag, when compared to the second parallel, explains the high Al recovery.

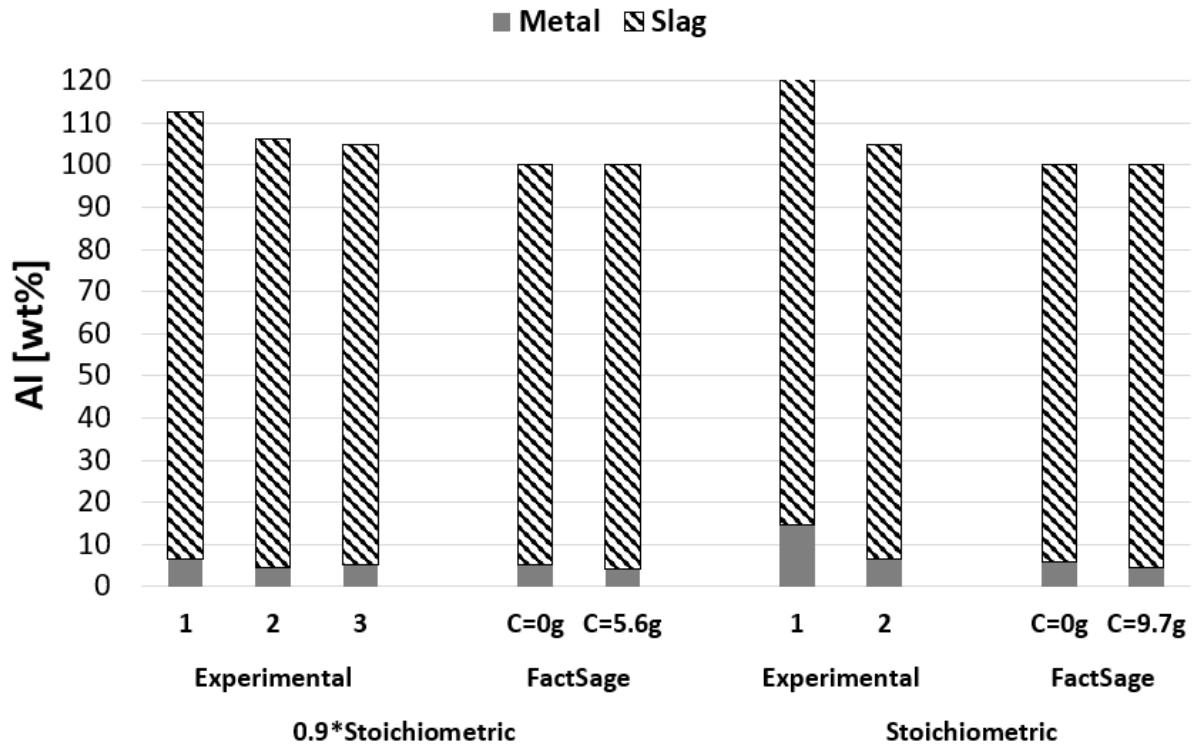

Figure 5.14: Calculated Al recovery for Basic slag, compared with the simulated values with and without C.

The calculated total Ca recovery for basic slag was between 91.4-95.4 wt% (see Figure 5.15). For 0.9*stoichiometric reduction amount was the Ca recovery in metal between 8.2-10.5 wt%, while it for slag was between 83.2-85.2 wt%. The simulated values without/with C were; 15.5-13.2 wt% for metal, and 84.5-86.8 wt% for slag.

For stoichiometric reduction amount was the Ca recovery in metal between 8.5-9.9 wt%, while it for slag was between 83.1-85.5 wt%. The simulated values without/with C were; 17.9-13.6 wt% for metal, and 82.1-86.4 wt% for slag.

There are no large surprises for neither stoichiometries. The overall Ca recovery is lower than simulated, in both metal and slag leading to a loss in the system. Again, it is important to remember the uncertainty in the slag analysis.

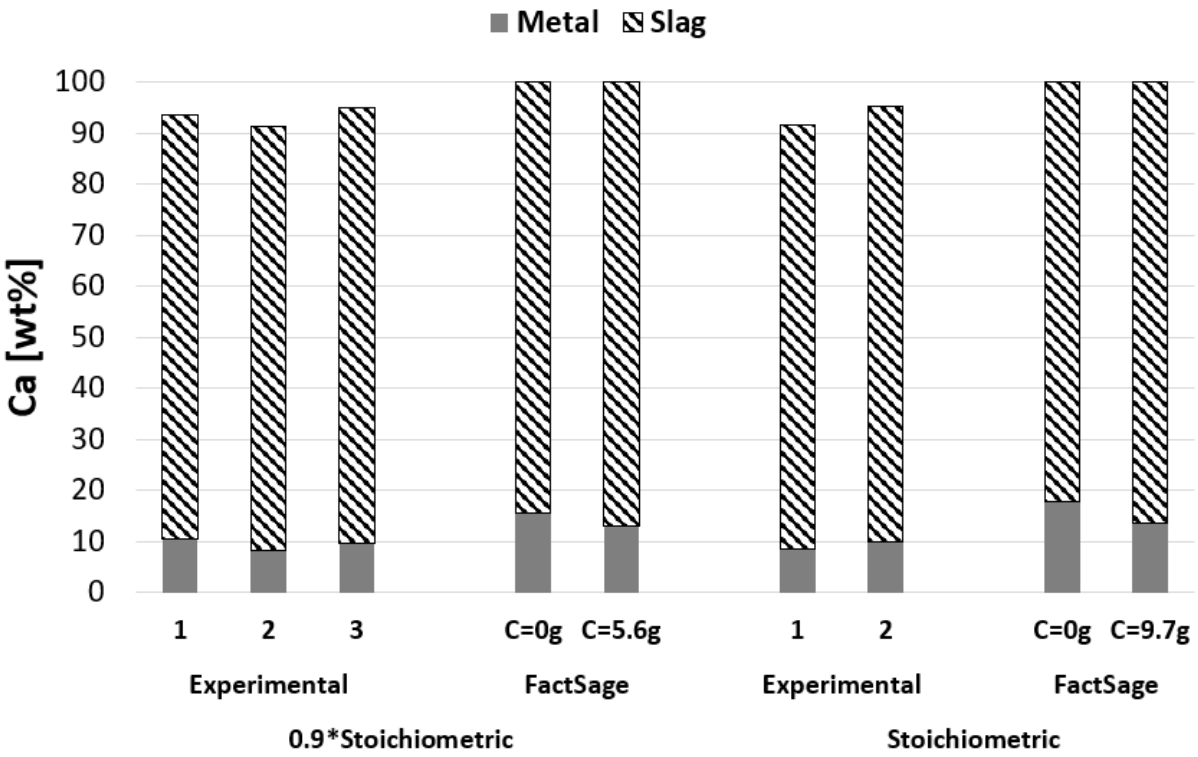

Figure 5.15: Calculated Ca recovery for Basic slag, compared with the simulated values with and without C.

The Basic slag had large variations in mass recovery. Part of this can be contributed to variation as a direct consequence of the cracked crucibles: larger metal losses during handling of the samples even before the separation process could begin, and slag analysis of only select parts of the slag due to the self-decrepitating Ca_2SiO_4. There were also the fact that the composition of the metal had large variations.

5.4 Effect of temperature and time on reaction rate and transport

As all experiments conducted with the REC slag was relatively stable in composition, temperature development (see Figure 4.8 and Figure 4.10), and metal yield, will it not be discussed in any further details.

5.4.1 Outliers from the Acidic slag

The first parallels with acidic slag and 0.9*stoichiometric-, and the first parallel with 1.1*stochiometric reductant addition were outliers with little to no amount of coalesced metal. The first parallel with 0.9*stoichiometric amount had only a 20.8g large ball of mainly Si metal (smaller concentration of Al and Ca than its following parallels), as well as large amount of dispersed metal throughout the slag. The experiment with 1.1*stoichiometric reductant addition did not have a solid piece of coalesced metal, but rather a dense cloud of metal droplet (high in Si) dispersed throughout the top half of the slag (see Figure 4.26), while the bottom slag had less droplets of metal, but it still had large amount of the Si_2Ca metal phase observed in the slag for all experiments. As described in section 4.2.1, it is believed the experiment with 1.1*stoichiometric reduction amount was conducted on a lower temperature than its parallel, (see Figure 4.6). A lower temperature in an acidic slag high in network formers usually means that the viscosity will dramatically increase. This can then be the reason for the slow mass transport of metal droplets. Figure 4.6 show that there was no distinct temperature peak, meaning that the exothermic reaction did not happened all at ones. This further lens credibility the theory of slow transport as it is found that transport of SiO_2 in a slag usually is the rate determining step, due to its network forming abilities that is enhanced on lower temperature [20], [29]. (There is also the possibility that the lack of coalescence in the metal is due to the slow reaction as described by White [31]. He found that Si was

more dispersed throughout the slag when the reaction energy was higher than the surface tension. Though for this to be the case would it be expected that the metal droplets and the small coalesced ball would be higher in Al concentration, and have a more irregular shape to increase its reactive surface. A comparison between the top and bottom thermocouple for the experiment with 0.9*stoichiometric reduction amount is not possible as the top thermocouple stopped working. The temperature did like the previous mentioned experiment not have a distinct temperature peak (see Figure 4.2). This makes it reasonable to assume that the temperature may have been too low also her, as no other differences between experiments between other parallels are observed. It is a well-known fact that C-type thermocouples can have large uncertainties at high temperatures, especially if they have been used before, and are in an induction field. All of which it was.

It should be mentioned that the temperature peaks on REC slag and stochiometric reduction amount varied between parallels (see Figure 4.10). Though these slags (REC- and acidic slag) are different and not directly comparable does this observation show that there are a different in reaction time for other slags as well. The flatter temperature curves show that the exothermic reduction with REC slags can be slower in between parallels (which can be due to lower temperatures). Though there should be more, and clearer date on this, do the observation lend credibility to the theory that the acidic slag is much more sensitive to lower temperatures. As mentioned earlier due the experiments with REC slag had a stable composition (see section 4.5.1) and a stable metal yield (see Table 5-1) compared to the acidic slag. This should be looked closer into in following studies.

5.4.2 Basic slag temperature dependence

When it comes to the basic slag was the parallels with 0.9*stoichiometric reduction amount consistent in composition. The temperature data show that the peaks came later and more irregular than other slags however (see Figure 4.12). Stoichiometric reduction amount showed differences in the metal compositions between the first two parallels. The first one had a higher Al concentration, while the second had a larger Si concentration. This is backed by the temperature data (see Figure 4.15) as the second had several temperature peaks, meaning several exotherm reactions, though both was more irregular compared to other slags. One explanation to the smaller temperature development for all experiments with the basic slag, can be the high Ca concentration present in its metal (both for stoichiometric and 0.9*stochiometric). As reduction of CaO with Al or Si would be endothermic. A kinetics study of REC slag and different reductants conducted by the author [34] found that there was relatively small changes in the Ca concentration after 20 minutes at 1650˚C. This tells us that Ca reacts early and can mitigate the energy from SiO_2 the reduction. Though this helps to explain the differences in temperature development between the basic slags and others, does it not explain the difference in metal composition for stochiometric reductant addition. Another explanation to the difference in temperature development for different slags is simply that the basic slag has high melting temperature. Figure 2.11 show that the melting temperature for the basic slag lies just around 1650˚C. This means that the irregular temperature development can be due to the slag melting in several steps at the holding temperature. The slag may simply have areas with heterogeneous concentration of CaO so that local areas will lie below the liquidus line. This is further backed as there was found a small, slag covered, mostly Al piece, at the bottom of the crucible for the second parallel with stoichiometric reduction amount (see section 4.4.3). If the slag around this piece did not melt completely, could the Al piece not rise to the surface like the rest of the metal. The possibility of solid slag particles would increase the viscosity of the melt thereby decreasing the mass transference [24], [25]. The local changes in concentration would make the system infinitely more complex. The possibility of: Al trapped in slag and not reacting, slag that does not react due to it being solid, and overall irregularities in mass transfer between parallels can explain the differences in metal compositions, and irregularities in temperature developments. It is hard to say exactly what has happened in the slag as a study of the cross section of the samples was not possible due to the self-decrepitating phase mentioned earlier. Though, with the observations mentioned, the high melting temperatures for slags high in CaO (see Figure 2.10), coupled

with the large temperature differences observed between the top and bottom of the crucible (see section 4.2) is there a high probability that the basic slag have stayed semisolid throughout the experiments.

The third parallel with stochiometric reduction amount had some interesting results. It was the one that failed 11 minutes after the holding temperature of 1650˚C was reached (the furnace was off and on again 1 time during this period). This was due to problems with the furnace (see section 4.4.2). What makes this interesting was that metal had coalesced on top of the slag even though it was not finished reaction yet. This was obvious as Al pearls was found on top for the bulk metal (see Figure 4.22), as well for the different concentration of the bulk metal Table 5-1. The bulk metal that had coalesced had a high Ca concentration (the same as the first parallel), though with a lower Si- and higher Al concentration. This sample are interesting for two reasons: This then confirms the fact that Ca will react early and imply that the simulations are wrong when it comes to the equilibrium compositions as it is not the transport of Ca that stops the reaction. The second is that transport of metal to the top of the slag will be fast for this slag composition. This is interesting as the metal for the outliers with acidic slag could not coalesce, even at a holding time of 60 minutes. This implies that temperature control on slags, low in basicity is of upmost importance to get a high metal yield. This should be looked further into at a later date.

5.5 Interfacial tension

On interesting observation is that slag did often contain round metal droplets with roughly the same composition as the bulk metal, though these would be closer to the top of the melt with the rest of the metal. What is interesting is that there was found Si_2Ca metal throughout the slag, both close to the surface, but also further down. What makes this more interesting is that these metal phases did not necessarily have a round shape, implying that the interfacial tension between this phase and slag are low. A low interfacial tension can mean that it will be hard to get this phase out of the slag as the driving force for it to coalesce will not be high enough, leading to a steady state metal emulsion as described by White [31]. There was no research into the interfacial tension between Si_2Ca phase and SiO_2-CaO-Al_2O_3 slags to the authors knowledge, but it would be interesting to look into this in further work.

6 Conclusion

6.1 Concentrations

- Less reductant gives a higher purity in silicon production. Higher Si- and lower Al-concentration. Ca concentration is be less affected.

- Increasing the reductant amount will increase the Al_2O_3- and lower the SiO_2 concentration in the slag.

- Increasing the CaO/SiO_2 mass fraction in start slag will increase the Ca concentration and lower the Si concentration in the metal product. The Al concentration are largely unaffected.

6.2 Si recovery to metal

- Acidic slags, high in SiO_2 reduces the mass transport for the metal increasing the possibility of metal being trapped in the slag, at lower temperature.

- Excluding the outliers, did the acidic slag have the highest Si recovery to metal. There can therefore be advantages to use slags high in SiO_2 as long as the process is under full control.

- The REC slag showed highest stability for composition of metal, and Si recovery

7 Further work

- The acidic slag had several instances where the metal only partly coalesced. It is believed that these experiments had a lower temperature than a control at 1650˚C. This coupled with the low amount of network modifiers in the slag meant that the slag itself would be highly viscous and therefore retard the transport of metal to the top of the crucible where it could form one single metal phase. Though the SisAl process can produce metal with a high Si content when high silica slags are used SiO_2-CaO (55-43.5), would it be of interest to investigate the effect temperatures lower than 1650˚C have. As this study has indicate that there is a risk that the metal and slag will not separate when the temperature drops.
- The reason for the irregularities in composition for the basic slag is not known but it is believed that it is due to the high melting temperature of the slag with 55.1wt% CaO. This coupled with the fact that a high CaO slag produces a metal high in Ca, is worth remembering when considering the energy consumption in the SisAl process. Two of the advantages with this new process is that the production can be conducted on a lower temperature, and that the main reaction are an exothermic reaction. If it becomes necessary to increase the operation temperature to keep the slag liquid, coupled with the fact that CaO reduction is endothermic, will the energy gains in switching process diminish.
- The reaction of Ca is found to be rapid, implying that the systematically difference between simulated and experimental Ca concentration can be explained by errors in the database, and not just that the system has not reached equilibrium. If this is the case, would it be interesting to look into further.
- There was theorised that a larger part of the reductant got lost in near the graphite walls, where they did not contribute to further reduction of SiO_2 when the reduction to SiO_2 mass was high. Though the data for this was spars could this be an interesting topic for further investigation, as implementation of high reductant amount not necessarily need to end up with a higher Si recovery in the produced metal, in practice.
- The formation, and possible losses of Si_2Ca metal in the slag due to its possible lower interfacial tension should be investigated further. This could be done with a more thorough investigation of the slags, possible with image analysing software like ImageJ.

8 Bibliography

[1] G. Tranell, 'SiSal Pilot: Innovative pilot for Silicon production with low environmental impact using secondary Aluminium and silicon raw materials', 2019.

[2] 'Global Market Outlook 2019-2023', *SolarPower Europe*, May 10, 2019. https://www.solarpowereurope.org/global-market-outlook-2019-2023/ (accessed Jun. 11, 2021).

[3] European Commission, 'European Commision. COMMUNICATION FROM THE COMMISSION TO THE EUROPEAN PARLIAMENT, THE COUNCIL, THE EUROPEAN ECONOMIC AND SOCIAL COMMITTEE AND THE COMMITTEE OF THE REGIONS', 2014.

[4] *Treatise on Process Metallurgy*. Elsevier, 2014. doi: 10.1016/C2010-0-67121-5.

[5] M. Tangstad and (ed), *Metal production in Norway*. Akademika Publishin, 2013.

[6] I. Kero, S. Grådahl, and G. Tranell, 'Airborne Emissions from Si/FeSi Production', *JOM*, vol. 69, no. 2, pp. 365–380, Feb. 2017, doi: 10.1007/s11837-016-2149-x.

[7] A. Schei, J. K. Tuset, and H. Tveit, *Production of high silicon alloys*. Trondheim: Tapir, 1998. Accessed: May 02, 2021. [Online]. Available: https://urn.nb.no/URN:NBN:no-nb_digibok_2010021004001

[8] B. Monsen, T. Lindstad, and J. Tuset, 'CO2 Emissions from the Production of Ferrosilicon and Silicon metal in Norway', Nov. 1998.

[9] T. Lindstad, S. E. Olsen, and G. Tranell, 'GREENHOUSE GAS EMISSIONS FROM FERROALLOY PRODUCTION', p. 10.

[10] 'The Norwegian PRTR - Frontpage'. https://www.norskeutslipp.no/en/Frontpage/ (accessed May 16, 2021).

[11] B. Ozturk and R. J. Fruehan, 'The rate of formation of SiO by the reaction of CO or H2 with silica and silicate slags', *Metall Mater Trans B*, vol. 16, no. 4, pp. 801–806, Dec. 1985, doi: 10.1007/BF02667516.

[12] T. Nohira, K. Yasuda, and Y. Ito, 'Pinpoint and bulk electrochemical reduction of insulating silicon dioxide to silicon', *Nature Materials*, vol. 2, no. 6, Art. no. 6, Jun. 2003, doi: 10.1038/nmat900.

[13] K. Yasuda, T. Nohira, R. Hagiwara, and Y. H. Ogata, 'Direct electrolytic reduction of solid SiO2 in molten CaCl2 for the production of solar grade silicon', *Electrochimica Acta*, vol. 53, no. 1, pp. 106–110, Nov. 2007, doi: 10.1016/j.electacta.2007.01.024.

[14] D. Elwell and G. M. Rao, 'Electrolytic production of silicon', *J Appl Electrochem*, vol. 18, no. 1, pp. 15–22, Jan. 1988, doi: 10.1007/BF01016199.

[15] Z. Xing, J. Lu, and X. Ji, 'A Brief Review of Metallothermic Reduction Reactions for Materials Preparation', *Small Methods*, vol. 2, Aug. 2018, doi: 10.1002/smtd.201800062.

[16] F. Habashi, 'Metallothemic reactions - Past, Present and Future', *Research and Reports on Metals*, vol. 2, no. 1, pp. 1–16, 2018.

[17] K. Yasuda and T. H. Okabe, 'Solar-grade silicon production by metallothermic reduction', *JOM*, vol. 62, no. 12, pp. 94–101, Dec. 2010, doi: 10.1007/s11837-010-0190-8.

[18] J. Dietl and C. Holm, 'New Aspects in Aluminothermic Reduction of SiO2', in *Seventh E.C. Photovoltaic Solar Energy Conference*, Dordrecht, 1987, pp. 726–730. doi: 10.1007/978-94-009-3817-5_129.

[19] K. Yasuda, K. Saegusa, and T. H. Okabe, 'New Method for Production of Solar-Grade Silicon by Subhalide Reduction', *Materials Transactions*, vol. 50, no. 12, pp. 2873–2878, 2009, doi: 10.2320/matertrans.M2009260.

[20] Y. Waseda and J. M. Toguri, *The Structure and Properties of Oxide Melts: Application of Basic Science to Metallurgical Processing*. WORLD SCIENTIFIC, 1998. doi: 10.1142/3646.

[21] T. Matsushita, T. Watanabe, M. Hayashi, and K. Mukai, 'Thermal, optical and surface/interfacial properties of molten slag systems', *International Materials Reviews*, vol. 56, pp. 287–323, Nov. 2011, doi: 10.1179/1743280411Y.0000000007.

[22] H. Sun, N. Yoneda, K. Nakashima, and K. Mori, 'Interfacial tensions between CaO-SiO2-Al2O3 slag and Fe-O-S, Fe-Si, Fe-Al, Fe-C, Fe-Cr or Fe-Ni alloys', *Iron & Steel Inst Japan-J (Testu-To-Hagane)*, vol. 83, no. 1, pp. 1–6, 1997, doi: 10.2355/tetsutohagane1955.83.1_1.

[23] T. E. Gammal, H.-J. Schrinner, and E. Wosch, ‘Influence of carbon, silicon and molybdenum on the separating and emulsifying behaviour of steel and slag’, *Steel Research*, vol. 67, no. 4, pp. 138–143, 1996, doi: https://doi.org/10.1002/srin.199605470.
[24] D. Siafakas, T. Matsushita, A. Jarfors, S. Hakamada, and M. Watanabe, ‘Viscosity of SiO2–CaO–Al2O3 slag with low silica – Influence of CaO/Al2O3, SiO2/Al2O3 ratio’, *ISIJ International*, vol. 58, pp. 2180–2185, Dec. 2018, doi: 10.2355/isijinternational.ISIJINT-2018-381.
[25] J.-F. Xu, T. Zeng, M.-Q. Sheng, C. Jie, K. Wan, and J.-Y. Zhang, ‘Viscosity of low silica CaO–5MgO–Al2O3–SiO2 slags’, *Ironmaking & Steelmaking*, vol. 41, no. 7, pp. 486–492, Aug. 2014, doi: 10.1179/1743281213Y.0000000142.
[26] T. Rosenquist, *Principles of extractive metallurgy*, Second. Trondheim, Norway: Tapir Academic Press, 2004.
[27] S. H. Ahn, L. Jakobsson, and G. Tranell, ‘Distribution of Calcium and Aluminum Between Molten Silicon and Silica-Rich CaO-Al2O3-SiO2 Slags at 1823 K (1550 °C)’, *Metallurgical and Materials Transactions B*, Oct. 2016, doi: 10.1007/s11663-016-0829-0.
[28] T. Abel Engh, *Principles of metal refining*. Oxford, New York: Oxford University Press, 1992.
[29] J. Park, S. Sridhar, and R. Fruehan, ‘Kinetics of reduction of SiO2 in SiO2-Al 2O3-CaO slags by Al in Fe-Al(-Si) melts’, *Metallurgical and Materials Transactions B*, vol. 45, pp. 1380–1388, Aug. 2014, doi: 10.1007/s11663-014-0076-1.
[30] M. Sandell, ‘Removal of Dissolved Al and Ca in Si by SiO2 Additions and Mechanical Stirring’, KTH, Stockholm, Sweden, Degree Project, 2015.
[31] J. F. White, ‘Equilibrium and Kinetic Considerations in Refining of Silicon’, Doctoral Thesis, KTH, Sweden, 2013.
[32] E. L. Bjørnstad and G. Tranell, ‘Nucleation of SiO$$_{2}$$-CaO-Al$$_{2}$$O$$_{3}$$Slag in Oxidative Ladle Refining of Metallurgical Grade Silicon’, *Metall Mater Trans B*, vol. 52, no. 3, pp. 1392–1412, Jun. 2021, doi: 10.1007/s11663-021-02132-7.
[33] S. Hassan, ‘Utilization of CaO-Al2O3 Slags from the SisAl Process - an Equilibrium Study between Silicon and CaO-Al2O3 Slags’, Master, NTNU, Trondheim, Norway, 2020.
[34] G. L. Solbakk, ‘Kinetics in Aluminothermic Production of Silicon using Dross as Reductant’, NTNU, Dec. 2020.
[35] K. Tang, ‘Iso-content curves for the Equilibrium between SiO2-CaO-Al2O3 Slag and Si-Al-Ca Metal’. SINTEF Industri, Oct. 19, 2020.
[36] J. F. White, L. Ma, K. Forwald, and D. Sichen, ‘Reactions Between Silicon and Graphite Substrates at High Temperature: In Situ Observations’, *Metall and Materi Trans B*, vol. 45, no. 1, pp. 150–160, Feb. 2014, doi: 10.1007/s11663-013-9947-0.
[37] I. Nettleship, J. L. Shull, and W. M. Kriven, ‘Chemical preparation and phase stability of Ca2SiO4 and Sr2SiO4 powders’, *Journal of the European Ceramic Society*, vol. 11, no. 4, pp. 291–298, Jan. 1993, doi: 10.1016/0955-2219(93)90028-P.
[38] V. D. Eisenhüttenleute (ed.)., *Slag Atlas*, 2. Verlag Stahleisen nbH, 1995.
[39] A. Hoseinpur and J. Safarian, ‘Mechanisms of graphite crucible degradation in contact with Si–Al melts at high temperatures and vacuum conditions’, *Vacuum*, vol. 171, p. 108993, Jan. 2020, doi: 10.1016/j.vacuum.2019.108993.

Appendix

A. XRF results of the master slags

All parallels from the XRF analysis of the three master slags are found underneath (Table 1).

Table 1: Results for all parallels of XRF analysis of the three master slags.

	REC Slag			*Acidic Slag*		*Basic Slag*	
Oxides in slag:	*Sample 1*	*Sample 2*	*Sample 3*	*Sample 1*	*Sample 2*	*Sample 1*	*Sample 2*
K_2O	0.010	0.014	0.015	0.012	0.015	0.007	0.003
MgO	0.253	0.253	0.250	0.211	0.205	0.275	0.270
Mn_3O_4	0.003	0.006	0.004	0.004	0.004	0.004	0.003
Na_2O	<LLD	<LLD	<LLD	<LLD	<LLD	<LLD	<LLD
Fe_2O_3	0.097	0.124	0.116	0.095	0.059	0.027	0.026
P_2O_5	<LLD	<LLD	<LLD	<LLD	<LLD	<LLD	<LLD
SiO_2	46.7	46.6	46.7	55.0	55.0	43.8	43.9
TiO_2	<LLD	<LLD	<LLD	<LLD	<LLD	<LLD	<LLD
Al_2O_3	0.155	0.157	0.164	0.131	0.135	0.147	0.151
CaO	51.3	51.2	51.5	43.5	43.5	55.1	55.1
SrO	0.013	0.016	0.014	0.001	0.013	0.014	0.010
V_2O_5	<LLD	<LLD	<LLD	<LLD	0.002	0.002	0.002
ZnO	<LLD	<LLD	0.001	0.001	<LLD	<LLD	<LLD
ZrO_2	0.007	0.005	0.008	0.005	0.010	0.007	0.014
PbO	<LLD	<LLD	<LLD	<LLD	<LLD	<LLD	<LLD
BaO	<LLD	<LLD	<LLD	<LLD	0.003	<LLD	0.001
Cr_2O_3	0.002	0.004	0.0.2	0.004	0.001	0.003	<LLD
CuO	0.001	0.001	0.002	0.002	<LLD	0.002	0.002
NiO	<LLD	<LLD	<LLD	<LLD	<LLD	<LLD	<LLD
HfO_2	<LLD	<LLD	<LLD	<LLD	<LLD	<LLD	<LLD
LOI 1000˚C	0.69	0.70	0.60	0.05	0.06	-0.02	0.00
Sum	99.2	99.1	99.4	99.1	99.1	99.4	99.5

B. All WDS results

The following Table 2 are a list of all WDS results for metal and slag phases. The results go from brightest (heaviest) to darkest (lightest) phase in the BSE-images. The results for slag marked with bold text were phases that was identified metals or carbides.

Table 2: All WDS results of phases seen in metal (left), and slag (right). Samples with bold numbers in slag are identified as metal of SiC.(The results goes from brightest (heaviest) to darkest (lightest) in the BSE-images.

WDS analysis of metal [wt%]							***WDS analysis of slag [wt%]***					
Acidic Slag							*Acidic Slag*					
Under stoichiometric reductant addition							*Under stoichiometric reductant addition*					
	Si	Al	Ca	Fe	Mn	Mg	SiO_2	Al_2O_3	CaO	FeO	MnO	MgO
Parallel 1	37.41	23.11	7.47	29.03	0.76	0.66	18.58	40.59	41.04	0	0	0.16
	58.99	0.89	40.10	0.11	0	0.05	2.73	62.77	35.80	0	0	0.11
	39.18	36.40	26.05	0.18	0.02	0.50	33.28	2.18	61.81	0.01	0.03	0.44
	101.72	0.31	0.41	0	0	0.01	21.04	38.08	40.94	0	0	0.09
Parallel 2	37.11	23.59	7.32	30.73	0.91	0.77	15.29	42.43	39.13	0	0.01	0.28
	59.17	1.00	40.43	0	0	0..8	3.46	59.67	38.96	0	0	0.09
	39.42	36.69	26.18	0	0	0.07						
	102.33	0.17	0.21	0.01	0	0						
Parallel 3	52.15	4.16	0.52	40.48	1.10	0.05	19.19	38.23	42.25	0	0	0.36
	58.83	0.92	42.22	0.23	0.03	0.18	3.34	59.85	37.10	0.01	0	0.11
	38.62	34.48	27.37	0.02	0	0.11						
	99.86	0.55	0.49	0.02	0	0.02						
Stoichiometric reduction addition							*Stoichiometric reduction addition*					
Parallel 1	44.89	8.37	2.37	37.47	0.10	0.08	28.91	8.78	62.00	0	0	0.10
	37.40	20.69	7.25	35.24	1.37	0.93	18.86	36.26	42.54	0	0	0.46
	58.48	1.33	41.26	0.20	0.02	0.44	0.19	59.51	36.93	0	0	0.03
	38.90	32.25	27.31	0	0.01	0.08						
	103.03	0.79	0.61	0.02	0	0						
Parallel 2	33.42	39.60	0.43	26.65	0.51	0.01	**67.60**	**68.60**	**38.21**	**0.04**	**0**	**0.45**
	38.63	35.10	27.22	0.09	0	0.04	17.48	40.94	42.22	0	0	0.50
	96.94	0.28	0.17	0.06	0.02	0	0.07	60.23	36.57	0	0	0
	1.56	93.21	0.49	0.03	0	0.50						
Parallel 3	31.04	40.76	0.27	27.22	0.64	0.02	17.70	38.99	42.11	0	0	0.49
	36.35	34.93	27.02	0.06	0	0.11	0.13	61.39	36.41	0	0	0.03
	96.11	0.22	0.12	0.03	0	0.01						
	1.62	99.24	0.31	0	0.01	0.41						
Over stoichiometric reductant addition							*Over stoichiometric reductant addition*					
Parallel 1	37.09	21.89	7.57	32.70	1.22	0.67	21.97	30.53	46.84	0.01	0.03	1.03
	57.05	0.79	42.23	0.02	0	0.05	0.07	61.15	36.69	0	0	0.02
	37.32	34.29	27.20	0.08	0.03	0.35						
	97.60	0.11	0.16	0	0	0						
Parallel 2	31.17	43.80	0.14	25.41	0.57	0.01	5.87	53.14	38.94	0	0.01	0.25
	39.00	34.82	27.07	0.01	0	0.05	0.02	61.12	36.39	0	0	0.01
	101.30	0.14	0.08	0	0.02	0						
	2.04	97.86	0.19	0.26	0	0.55						

REC Slag							*REC Slag*					
Under stoichiometric reductant addition							*Under stoichiometric reductant addition*					
Parallel 1	37.26	22.23	7.48	26.61	0.48	0.72	30.55	12.07	59.63	0	0	0.22
	58.44	0.92	42.02	0.18	0.01	0.15	7.77	34.27	60.15	0	0.06	0.57
	38.65	36.15	27.09	0.05	0	0.22	0.10	59.03	37.45	0	0.06	0
	101.82	0.07	0.07	0.01	0	0.01	8.97	42.62	46.39	0	0.01	0.22
Parallel 2	36.92	21.17	7.53	31.47	0.81	0.92	4.00	43.65	51.88	0	0	1.05
	59.11	0.69	42.91	0.02	0	0.07	0.02	62.19	37.41	0	0.01	0.01
	38.56	33.01	27.95	0	0	0.08						
	102.63	0.10	0.09	0	0.01	0						
Parallel 3	35.64	20.55	7.02	32.87	0.60	0.72	28.84	3.03	66.42	0	0	0.03
	58.41	0.70	42.65	0.15	0	0.11	3.87	32.82	60.37	0	0.01	0.59
	38.15	32.75	27.68	0.02	0	0.16	0.07	58.32	37.47	0.05	0	0.03
	101.13	0.08	0.23	0	0	0	9.68	41.14	47.39	0	0.04	0.26
Basic Slag							*Basic Slag*					
Under stoichiometric reductant addition							*Under stoichiometric reductant addition*					
Parallel 1	37.05	23.48	6.83	29.17	0.74	0.64	**124.2**	**1.57**	**59.83**	**0.02**	**0**	**0.42**
	58.77	0.74	41.74	0.12	0	0.27	29.40	5.90	65.01	0	0	0.08
	39.15	34.51	26.04	0.10	0.01	0.53	1.08	62.20	37.42	0	0	0.27
	101.81	0.52	0.59	0	0.03	0.01	**153.7**	**4.78**	**1.48**	**0.03**	**0.03**	**0.01**
Parallel 2	37.49	21.11	7.74	33.47	0.88	0.82	29.41	11.44	62.92	0.02	0.03	0.02
	58.93	0.72	43.2	0.01	0.02	0.03	0.30	62.61	37.44	0	0	0.04
	38.55	32.92	27.63	0.06	0.01	0.12						
	100.71	0.02	0.04	0	0.05	0						
Parallel 3	39.08	18.92	6.33	31.54	1.14	0.84	21.38	13.27	62.72	0	0.02	0.08
	58.07	0.67	42.13	0.07	0	0.09	4.02	34.47	60.56	0.01	0.01	0.46
	38.27	34.54	27.05	0.04	0.03	0.14	0.11	61.40	36.62	0	0	0.01
	100.73	0.10	0.11	0	0.01	0	**156.5**	**3.49**	**1.14**	**0**	**0**	**0.01**
Stoichiometric reductant addition							*Stoichiometric reductant addition*					
Parallel 1	58.77	0.96	41.80	0.08	0	0.31	4.74	32.49	61.25	0	0	0.39
	38.07	36.03	27.24	0	0.01	0	0	58.99	36.89	0	0.01	0
	101.21	0.08	0..6	0	0.01	0						
	69.40	3.05	1.87	0	0.02	0.02						
Parallel 2	38.40	21.49	7.21	31.39	0.33	0.89	98.06	10.13	57.22	0	0.04	0.12
	58.24	0.76	41.00	0	0.03	0.04	0.95	62.36	37.23	0.03	0.01	0.02
	39.02	36.11	25.46	0.02	0	0.14	134.4	10.98	2.85	0	0.01	0.02
	100.27	0.33	0.50	0.01	0	0						
Parallel 3	17.79	58.60	0.22	23.86	0.56	0.15	6.99	38.71	52.45	0.03	0.01	0.38
	38.55	36.83	25.58	0	0.02	0.02	0	61.10	36.51	0	0.02	0
	99.09	0.211	0.03	0	0.02	0						
	1.52	99.59	0.09	0.07	0.02	0.43						

C. Results from the ICP-MS analysis

The following (see Table 3) are the results from the ICP-MS analysis of the three parallels with REC slag and stoichiometric reductant addition.

Table 3: ICP-MS results of three main elements (Si, Al, and Ca) in metal and slag, for REC slag with stoichiometric reduction amount.

	ICP-MS analysis of REC slag with stoichiometric reductant addition [wt%]		
	Metal samples		
	Si	*Al*	*Ca*
Parallel 1	71.8	8.6	19.3
Parallel 2	71.8	8.6	19.3
Parallel 3	73.2	7.9	18.4
	Slag samples		
	Si	*Al*	*Ca*
Parallel 1	4.00	24.5	28.4
Parallel 2	3.71	25.3	28.6
Parallel 3	4.04	26.3	29.6

D. EPMA analysis of slag on low and high magnification

Results from the EPMA analysis of the produced slags on low magnification (*40x*), and on high magnification (*600x*), separate.

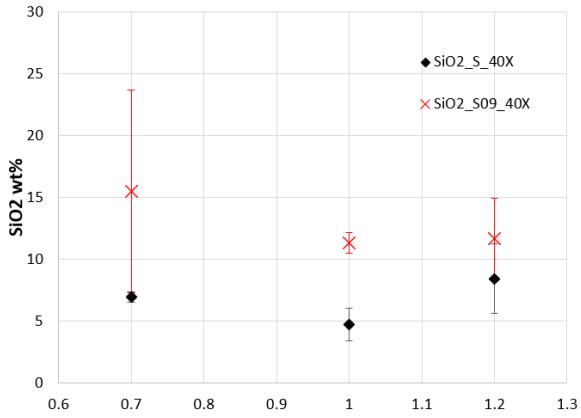

Figure 1: Average wt% SiO_2 (40x magnification) in slag for the different input slags and reductant amount. (Red x) under stoichiometric, (black diamantes) stoichiometric

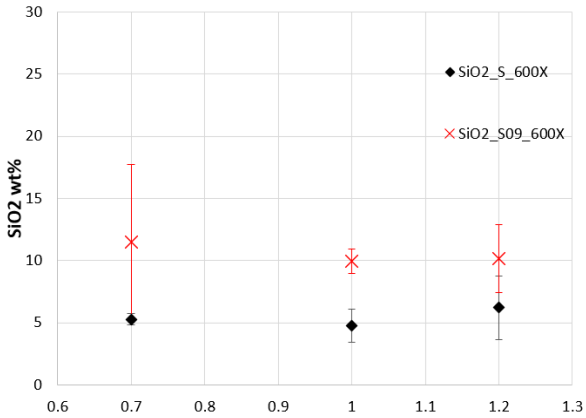

Figure 2: Average wt% SiO_2 (600x magnification) in slag for the different input slags and reductant amount. (Red x) under stoichiometric, (black diamantes) stoichiometric

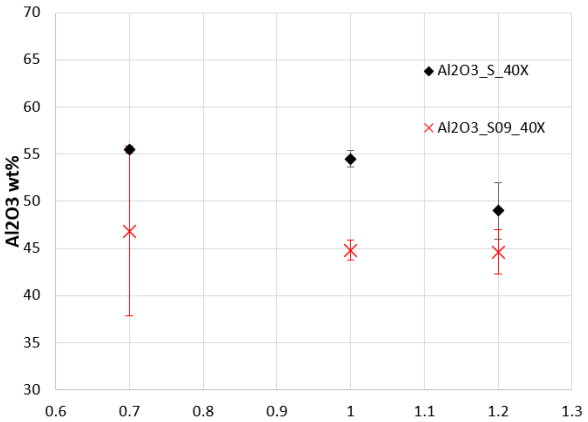

Figure 3: Average wt% Al_2O_3 (40x magnification) in slag for the different input slags and reductant amount. (Red x) under stoichiometric, (black diamantes) stoichiometric

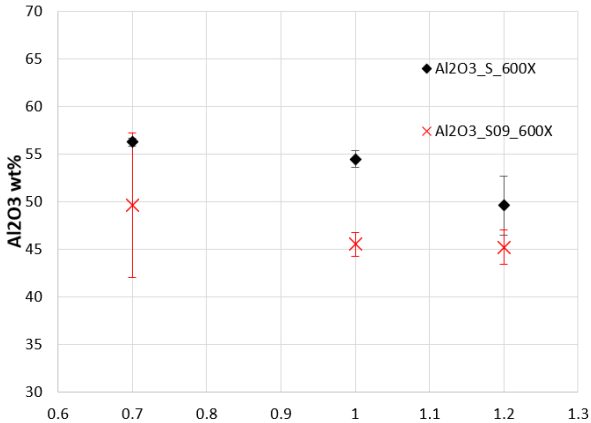

Figure 4: Average wt% Al_2O_3 (600x magnification) in slag for the different input slags and reductant amount. (Red x) under stoichiometric, (black diamantes) stoichiometric

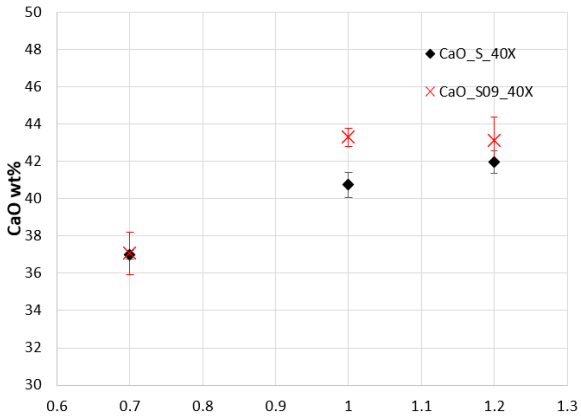

Figure 5: Average wt% CaO (40x magnification) in slag for the different input slags and reductant amount. (Red x) under stoichiometric, (black diamantes) stoichiometric

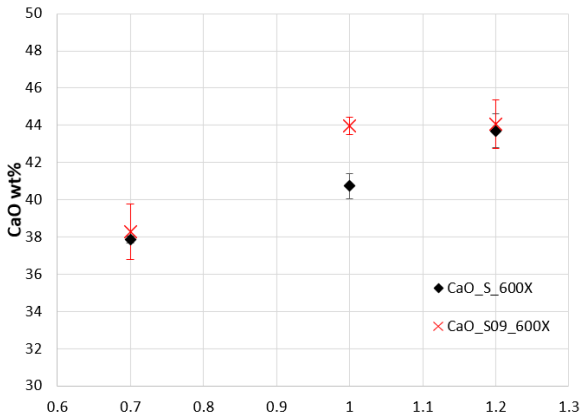

Figure 6: Average wt% CaO (600x magnification) in slag for the different input slags and reductant amount. (Red x) under stoichiometric, (black diamantes) stoichiometric

E. EPMA results for all parallels

The EPMA analysis of pure elements (in other words, no oxides) for both produced metal (Table 4) and slag (Table 5) are fund underneath. This is the results for each individual parallel.

Table 4: EPMA results for all metal samples.

			EPMA analysis of the bulk metal [wt%]								
		Parallels:	*Si*	*Al*	*Ca*	*V*	*Mg*	*Ti*	*Mn*	*Fe*	*P*
Acidic Slag	*0.9*Stoichiometric*	*1*	93.46	1.29	4.96	0.01	0.06	0.02	0.03	0.18	0
		2	81.02	8.38	10.27	0	0.12	0.02	0.05	0.14	0
		3	82.39	7.93	9.41	0.01	0.13	0	0.03	0.1	0
	Stoichiometric	*1*	75.75	12.70	11.13	0.03	0.14	0.02	0.02	0.21	-
		2	78.42	11.87	9.40	0.03	0.140	0	0.01	0.13	0
		3	75.10	13.78	10.70	0.02	0.17	0.01	0.04	0.18	0
	*1.1*Stoichiometric*	*1*	-	-	-	-	-	-	-	-	-
		2	76.35	13.43	9.80	0.04	0.14	0.02	0.02	0.20	0
REC Slag	*0.9*Stoichiometric*	*1*	76.08	5.57	17.87	0.05	0.12	0.04	0	0.27	0
		2	78.69	5.08	15.84	0.03	0.10	0.01	0.03	0.22	0
		3	76.22	5.51	17.81	0.05	0.11	0	0.03	0.25	0
	Stoichiometric	*1*	71.84	8.61	19.06	-	-	-	0.01	0.49	-
		2	71.61	8.60	19.33	-	-	-	0.01	0.45	-
		3	73.19	7.94	18.44	-	-	-	0.01	0.41	-
Basic Slag	*0.9*Stoichiometric*	*1*	70.34	8.10	21.23	0.01	0.16	0.04	0	0.11	-
		2	74.85	6.45	18.39	0.01	0.11	0.01	0.01	0.16	-
		3	72.07	6.84	20.77	0.03	0.13	0.01	0.01	0.14	-
	Stoichiometric	*1*	61.50	20.71	17.49	0	0.18	0.05	0	0.8	-
		2	68.80	9.69	21.09	0.3	0.17	0.02	0.03	0.17	-

Table 5: EPMA results for all slag samples. Calculated to pure elements (not oxides).

			EPMA analysis of the bulk slag calculated to pure elements [wt%]								
		Parallels:	*Si*	*Al*	*Ca*	*V*	*Mg*	*Ti*	*Mn*	*Fe*	*P*
Acidic Slag	*0.9*Stoichiometric*	*1*	10.55	20.02	27.95	0	0.25	0.02	0.01	0.01	0
		2	4.29	28.48	25.99	0.02	0.24	0.03	0.01	0.01	0.04
		3	4.09	28.07	26.82	0.01	0.26	0.01	0.03	0.02	0.04
	Stoichiometric	*1*	2.82	29.62	26.75	0.01	0.22	0.02	0	0.01	0.04
		2	2.98	29.46	26.70	0.01	0.26	0.02	0.01	0.02	0.02
		3	2.78	29.61	26.78	0.01	0.25	0.02	0.01	0.01	0.03
	*1.1*Stoichiometric*	*1*	15.96	11.64	31.02	0.01	0.22	0.01	0.02	0.04	0
		2	1.91	30.93	26.30	0.02	0.25	0.01	0.02	0.02	0.04
REC Slag	*0.9*Stoichiometric*	*1*	5.10	23.53	31.51	0.02	0.24	0.01	0.03	0.01	0.01
		2	4.34	24.89	30.77	0.03	0.24	0.02	0.01	0.03	0.03
		3	5.15	23.56	31.37	0.01	0.25	0.02	0.01	0.04	0.01
	Stoichiometric	*1*	4.0	24.5	28.4	-	-	-	-	-	-
		2	3.7	25.3	24.6	-	-	-	-	-	-
		3	4.0	26.3	29.6	-	-	-	-	-	-
Basic Slag	*0.9*Stoichiometric*	*1*	4.12	24.86	31.16	0.01	0.25	0.02	0.04	0.02	0.01
		2	5.81	23.36	30.65	0.02	0.23	0.01	0.01	0.01	0.02
		3	5.39	23.11	31.66	0.01	0.22	0.02	0.01	0.02	0.01
	Stoichiometric	*1*	2.36	27.53	30.27	0.02	0.23	0.3	0.02	0.02	0.02
		2	4.48	24.64	30.97	0.02	0.24	0.01	0.01	0	0.01

F. Plotted analysed and simulated values with C introduced

Experimental composition plotted with the simulated values where carbon was introduced to the system. The amount of the introduced carbon was enough, so that the simulated metal yield was equal to the experimental yield. (Carbon reacted with silicon to form SiC).

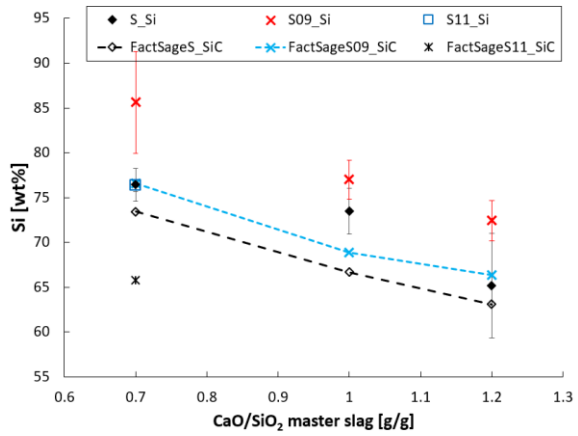

Figure 7: Simulated (with C) and experimental Si concentration in metal.

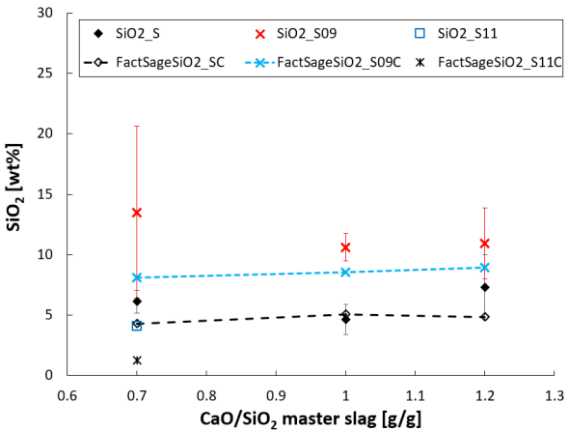

Figure 8: Simulated (with C) and experimental SiO_2 concentration in metal.

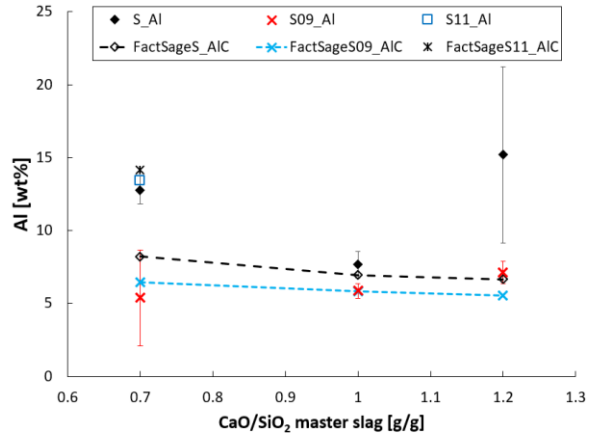

Figure 9: Simulated (with C) and experimental Al concentration in metal.

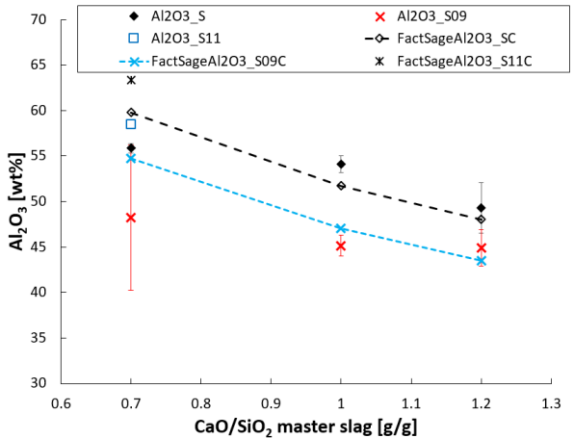

Figure 10: Simulated (with C) and experimental Al_2O_3 concentration in metal.

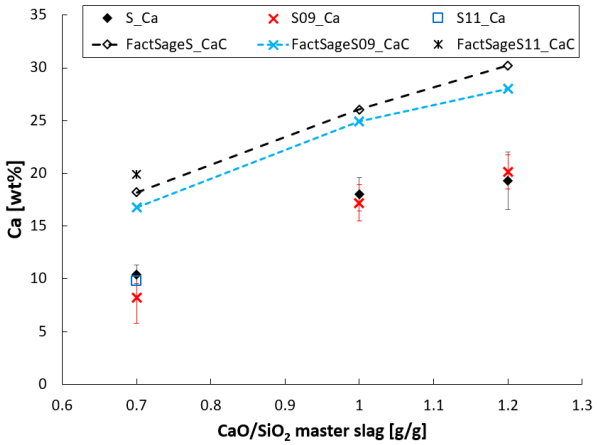

Figure 11: Simulated (with C) and experimental Ca concentration in metal.

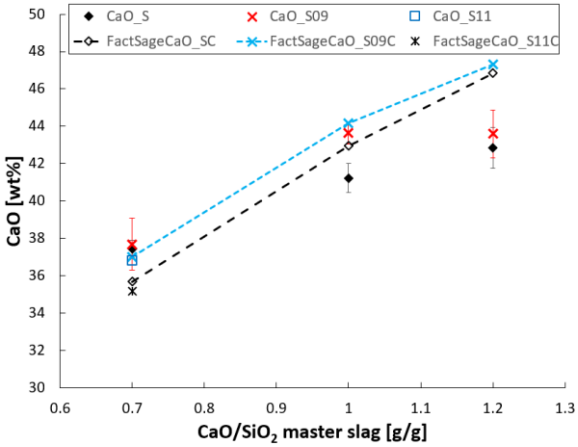

Figure 12: Simulated (with C) and experimental CaO concentration in metal.

G. Calculated metal yield from analysed composition

The calculations for a theoretical metal yield based on the analysed composition (assuming only Al, Si, and Ca present) of the metal products and the input of reductant are as follow: The metal start out as pure Al that is gradually replaced by Ca and Si in accordance with eq. (*1*) and (*2*).

$$2Al + 3CaO = 3Ca + Al_2O_3 \tag{1}$$

$$4Al + 3SiO_2 = 3Si + 2Al_2O_3 \tag{2}$$

The wt% from the EPMA analysis need to be calculated to at%. This is done in accordance with eq. (*3*).

$$at\%_a = \left(\frac{\frac{wt\%_a}{M_a}}{\frac{wt\%_a}{M_a} + \frac{wt\%_b}{M_b} + \frac{wt\%_c}{M_c}} \right) \tag{3}$$

The total mol of all species in the metal can be described by eq. (*4*). As mol Al are a function of start mass, and of amount Ca and Si that have replaced Al (as described above) can eq. (*4*) be rewritten as eq. (*5*).

$$n_{tot} = (n_{Al}) + n_{tot} at\%_{Ca} + n_{tot} at\%_{Si} \tag{4}$$

$$n_{tot} = (\frac{m_{Al\_in}}{M_{Al}} - \frac{2}{3} n_{tot} at\%_{Ca} - \frac{4}{3} n_{tot} at\%_{Si}) + n_{tot} at\%_{Ca} + n_{tot} at\%_{Si} \tag{5}$$

Dividing all terms in eq. (*5*) with n_{tot} gets eq. (*6*)

$$1 = \frac{m_{Al\_in}}{n_{tot} M_{Al}} + \frac{1}{3} at\%_{Ca} - \frac{1}{3} at\%_{Si} \tag{6}$$

Total mol of metal will then be described by eq. (*7*).

$$n_{tot} = \frac{m_{Al\_in}}{M_{Al}(1 - \frac{1}{3} at\%_{Ca} + \frac{1}{3} at\%_{Si})} \tag{7}$$

The equation for total metal mass is described by eq. (*8*)

$$m_{tot} = n_{tot}(at\%_{Al} M_{Al} + at\%_{Ca} M_{Ca} + at\%_{Si} M_{Si}) \tag{8}$$

By replacing the n_{tot} term in eq. (*8*) with the expression in eq. (*7*) can the theoretical mass be express by the input mass for Al, and the analysed amount of Ca, Al, and Si. This is expresses in eq. (*9*).

$$m_{tot} = \frac{m_{Al\_in}}{M_{Al}\left(1 - \frac{1}{3} at\%_{Ca} + \frac{1}{3} at\%_{Si}\right)} (at\%_{Al} M_{Al} + at\%_{Ca} M_{Ca} + at\%_{Si} M_{Si}) \tag{9}$$

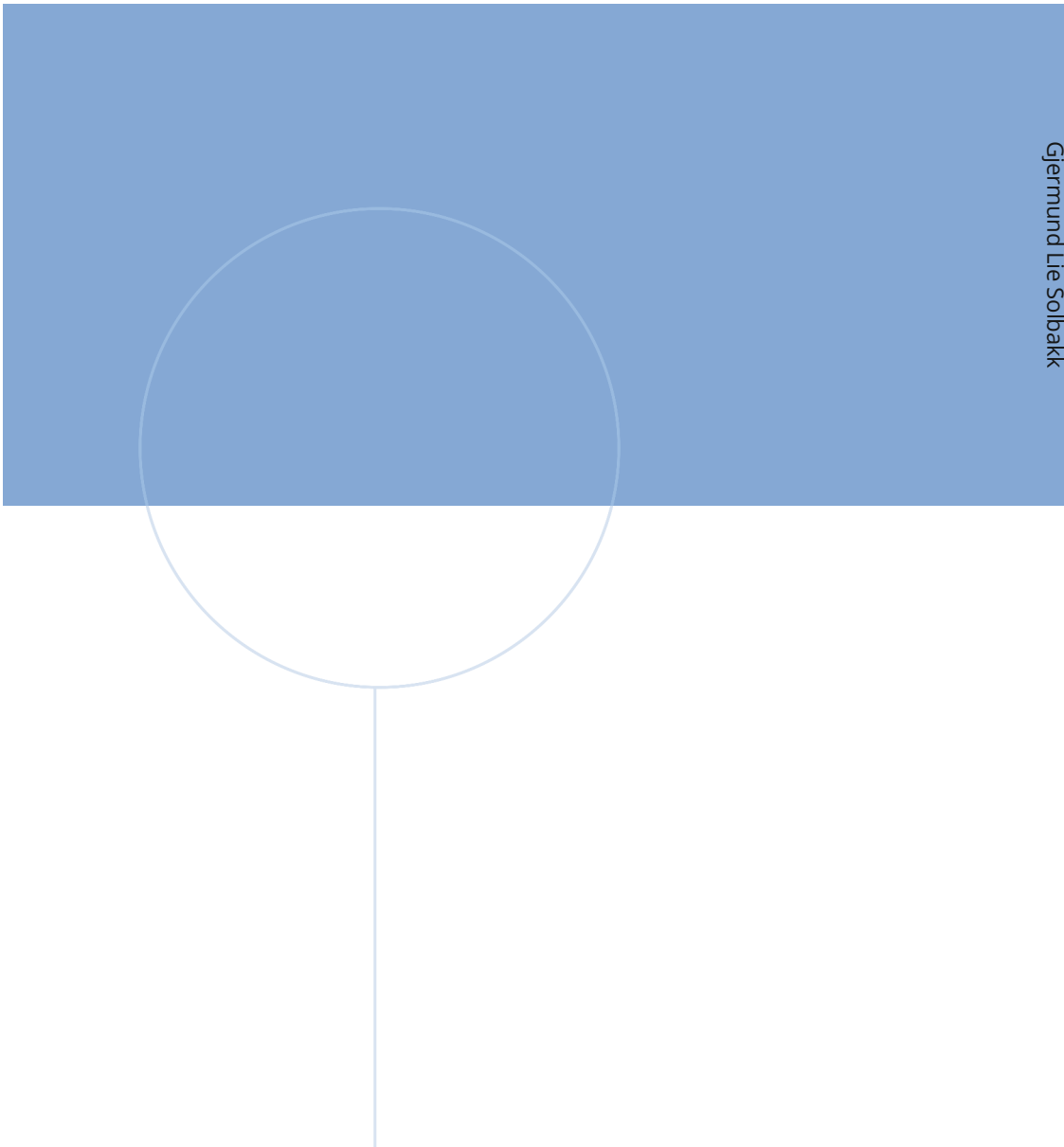

Gjermund Lie Solbakk

NTNU
Norwegian University of
Science and Technology